Development of new fluorescence spectroscopy approaches for the study of silica

Mithun Parambath

A thesis submitted in partial
fulfilment of the requirements of
Nottingham Trent University for the
degree of doctor of philosophy

February 2016

Abstract

PDMPO (2-(4-pyridyl)-5-((4-(2dimethylaminoethylaminocarbamoyl)methoxy)phenyl) oxazole), has unique silica specific fluorescence and is used in biology to understand biosilicification. This 'silicaphilic' fluorescence is not well understood nor is the response to local environmental variables like solvent and pH. We investigated PDMPO in a range of environments: using UV-visible and fluorescence spectroscopy supported by computational data, dynamic light scattering and zeta potential measurements to understand the PDMPO-silica interaction. From absorption data, PDMPO exhibited a pK_a of 4.20 for ($PDMPOH_2^{2+}$ to $PDMPOH^+$).

Fluorescence emission measurements revealed large shifts in excited state pK_a^* values with different behaviour when bound to silica (pK_a^* of 10.4). There is size dependent shift in pK_a^*. pK_a^* value of 9.60, 10.20, 10.50, 11.40, 11.44 was retrieved for 22 nm, 30 nm,50 nm, 77 nm and 133 nm particles respectively. PDMPO bound to silica particles is located in the Stern layer with the dye exhibiting pH dependent depolarising motion. In aqueous solution, PDMPO showed strong chromaticity with correlation between the maximum emission wavelength for $PDMPOH^+$* and dielectric constant (4.8-80). Chromatic effects were also observed for silica bound dye which allow its use as a direct probe of bulk pH over a range far in excess of what is possible for the dye alone (3-5.2). The unique combination of chromaticity and excited state dynamics allows PDMPO to monitor pH from 3 to 13 while also reporting on surface environment opening a new frontier in the quantitative understanding of (bio)silicification. A linear relationship was observed between PDMPO emission ratio and zeta potential measurements were used to determine charge on the silica nanostructures exhibited by *Equisetum arvense* and *Nitzschia stellate.* This thesis also report an optical sectioned planar format assay (OSPFA) using confocal microscopy to study silica biomolecule interaction (amino acids and silica binding peptides (pep 1)) using a PDMPO displacement assay.

Acknowledgements

First and foremost, I would like to express my infinite gratitude to my advisor Prof Carole C. Perry who made this research possible by providing this opportunity, her time and ideas. I also would like to express my sincere gratitude to my co-advisor Dr Quentin Hanley for introducing me to the area of fluorescence spectroscopy, his guidance and suggestions throughout my PhD studies. I am so grateful for the PhD studentship from NTU, Air Force Office of Scientific Research (AFOSR) grants FA9550-10-1-0024 and FA9550-13-1-0040. I want to thank Dr Francisco J. Martin-Martinez, Dr Tristan Giesa, Prof Markus J. Buehler, Massachusetts Institute of Technology, USA for carrying out the computational analysis.

I would like to address a very special thanks to my colleagues Dr David Belton and Dr Marion Limo for their support and friendship both on and off the laboratory. I am deeply grateful to Mrs Anna Sola Rabada, Dr Graham Hickman, Mr Matthew Nicklin and Mr Zayd Westcott for spending their valuable time for the proof reading of my thesis. I also thank Mr Veeru Thota, Ms Robyn Plowright and all my fellow lab mates for the stimulating discussions, exchange of ideas and all the fun we had for the last four years that made this journey a memorable experience in my life. I also thank my previous lab mates Dr Estefania Boix and Dr Homanaz Ghafari for their encouragement and support.

I want to thank my house mates Ms Elisa Tonoli, Ms Debora Del Cogliano and Ms Gandhali Bapat for their considerations during the write up term of my thesis and for the pizzas on Saturdays.

I am also grateful to my lifelong friends Mr Vipin T.S, Dr C.P.Antony and Mr Jithil.K. Jayan who have been always willing to listen, support and help over the years.

I express my warmest gratitude to *Achan*, *Amma,* and *Ammamma* for being with me with their never ending prayers in all ups and downs of my life. And most of all I appreciate Vandana for her love, encouragement and support during the final stages of my PhD.

Table of Contents

LIST OF FIGURES

1. Introduction

1.1 Scope and applications of silica

Silica is formed by the combination of silicon and oxygen and is being one of the most technologically important inorganic materials with a wide range of applications in catalyst support, as separation media (i.e. chromatographic columns), as fillers in polymeric items and many biomedical applications (Belton, Deschaume and Perry 2012). The global market for silica is more than 2 billion USD a year and, thus very important material in the modern age. There is great interest in bioinspired silica formation and in the study of the silica water interface as this has impact in understanding, for example, optical biosensing (Monton, Forsberg and Brennan 2012), cell imaging (Korzeniowska, et al. 2013), tissue engineering (Wang, et al. 2012), phage display (Puddu and Perry 2012) and drug delivery systems (Barisik, et al. 2014). Silica is found in nature as crystalline and amorphous forms. Major crystalline forms of silica are quartz (Wang, et al. 2015a), cristobalite (Tang, et al. 2015) and tridymite (Solc, et al. 2015). Amorphous silica does not exhibit the order displayed by crystalline silica. Major forms of amorphous silica are diatomaceous earth (Tavares, et al. 2016), silica gel (Shi, et al. 2005), fused silica (Isaienko and Borguet 2013) and precipitated silica (Xiao, et al. 2016). In the food industry amorphous silica is widely used as an anti-caking agent (Howard, Hung and McWatters 2010) It is also used as a dentifrices in toothpaste (Creeth, et al. 2015). It is widely applied as a defoamer in the food, paint and paper industries. Silica also has wide biomedical applications, particularly, tissue engineering (Shadjou and Hasanzadeh 2015). Nicklin et al in 2014 have demonstrated that hydrophobic fluoro-silica surface can be used for homotypic cancer cell aggregation and disaggregation studies (Nicklin, et al. 2014).

1.2 Chemistry of silica

The properties of silica from the smallest colloidal particles to macroscopic gels depend, in its majority, on the chemistry at the silica surface. Silica consists of siloxane bonds (Si-O-Si), that can react with water, hence covering the silica surface with silanol groups (Si-OH). Research studies in the last decade have demonstrated that water molecules and many organic molecules with polar groups are adsorbed onto the silica surface via hydrogen bonding with the silanol sites. Silanol groups can donate or accept a proton to give to the surface negative or positive charge, respectively. The pH of zero charge, the so called isoelectronic point, is the pH at which the concentration of protonated groups [$-SiOH_2^{2+}$] should be equal to the concentration of deprotonated silanol groups [SiO-]. The isoelectric pH of silica was determined to be between pH 2 and pH 3. Surface properties of silica can be changed by changing the functional groups on silica nanoparticles. The interface between silica and water is typically explained by the Gouy-Chapman-Stern model (Brown, Bossa and May 2015). It is explained using an electrical double layer which consists of three electrostatically charged regions. The inner layer also known as the Stern layer, consisting of hydrogen ions coordinated with unsaturated sites. This layer is followed by a double layer which consists of a inner sphere complex and an outer sphere complex containing sodium and other weakly bound cations and anions .

1.3 Silica polymerization

In aqueous solution, monosilicic acid at levels above 100 ppm and circumneutral pH will condense spontaneously to large silicate oligomers followed by stable particles that will eventually form a network . The process can be broadly classified into three stages. One, polymerization of monomers to very small particles; two, growth of the particles and three, formation of a branched network . The earliest stage of the condensations is the formation of dimers, followed by trimers and oligomers which are kinetically distinct with each other. The

reaction order observed during condensation is determined by a range of variables which includes precursor concentration, and pH (Belton, et al. 2010, Ralph K. Iler 1979).

1.4 Biosilicification

Biological organisms, particularly diatoms, some sponges and higher plants, are able to uptake, store and process soluble silicon and mould it into hierarchical patterned biosilica by genetically controlled processes (Hildebrand 2003). In addition, natural silica production in diatoms occurs under mild conditions compared to the harsh conditions of silica production generally found in industrial processes (Belton, Deschaume and Perry 2012). In order to develop new environmentally friendly conditions for *in vitro* synthesis, it is important to identify the mechanisms involved in biosilicification (Perry 2003b, Patwardhan, Clarson and Perry 2005a). Furthermore, a better understanding of how biomolecules are involved during the biosilicification process is of great interest for scientists to carry out biomimetic studies and produce better silicon based materials without pollution or high energy loss. In diatoms, silicic acid transporters carry silicic acid into the diatom cell wall, where it is further concentrated in silica deposition vesicles (SDV) followed by polymerization to form silica (Kroger, et al. 2000, Crawford, et al. 2009). Molecules isolated from diatoms thought to be key in the biosilicification process which include peptides and polyamines, with a propylamine backbone (Patwardhan, Clarson and Perry 2005a, Hildebrand 2003).

1.5 Silica-biomolecule interactions

The nature of the interaction of biomolecules with silica is a subject of extraordinary relevance due to its direct implication in promising fields such as bionanotechnology, where the disciplines of chemistry, material science, and medicine merge. Silica biomolecule interactions are very important to understand the process of biosilicification. Another area where this understanding is important is when using phage display technique, which is widely used to study silica peptide interaction using bacteriophages. By phage display, silica binding peptides like 7-mer peptides S1 (KLPGWSG), S2 (AFILPTG), and S3 (LDHSLHS) were

identified (Puddu and Perry 2012). At the molecular level, silica adsorption ~~is~~ was seen to be predominantly by ammonium groups in the N-terminus, Lysine residues and further modulated by Arginine residues through formation of ion pairs with siloxide groups on silica. Similar behaviour was also observed for serine, histidine and aspartic acid through hydrogen bonds and polar interactions (Patwardhan, et al. 2012). A fusion protein of silk and silica binding peptide has been used to control silicification (Zhou, et al. 2015). Particle size and surface functionality on silica nano-particles are significantly important parameters that can substantially influence (bio)molecule uptake via modulation or selection of specific binding modes at the silica/peptide interface (Puddu and Perry 2014).

1.6 Techniques used to study silica chemistry and biosilicification

The size of silica structures and interconnections are primarily studied using electron microscopy (scanning and transmission mode). For example, studies on silica distribution in plants horsetails, *Equisetum arvense*, was based on scanning electron microscopy (SEM)(Anderson, Perry and Hughes 1990). Proton-induced X-ray emission combined with a scanning proton microprobe has been used to investigate the distribution of inorganic elements in silicifying macrohairs from the lemma of the grass *Phalaris canariensis* (Perry, et al. 1984). Energy dispersive X-ray analysis can be used along with scanning and transmission microscopy to locate the mineral within an organism as well as to identify co-localized inorganic species (Silva, Andrade de, Dias and de Mendonca 2014). Small angle and wide angle X –ray diffraction along with transmission electron microscopy TEM were used to study the size of the silica particles (Holzhuter, Narayanan and Gerber 2003). Interspecific differences in structural and fractal properties from the subnanometer level up to dimensions of several microns) are species-specific in fractal properties of biosilica was studied using ultra small angle X-ray diffraction (USAXS) (Vrieling, et al. 2004). Nanoscale uniformity of pore architecture in diatomaceous earth silica was studied using wide angle X-ray diffraction

(WAXS)(Anderson, Perry and Hughes 1990, Vrieling, et al. 2000). At the molecular level, solid state ^{29}Si NMR allows studies on the degree of condensation in solid siliceous materials (Patwardhan, Clarson and Perry 2005b). Infrared spectroscopy (Roach, Farrar and Perry 2006) and Raman spectroscopy (Rai and Perry 2012) have been used to study colloidal and solid state properties of silica. Reflection techniques like attenuated total reflection (ATR) and diffuse reflection infrared Fourier transform spectroscopy (DRIFTS) are used to observe first monolayers of materials (Daboczi, et al. 2016, Parlett, et al. 2013) while the bulk properties observed by transmission techniques (Shi, et al. 2013). Solution studies on silica precipitation are mostly done using UV-Vis absorbance spectroscopy with detection of scattering at 595 nm (Iler 1979, Belton, et al. 2012). The most popular method for the measurement of silica is the molybdenum blue based colorimetric assay (Perry and Yun 1992). The formation of silicomolybdous (blue) complexes was utilized to monitor and study diverse stages of silicic acid condensation (Perry and Yun 1992). In more recent studies, the rates of silicomolybdic (yellow) complex formation, with mathematical modelling of the species present was used to monitor the solution speciation of polysilicic acids (Belton, et al. 2010b).

1.7 Fluorescent approaches in silica chemistry and its advantage

Fluorescence spectroscopy is a powerful technique in chemical and biological sciences (Cambi and Lidke 2012). Examples include interaction of solvent molecules with flurophores; rotational diffusion of molecules; distance between molecules; and molecular conformation and binding (An 2009, Jaeger, Brand and Eggeling 2003). Fluorescent nanoparticles have many advantageous over conventional fluorophores in the area of nanobiophotonics (Al Dwayyan, et al. 2012), being applied in cancer imaging (Geng, et al. 2013), as sensors (Ho, et al. 2013) and photon sources (Das, et al. 2013). Silica nanoparticles with their

biocompatablity and non toxic nature make them an excellent candidate for biomedical imaging (Veeranarayanan, et al. 2012, Gandhi, et al. 2011).

Attempts to label silica fluorescently in nature was performed initially using common fluorophores like rhodamine 123 (Li, Chu and Lee 1989). This dye enters into the cell immediately and it is trapped in the silica deposition vesicle (SDV), probably by the high reducing potential of the SDV and silica is co-deposited with rhodamine 123 in the SDV with the subsequently formed valves and girdle bands becoming fluorescent . However, this molecule has low accumulation efficiency relative to the bright auto fluorescence of the cells (Li, Chu and Lee 1989). Bis(cytopentadienyl)titanium dichloride was also reported as a surface hydroxyl staining agent for biological silica (Perry, Moss and Williams 1990); however, this compound is insoluble in aqueous solution and, therefore, it is not applicable for living specimens. On another study, the dye fluorescein was covalently linked to isolated purified silica fibres with the silane coupling agent 3-aminopropyl triethoxysilane; however, this method was only practical for post-staining of silica exposed on the surface of materials (Hodson, et al. 1994).

1.8 Nature of Fluorescence

The nature of fluorescence can be best explained by the Jablonski diagram (Jablonski 1933) as shown in **Figure 1.1** Electronic states of molecules can be in the ground electronic state (S_0), first electronic state (S_1), second electronic state (S_2) and so on. At each of these electronic states fluorescent molecule can exist in number of vibrational energy levels represented as 0, 1, 2, etc. When fluorescent molecules absorb light this result in transitions between the electronic states which are represented as vertical lines in the Jablonski diagram with transitions occurring at about 10^{-15} s. After light absorption, a fluorescent molecule gets excited to vibrational levels of S_1 or S_2 followed by relaxation to the lowest vibration level of

S_1, this process is called internal conversion and occurs at a time scale of 10^{-12} s and it is completed prior to emission.

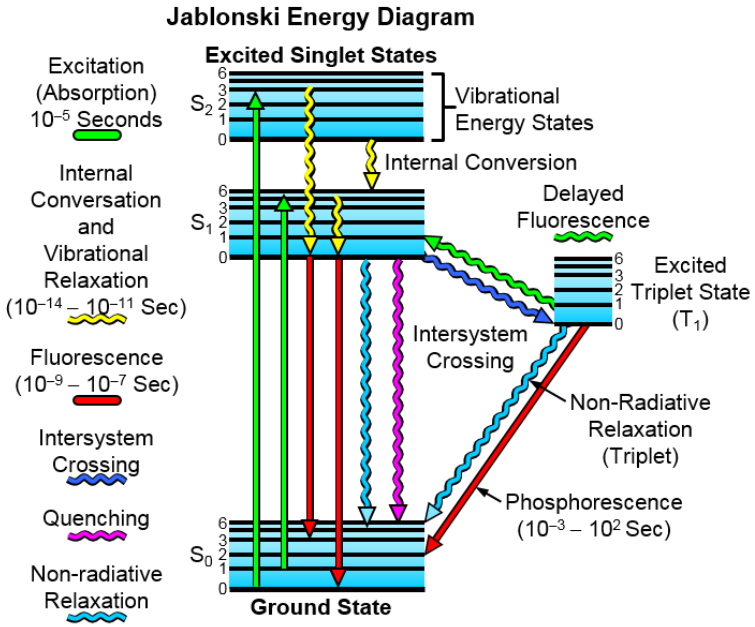

Figure 1.1: Jablonski diagram of excitation of a molecule to its singlet excited state followed by intersystem crossing to the triplet state which further relaxes to the ground state by phosphorescence (Lakowicz 2006).

Energy absorbed is released in the form of a photon (fluorescence) and the electron moves back down to the lower energy level. The energy released will be determined by how far the electron drops down the energy levels. This will determine the wavelength of the photon, and the 'colour' of the fluorescence observed giving the fluorescent dye its distinct emission wavelength.

Molecules in the S_1 state can undergo a spin conversion to the first triplet state (T_1) which is termed as phosphorescence. Phenomena of fluorescence exhibits general characteristics; energy of the emissions is typically less than that of absorption; or emission wavelength is higher than excitation wavelength which is described as Stokes shift (Stokes GG 1852). The

average time the molecules spend in the excited state prior to return to the ground state is referred to as the fluorescence lifetime and the ratio between the number of photons emitted and the number of photons absorbed is called as quantum yield (Q). Emissive rate of the fluorophore is denoted by (Γ) and its rate of nonradiative decay to S_0 (k_{nr}).

1.9 Factors affecting fluorescence emissions

Solvent polarity and local environments have large effects on fluorescence emission properties (Lakowicz 2006). Major factors which affect fluorescence emission include solvent polarity and viscosity, probe conformation change, rigidity of the local environment, internal charge transfer, proton transfer and excited state reactions, probe-probe interaction and the change in radiative and non-radiative decay rates (Lakowicz 2006).

1.9.1 Solvent effects on fluorescence

Solvatochromisim can be defined as the ability of a chemical substance to change colour due to change in solvent polarity (Marini, et al. 2010). Fluorescence emission generally occurs at a longer wavelength than the absorption maximum as there is loss in energy during internal conversion (IC). Solvent effects further shift the emissions to lower wavelength due to stabilization of excited state by polar solvents. Fluorophores may exhibit different dipole moments in the ground state (μ_g) and excited state (μ_E). Typically, the excited state has a higher dipole moment compared to the ground state, as solvent polarity increases, the excited state dipole moments increase compared to the ground state which results in fluorescence emission at lower energy and higher wavelength. Normally fluorophores that display polar nature exhibit more sensitivity to solvent polarity compared to nonpolar fluorophores (Loving, Sainlos and Imperiali 2010, Haidekker, et al. 2005). Solvatochromic probes can be used to study local dielectric constants of an unknown surface as demonstrated by Safarzedeh *et al* (Safarazadehamiri, Thompson and Krull 1989) using trans 4-dimethylamino-4'-(1-oxobutyl)stilbene (DOS) on membrane surfaces. DOS has an emission maximum 575 nm in butanol , 510 nm in ethyl acetate, 425 nm in cyclohexane, 475 nm in toluene when DOS is

bound to membranes, fluorescence emission maximum displayed was between that expected for ethyl acetate and toluene, from this fluorescence emission the solvent environment of the bound fluorophore was predicted as being an intermediate polarity between ethyl acetate and toluene. The dielectric constant on the membrane was determined as being approximately as 5.8 similar to that of ethyl acetate. However, single theory is not sufficient to explain solvathochromisim, but most generally accepted theory to explain solvathochromisim is Lippert – Mataga equation (Mataga, Kaifu, 1956, Lakowicz 2006).This is explained in greater details in the discussion section of chapter 3.

1.9.2 Excited state reactions and its effect on fluorescence

If a fluorophore contains an electron accepting group and an electron donating group, upon excitation there will be increases in charge separation, if the solvent is a polar solvent this results in an internal charge transfer state (ICT), if the solvent is non polar it results in local excited state (LE) state, therefore, the solvent can govern the state of the molecule. In some cases, the molecule undergoes rotation or twisting to form twisted internal charge transfer or exciplex (TICT). Laurdan (6-Dodecanoyl-2-Dimethylaminonaphthalene) has been extensively used to study lipid organization in membranes at -30 ^{O}C (Viard, et al. 1997). It has fluorescence emission from local excited state (LE) at 400 nm and with increasing temperature there is emission shift from 455 nm to 490 nm due to the ICT. A temperature dependent emission shift is observed between 420 nm to 455 nm due to the twisting of dimethyl amino group of the dye to allow the nitrogen electrons to be in conjugation with the naphthalene ring to form a twisted internal charge transfer complex (Viard, et al. 1997). Protonation and deprotonation can occur in the excited state which process is called excited state proton transfer. Phenol is a typical example for an excited state reaction. At neutral pH, phenol can deprotonate at excited state, this deprotonation occurs more readily in the excited

state because electrons on the hydroxyl groups are shifted into aromatic rings making hydroxyl group more acidic (Tolbert and Solntsev 2002). Excited state process displays characteristics time dependent decay. An excited state dissociation constant is denoted as pK_a^*. If $pK_a^* < pK_a$, then a fluorophore tend to lose a proton in the excited state whereas if $pK_a^* > pK_a$ a fluorophore may pick up a proton in the excited state. Electron donors such as -OH, -SH, $-NH_2$ that have a lone pair of electrons tend to become more conjugated to aromatic ring systems in the excited state resulting in $pK_a^* < pK_a$. Electron acceptors such as $-CO_2^-$, $-CO_2H$ have vacant π orbitals into which electrons can be transferred in the excited state resulting a $pK_a^* > pK_a$ (Szczepanik 2015, Esboui and Jaidane 2015).

1.10 Fluorophores

All the information obtained from experiments depends on the properties of the fluorescent probes or fluorophores. Fluorophores can be broadly divided into intrinsic probes and extrinsic probes. Intrinsic fluorophores are those that occur naturally (i.e. aromatic amino acids, NADH and flavins). Extrinsic fluorophores are added to samples to provide fluorescence. As an example the sol gel method is widely used to produce fluorescent silica particles by using both intrinsic fluorophores and extrinsic fluorophores (Lakowicz 2006).

1.10.1 Silica nano particles using intrinsic fluorophore

Intrinsic fluorescence originates with aromatic amino acids such as tryptophan (Trp), tyrosine (Tyr) and phenylalanie (Phe). The indole group of the tryptophan residue are the dominant source of UV absorbance and emission source. Jie Sui *et al in* 2005 demonstrated that the intrinsic fluorescence of the tryptophan residue can be used to study silica peptide adsorption using steady-state anisotropy (Sui, Tleugabulova and Brennan 2005). Studies using intrinsic fluorescence provide the following advantages: (1) There is no need for labelling the competing compound, which may be challenging or may introduce unwanted changes; (2) the capacity to use the method for many diverse species (polymers, peptides, proteins); and (3) the ability to change the nature of the probe to assess different types of

interactions (electrostatic, H-bonding, hydrophobic); thus, providing a more versatile method for studying interactions of compounds with surfaces (Sui, Tleugabulova and Brennan 2005). As an example, Spallino *et al* in 2014 studied the spectroscopic characterization of visible intrinsic photoluminescence associated with silica and the surface defects and the effects induced by vacuum treatment on silica (Spallino, et al. 2014).

1.10.2 Silica nanoparticles using extrinsic fluorophores

In most cases, silica is non-fluorescent or weakly fluorescent. For this reason, fluorescence signal when working with this material can be obtained by labelling the molecule with extrinsic probes. Fluorescent dyes can be non-covalently attached by physical encapsulation in silica spheres prepared by the Stöber process (**Figure 1.2**) or covalently grafted onto the surface of silica. Monodispersed silica spheres can be produced and their size can be modulated by variation of the reaction conditions (Stober 1968). These fluorescent particles are further coupled by amine groups and carboxyl groups for specific applications .

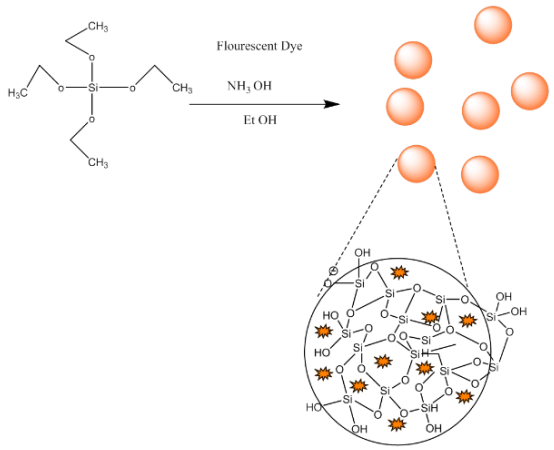

Figure 1.2: Schematic representation of the Stöber process and incorporation of fluorescent labels.

Major fluorophores used for encapsulation include organic dyes such as Rhodamine 6G, BODIPY (Choi, Lee and Jung 2014), FITC (Veeranarayanan, et al. 2012), TRITC (Ogneva, et al. 2014). Semiconductor nanoparticles like quantum dots provide higher photo stability

and the most commonly used nano particle is a core shell nano particle where the core is cadmium selenide and the shell is zinc sulphide (Wu, et al. 2015).

1.10.3 Fluorophore – colloid interaction

The presence of a colloid can change the spontaneous emission of the fluorophore, although these can affect the fluorophore, it can also give some useful effects such as an increase of the quantum yield, an increase of the photo stability, etc. These kind of processes are collectively called radiative decay engineering. Radiative decay engineering is defined by the process by which the environment around the fluorophore is modified or engineered to change the radiative decay (Lakowicz 2006). Our current understanding on radiative decay engineering can be categorised into (a) metal enhanced fluorescence and (b) surface plasmon coupled emission (Lakowicz 2006).

1.10.3.1 Silica nanoparticles using metal enhanced fluorescence

In typical fluorescence measurements, when a fluorophore interacts with a colloid there will be minor changes like refractive index and these changes have insignificant effects on fluorescence spectral properties. In contrast, in the case of metal enhanced fluorescence measurements the electric field felt by the fluorophore is affected by the interaction of light with the near metal surface and fluorophore dipole oscillations induce a field on the metal surface. These interactions can increase or decrease the field incident on the fluorophore which can result in the increase or decrease of the radiative decay rate. Colloidal solutions of Au/SiO_2 core-shell nanoparticles then mixed with CdTe quantum dots (QDs) leads to an enhancement fluorescence by a factor of eight due to metal enhanced fluorescence (Chen, et al. 2015).

1.10.3.2 Surface plasmon coupled emission using silica spacer

Surface plasmon–coupled emission (SPCE) arose from the combination of fluorescence and plasmonics, two rapidly expanding research fields. SPCE is revealing innovative phenomena

and has potential applications in bioanalysis, medical diagnostics, drug discovery, and genomics (Cao, et al. 2012). It is achieved by exciting a fluorophore positioned above a thin metallic surface like silver. The exact mechanism behind this phenomena is still under investigation. Asian *et al* in 2008 demonstrated that silica can be used as spacer between the fluorophore and the metallic surface to protect the surface and minimize metal quenching effects (Asian, et al. 2008).

1.11 Fluorescence based sensing using silica nano particles

Fluorescence based sensing was developed traditionally as an alternative to radioactive methods which are costly to use and dispose (Lakowicz 2006). Fluorescence methods compared to absorbance methods are more sensitive as absorbance is measured as the difference in intensity between light passing through a reference and the sample whereas fluorescence is measured directly which provides a relative dark background compared to the bright reference beam in absorbance measurements. Fluorescence-based techniques are non-invasive. Fluorescence sensing requires a change in spectral response to the analyte. This change can occur in intensity, excitation spectrum, emission spectrum, wavelength, anisotropy or lifetime (Lakowicz 2006). In this work, we describe mostly fluorescence sensing based on silica nano particles.

1.11.1 Sensing based on collisional quenching using silica nano particles

The intensity based method is very direct where the fluorescence intensity of the probe changes in response to an analyte. Such changes normally occur for fluorophores that are subjected to collisional quenching. Quenching depends on the ability of the fluorophore to transfer energy to the quencher without the emission of light (Lakowicz 2006). Collisional quenchers do this by partaking in close molecular interactions with the fluorophore, e.g. aromatic stacking. The quenching efficiency of collisional quenchers, in contrast to FRET quenchers, is not strongly wavelength-dependent. Chen *et al* in 2009 has probed into the mechanisms for enzymatic activity enhancement of organophosphorus hydrolase in

functionalized mesoporous silica (Chen, et al. 2009). Althought this method is conceptually simple it is often inconvenient due to the intensity change observed occur for a wide variety of reasons (Chen, et al. 2009).

1.11.2 Sensing based on resonance energy transfer (RET) using silica nanoparticles

RET is a commonly used and valuable sensing technique to probe chemical process that bring the donor and acceptor into a close proximity which result in a decrease of the donor intensity or decay time. Sha *et al* in 2015 reported a new strategy for constructing a fluorescence resonance energy transfer (FRET) based on the use of a ratiometric sensor for Hg^{2+} detection with organic-inorganic hybrid mesoporous silica nanoparticles (MSNs) as the scaffolds (Sha, et al. 2015a). Silica nanoparticles loaded organic dyes (Demchenko 2013), conjugated polymers (Sha, et al. 2015b) or inorganic material such as semiconductor (quantum dots), colloidal clusters of silver and gold (Wang, et al. 2015b) or carbon dots (Hua, et al. 2015) either act as donor or acceptor and works on the principles of RET has now been used to probe wide variety of analytes such as pH, $Hg^{2+.}$

1.11.3 Sensing based on two state fluorophores using silica nanoparticles

This method of sensing is used when the fluorophore exists in two states and the reaction in each state depends on the analyte concentration. Typically, there is an equilibrium between the fluorophore free in solution and the fluorophore bound to the analyte. In some cases, one can be non-fluorescent and emission can only be observed in the presence or absence of the probe. For example, silica coated superparamagnetic Fe_3O_4 nanoparticles designed to probe for ratiometric and visualization detection of mercuric ions work on the above principle (Hua et al 2015). In some cases, both forms may be fluorescent but have different quantum yields or emissions spectrum (Lakowicz 2006). This behaviour is widely observed in sensors for pH determination.

1.11.4 Sensing using excited state complex using silica nanoparticles

Fluorescence probes can form an excited complex known as twisted intermolecular charge transfer complex (TICT), photoinduced electron transfer and exciplex complex. An analyte can react with excited state complex resulting in an increase or decrease in fluorescence which can be used as fluorescent sensors. For example, coumarin-based pluronic–silica (PluS) nanoparticles form TICT complex can be used as super-bright emitters for ultrasensitive detection (Pedone, et al. 2013)

or 2,4-dichlorophenoxyacetic acid is sensed using a nitrobenzoxadiazole (NBD) fluorophore with the organic amine covalently modified onto the surface of silica (Gao, et al. 2012). On the other hand, exciplex emission was observed between pyrenyl units linked on the silica surface and N,N-dimethylaniline (DMA) units of polymer segments coated on the silica (Hayashi and Ichimura 2003).

1.12 Fluorescence microscopy

Fluorescence microscopy is very powerful technique to study molecules in a confined surface or a defined region or space such as silicified structures on diatoms. Recent advancement in development bright fluorophores and sensitive detectors have made possible to analyse fluorescence from single molecules (Peterson and Harris 2013). Fluorescence imaging when compared to other imaging techniques such as SEM or TEM is limited to low spatial resolution due to the diffraction of light. In recent years, super resolution fluorescence microscopy techniques have been invented to overcome the resolution barrier. This include techniques like confocal laser scanning microscopy, stimulated emission depletion (STED) microscopy for which Peuschel won the Nobel prize for chemistry in 2014 (Peuschel, et al. 2015), saturable optically linear fluorescence transitions (RESOLFTs) (Kwon, et al. 2015) and saturated structured-illumination microscopy (SSIM), as well as techniques that are based on the localization of individual fluorescent molecules, such as stochastic optical reconstruction microscopy (STORM) (Tam and Merino 2015), photoactivated localization

microscopy (PALM) (Betzig, et al. 2006), and fluorescence photoactivation localization microscopy (FPALM)(Alan, et al. 2014).

1.12.1 Fluorescence microscopy for silica nanotechnology

Confocal microscopy has limited image resolution compared to SEM and TEM, henceforth, the major contribution using confocal microscopy is not in imaging nanoscale objects. However, using spectral imaging in confocal microscopy can be used to analyse how photons interact with nanoscale particles as well as to identify energies of interaction, polarization, etc. (Amos and White 2003). Confocal microscopy is nowadays widely used to image the uptake of fluorophores by biological organisms (Ruggiero, et al. 2014). Friedrichs *et al.* combined scanning electron microscopy and confocal laser scanning microscopy to generate three-dimensional models of diatoms (Friedrichs, Maier and Hamm 2012). Confocal microscopy coupled with an image analysis system (NIS Elements AR software, Nikon) has been used to determine shape and biovolume by means a 3D reconstruction which finds many applications (Roselli, et al. 2013). McNair *et al* in 2015 attempted to measure silica deposition in diatoms using the fluorescence property of PDMPO. Fluorescence emissions from PDMPO incorporated in diatoms was converted to the amount of silica deposited (McNair, Brzezinski and Krause 2015). The technology at this scale has advantages such as fitting more functionalities in a smaller space, developing new technology where the size was the rate limiting factor previously. Henceforth, fluorescence microscopic techniques can be a potential and powerful tool to study nano processes involved in bioinspired nanotechnology.

1.13 Thesis outline: PDMPO a fluorescent probe for silica

The work presented here is an attempt to understand the ground state and excited state properties of a fluorescent molecule, PDMPO, explore its interaction when it binds to silica and further use the molecule in four different applications such as pH determination, surface acidity measurements, silica condensation and silica biomolecule interaction using

spectroscopic and imaging techniques. My thesis has six chapters. Each chapter has its own introduction, materials and methods, results and discussion.

Chapter 2 discuss the background to the experimental and mathematical methods used for my studies.

Chapter 3 is about the nature of the silicaphilic fluorescence of PDMPO. This chapter discusses the chemistry involved in the interaction of this fluorescent dye with silica, understanding the excited state processes of the fluorescent probe, location of the dye on silica, the effect of polarity on the fluorescent probe, and ask the following questions: how does the dye bind on silica?, why the dye bind on silica? and further used the understanding gained is silicaphilic fluorescence is used for pH determination.

Chapter 4 explores the applications of silicaphilic fluorescence of PDMPO to understand the surface acidity silica surfaces and translating spectroscopic knowledge into imaging applications using confocal microscopy. Estimates the charge of the biosilica deposited in living organisms such as *Equisetum arvense* and *Nitzschia stellata*. Finally, the application of silicaphilic fluorescence in studying silica condensation are all described.

Chapter 5 explores a newly developed optical interrogation method using confocal microscopy to study silica biomolecule interactions using PDMPO silicaphilic fluorescence. This technique is further used to screen silica binding interactions using aminoacids, polyamines and peptides.

Chapter 6 –provides general discussion and scope of future work.

References

Al Dwayyan, A.S., Qaid, S.M.H., Khan, M.A.M. and Al Salhi, M.S., 2012. Structural and spectral investigations of Rhodamine (Rh6G) dye-silica core-shell nanoparticles. *Optical Materials,* 34 (5).

Alan, L., Dlaskova, A., Spacek, T., Zelenka, J., Olejar, T. and Jezek, P., 2014. Mitochondrial DNA Nucleoid Distribution at Simulated Pathologies as Visualized by 3D Super-Resolution Biplane FPALM / dSTORM Microscopy. *Biophysical Journal,* 106 (2), 203A-203A.

Amos, W.B., and White, J.G., 2003. How the Confocal Laser Scanning Microscope entered Biological Research. *Biology of the Cell,* 95 (6), 335-342.

An, W.F., 2009. Fluorescence-Based Assays Cell-Based Assays for High-Throughput Screening. *Methods in Molecular Biology,* 97-107.

Anderson, O.R., Perry, C.C. and Hughes, N.P., 1990. Transmission and Scanning Electron-Microscopic Evidence for Cytoplasmic Deposition of Strontium Sulfate Crystals in Colonial Radiolaria. *Philosophical Transactions of the Royal Society of London Series B-Biological Sciences,* 329 (1252), 81-86.

Asian, K., Previte, M.J.R., Zhang, Y. and Geddes, C.D., 2008. Surface plasmon coupled fluorescence in the ultraviolet and visible spectral regions using zinc thin films. *Analytical Chemistry,* 80 (19), 7304-7312.

Barisik, M., Atalay, S., Beskok, A. and Qian, S., 2014. Size Dependent Surface Charge Properties of Silica Nanoparticles. *Journal of Physical Chemistry C,* 118 (4), 1836-1842.

Belton, D.J., Patwardhan, S.V., Annenkov, V.V., Danilovtseva, E.N. and Perry, C.C., 2008. From biosilicification to tailored materials: Optimizing hydrophobic domains and resistance to protonation of polyamines. *Proceedings of the National Academy of Sciences of the United States of America,* 105 (16), 5963-5968.

Belton, D.J., Deschaume, O., Patwardhan, S.V. and Perry, C.C., 2010. A Solution Study of Silica Condensation and Speciation with Relevance to in Vitro Investigations of Biosilicification. *Journal of Physical Chemistry B,* 114 (31), 9947-9955.

Belton, D.J., Deschaume, O. and Perry, C.C., 2012. An overview of the fundamentals of the chemistry of silica with relevance to biosilicification and technological advances. *Febs Journal,* 279 (10), 1710-1720.

Belton, D.J., Mieszawska, A.J., Currie, H.A., Kaplan, D.L. and Perry, C.C., 2012. Silk-Silica Composites from Genetically Engineered Chimeric Proteins: Materials Properties Correlate with Silica Condensation Rate and Colloidal Stability of the Proteins in Aqueous Solution. *Langmuir,* 28 (9), 4373-4381.

Brown, M.A., Bossa, G.V. and May, S., 2015. Emergence of a Stern Layer from the Incorporation of Hydration Interactions into the Gouy-Chapman Model of the Electrical Double Layer. *Langmuir,* 31 (42), 11477-11483.

Cambi, A., and Lidke, D.S., 2012. Nanoscale Membrane Organization: Where Biochemistry Meets Advanced Microscopy. *Acs Chemical Biology,* 7 (1), 139-149.

Cao, S., Cai, W., Liu, Q. and Li, Y., 2012. Surface Plasmon-Coupled Emission: What Can Directional Fluorescence Bring to the Analytical Sciences? *Annual Review of Analytical Chemistry, Vol 5,* 5, 317-336.

Chen, B., Lei, C., Shin, Y. and Liu, J., 2009. Probing mechanisms for enzymatic activity enhancement of organophosphorus hydrolase in functionalized mesoporous silica. *Biochemical and Biophysical Research Communications,* 390 (4), 1177-1181.

Chen, J., Wang, K., Wu, K., Qian, L., Long, H., Wang, B. and Lu, P., 2015. Optimization of metal-enhanced fluorescence by different concentrations of gold-silica core-shell nanoparticles. *Optics Communications,* 349, 180-184.

Choi, H., Lee, J.H. and Jung, J.H., 2014. Fluorometric/colorimetric logic gates based on BODIPY-functionalized mesoporous silica. *Analyst,* 139 (16), 3866-3870.

Crawford, S.A., Chiovitti, A., Pickett-Heaps, J. and Wetherbee, R., 2009. Micromorphogenesis during Diatom Wall Formation Produces Siliceous Nanostructures with Different Properties1. *Journal of Phycology,* 45 (6), 1353-1362.

Creeth, J.E., Kelly, S.A., Martinez-Mier, E.A., Hara, A.T., Bosma, M.L., Butler, A., Lynch, R.J.M. and Zero, D.T., 2015. Dose-response effect of fluoride dentifrice on remineralisation and further demineralisation of erosive lesions: A randomised in situ clinical study. *Journal of Dentistry,* 43 (7), 823-831.

Daboczi, M., Albert, E., Agocs, E., Kabai-Faix, M. and Horvoelgyi, Z., 2016. Bilayered (silica-chitosan) coatings for studying dye release in aqueous media: The role of chitosan properties. *Carbohydrate Polymers,* 136, 137-145.

Das, S., Banerjee, C., Kundu, A., Dey, P., Saha, H. and Datta, S.K., 2013. Silica nanoparticles on front glass for efficiency enhancement in superstrate-type amorphous silicon solar cells. *Journal of Physics D-Applied Physics,* 46 (41), 415102.

Demchenko, A.P., 2013. Nanoparticles and nanocomposites for fluorescence sensing and imaging. *Methods and Applications in Fluorescence,* 1 (2), 022001.

Esboui, M., and Jaidane, N., 2015. Non-radiative deactivation in phenol-pyridine complex: theoretical study. *Photochemical & Photobiological Sciences,* 14 (6), 1127-1137.

Ferreira Silva, R.J., Andrade de Aguiar-Dias, A.C. and de Mendonca, M.S., 2014. Silicified crystal concretions and rosettes in Piper (Piperaceae): unpublished reports on their macropatterns. *Acta Amazonica,* 44 (4), 435-445.

Friedrichs, L., Maier, L. and Hamm, C., 2012. A new method for exact three-dimensional reconstructions of diatom frustules. *Journal of Microscopy,* 248 (2), 208-217.

Gandhi, S., Venkatesh, S., Sharma, U., Jagannathan, N.R., Sethuraman, S. and Krishnan, U.M., 2011. Superparamagnetic nanosystems based on iron oxide nanoparticles &

mesoporous silica: synthesis & evaluation of their magnetic, relaxometric and biocompatability properties. *Journal of Materials Chemistry,* 21 (39), 15698-15707.

Gao, D., Sun, H., Si, J., Chen, H., Zhu, D. and Shi, J., 2012. Ultrasensitive detection of 2,4-D at surface of a hybrid silica nanoparticle based on photoinduced-electron transfer Enhanced Fluorescence. *Asian Journal of Chemistry,* 24 (9), 4031-4034.

Geng, J., Liu, J., Liang, J., Shi, H. and Liu, B., 2013. A general approach to prepare conjugated polymer dot embedded silica nanoparticles with a SiO_2@CP@SiO2 structure for targeted HER2-positive cellular imaging. *Nanoscale,* 5 (18), 8593-8601.

Haidekker, M.A., Brady, T.P., Lichlyter, D. and Theodorakis, E.A., 2005. Effects of solvent polarity and solvent viscosity on the fluorescent properties of molecular rotors and related probes. *Bioorganic Chemistry,* 33 (6).

Hayashi, Y., and Ichimura, K., 2003. Movement of polymer segments by exciplex emission of pyrene and N,N-dimethylaniline at the polymer-silica interface. *Journal of Fluorescence,* 13 (2), 129-137.

Hildebrand, M., 2003. Biological processing of nanostructured silica in diatoms. *Progress in Organic Coatings,* 47 (3-4), 256-266.

Ho, L., Ou, C., Li, C., Chen, S., Li, H. and Chang, H., 2013. Sensitive pH probes of retro-self-quenching fluorescent nanoparticles. *Journal of Materials Chemistry B,* 1 (18), 2425-2432.

Hodson, M.J., Smith, R.J., Vanblaaderen, A., Crafton, T. and Oneill, C.H., 1994. Detecting plant silica fibers in animal tissue by confocal fluorescence microscopy. *Annals of Occupational Hygiene,* 38 (2), 149-160.

Holzhuter, G., Narayanan, K. and Gerber, T., 2003. Structure of silica in Equisetum arvense. *Analytical and Bioanalytical Chemistry,* 376 (4), 512-517.

Howard, B.M., Hung, Y. and McWatters, S.K., 2010. Analysis of ingredient functionality and formulation optimization of an instant peanut beverage mix. *Journal of Food Science,* 75 (1), S8-S19.

Hua, M., Wang, C., Qian, J., Wang, K., Yang, Z., Liu, Q., Mao, H. and Wang, K., 2015. Preparation of graphene quantum dots based core-satellite hybrid spheres and their use as the ratiometric fluorescence probe for visual determination of mercury(II) ions. *Analytica Chimica Acta,* 888, 173-181.

Iler,R.K 1979. *The Chemistry ot Silica.* , New York: John Wiley and Sons.

Isaienko, O., and Borguet, E., 2013. Hydrophobicity of hydroxylated amorphous fused silica Surfaces. *Langmuir,* 29 (25), 7885-7895.

Jablonski, A., 1933. Efficiency of anti-Stokes fluorescence in dyes. *Nature,* 131, 839 - 840.

Jaeger, S., Brand, L. and Eggeling, C., 2003. New fluorescence techniques for high-throughput drug discovery. *Current Pharmaceutical Biotechnology,* 4 (6), 463-476.

Korzeniowska, B., Nooney, R., Wencel, D. and McDonagh, C., 2013. Silica nanoparticles for cell imaging and intracellular sensing. *Nanotechnology,* 24 (44), 442002-442002.

Kroger, N., Deutzmann, R., Bergsdorf, C. and Sumper, M., 2000. Species-specific polyamines from diatoms control silica morphology. *Proceedings of the National Academy of Sciences of the United States of America,* 97 (26), 14133-14138.

Kwon, J., Hwang, J., Park, J., Han, G.R., Han, K.Y. and Kim, S.K., 2015. RESOLFT nanoscopy with photoswitchable organic fluorophores. *Scientific Reports,* 5, 17804.

Lakowicz, J., 2006. *Principles of Fluorescence Spectroscopy.* USA: Springer.

Li, C.W., Chu, S. and Lee, M., 1989. Characterizing the silica deposition vesicle of diatoms. *Protoplasma,* 151 (2-3), 158-163.

Loving, G.S., Sainlos, M. and Imperiali, B., 2010. Monitoring protein interactions and dynamics with solvatochromic fluorophores. *Trends in Biotechnology,* 28 (2), 73-83.

McNair, H.M., Brzezinski, M.A. and Krause, J.W., 2015. Quantifying diatom silicification with the fluorescent dye, PDMPO. *Limnology and Oceanography-Methods,* 13 (10), 587-599.

Marini, A., Munoz-Losa, A., Biancardi, A. and Mennucci, B., 2010. What is Solvatochromism? *Journal of Physical Chemistry B,* 114 (51), 17128-17135.

Mataga.N. Kaifu Y, K.M. Solvent effects upon fluorescence spectra and the dipole

moments of excited molecules, 1956. *Bull Chem Soc Jpn,* 29, 465-470.

Monton, M.R.N., Forsberg, E.M. and Brennan, J.D., 2012. Tailoring sol-gel-derived silica materials for optical biosensing. *Chemistry of Materials,* 24 (5), 796-811.

Nicklin, M., Rees, R.C., Pockley, A.G. and Perry, C.C., 2014. Development of an hydrophobic fluoro-silica surface for studying homotypic cancer cell aggregation-disaggregation as a single dynamic process in vitro. *Biomaterials Science,* 2 (10), 1486-1496.

Ogneva, I.V., Buravkov, S.V., Shubenkov, A.N. and Buravkova, L.B., 2014. Mechanical characteristics of mesenchymal stem cells under impact of silica-based nanoparticles. *Nanoscale Research Letters,* 9, 284.

Parlett, C.M.A., Bruce, D.W., Hondow, N.S., Newton, M.A., Lee, A.F. and Wilson, K., 2013. Mesoporous Silicas as Versatile Supports to Tune the Palladium-Catalyzed Selective Aerobic Oxidation of Allylic Alcohols. *Chemcatchem,* 5 (4), 939-950.

Patwardhan, S.V., Clarson, S.J. and Perry, C.C., 2005a. On the role(s) of additives in bioinspired silicification. *Chemical Communications,* 1113-1121.

Patwardhan, S.V., Belton, D., Tilburey, G. and Perry, C.C., 2010. The role of non-bonded interactions in silica formation in vitro. *Advances in Silicones and Silicone-Modified Materials,* 1051, 229-240.

Patwardhan, S.V., Emami, F.S., Berry, R.J., Jones, S.E., Naik, R.R., Deschaume, O., Heinz, H. and Perry, C.C., 2012. Chemistry of aqueous silica nanoparticle surfaces and the mechanism of selective peptide adsorption. *Journal of the American Chemical Society,* 134 (14), 6244-6256.

Pedone, A., Gambuzzi, E., Barone, V., Bonacchi, S., Genovese, D., Rampazzo, E., Prodi, L. and Montalti, M., 2013. Understanding the photophysical properties of coumarin-based Pluronic-silica (PluS) nanoparticles by means of time-resolved emission spectroscopy and accurate TDDFT/stochastic calculations. *Physical Chemistry Chemical Physics,* 15 (29), 12360-12372.

Perry, C.,C., 2003a. Silicification: The processes by which organisms capture and mineralize silica. *In:* P. Dove M, Yoreo,J,J,D and S. Weiner, eds., *Biomineralization.* USA: Reviews in Mineralogy and Geochemistry, 2003a, pp. 291-328.

Perry, C.C., 2003b. Silicification: The processes by which organisms capture and mineralize silica. *Biomineralization,* 54, 291-327.

Perry, C.C., Mann, S., Williams, R., Watt, F., Grime, G. and Takacs, J., 1984. A scanning proton microprobe study of macrohairs from the lemma of the grass *Phalaris-Canariensis* L. *Proceedings of the Royal Society Series B-Biological Sciences,* 222 (1229), 439-+.

Perry, C.C., Moss, E. and Williams, R., 1990. A staining agent for biological silica. *Proceedings of the Royal Society B-Biological Sciences,* 241 (1300), 47-50.

Perry, C.C., and Yun, L., 1992. Preparation of silicas from silicon complexes - role of cellulose in polymerization and aggregation Control. *Journal of the Chemical Society-Faraday Transactions,* 88 (19), 2915-2921.

Peuschel, H., Ruckelshausen, T., Cavelius, C. and Kraegeloh, A., 2015. Quantification of internalized silica nanoparticles via STED Microscopy. *BioMed Research International,* 2015, 961208.

Peterson, E.M., and Harris, J.M., 2013. Single-molecule fluorescence imaging of DNA at a potential-controlled interface. *Langmuir,* 29 (26), 8292-8301.

Puddu, V., and Perry, C.C., 2014. Interactions at the silica-peptide interface: the Influence of Particle Size and Surface Functionality. *Langmuir,* 30 (1), 227-233.

Puddu, V., and Perry, C.C., 2012. Peptide adsorption on silica nanoparticles: evidence of Hydrophobic Interactions. *Acs Nano,* 6 (7), 6356-6363.

Rai, A., and Perry, C.C., 2012. Mussel adhesive protein inspired coatings: a versatile method to fabricate silica films on various surfaces. *Journal of Materials Chemistry,* 22 (11), 4790-4796.

Roach, P., Farrar, D. and Perry, C., 2006. Surface tailoring for controlled protein adsorption: Effect of topography at the nanometer scale and chemistry. *Journal of the American Chemical Society*, 128 (12), 3939-3945.

Roselli, L., Stanca, E., Paparella, F., Mastrolia, A. and Basset, A., 2013. Determination of Coscinodiscus cf. granii biovolume by confocal microscopy: comparison of calculation models. Journal of Plankton Research, 35 (1), 135-145.

Ruggiero, I., Terracciano, M., Martucci, N.M., De Stefano, L., Migliaccio, N., Tate, R., Rendina, I., Arcari, P., Lamberti, A. and Rea, I., 2014. Diatomite silica nanoparticles for drug delivery. *Nanoscale Research Letters*, 9, 329.

Safarzadhamiri, A., Thompson, M. and Krull, U. Trans-4-dimethylamino-4-(1-oxobutyl)stilbene - a new fluorescent probe of the lipid membrane. *Journal of photochemistry and phtonbiology A-chemistry*, 47} (3), 299-308.

Sha, J., Song, Y., Liu, B. and Lu, C., 2015a. Host-guest-recognition-based polymer brush-functionalized mesoporous silica nanoparticles loaded with conjugated polymers: A facile FRET-based ratiometric probe for Hg2+. *Microporous and Mesoporous Materials*, 218, 137-143.

Shadjou, N., and Hasanzadeh, M., 2015. Bone tissue engineering using silica-based mesoporous nanobiomaterials:Recent progress. *Materials Science & Engineering C-Materials for Biological Applications*, 55, 401-409.

Shi, B., Shin, Y.K., Hassanali, A.A. and Singer, S.J., 2015. DNA binding to the silica Surface. *Journal of Physical Chemistry B*, 119 (34), 11030-11040.

Shi, J., Wang, Y., Yao, Q., Zhou, G. and Fu, S., 2013. Bio-inspired synthesis of silica ribbons with through-holes. *Colloids and Surfaces A-Physicochemical and Engineering Aspects*, 436, 664-674.

Shi, F., Zhang, Q., Li, D. and Deng, Y., 2005. Silica-gel-confined ionic liquids: A new attempt for the development of supported nanoliquid catalysis. *Chemistry-a European Journal*, 11 (18), 5279-5288.

Sillibourne, J.E., Specht, C.G., Izeddin, I., Hurbain, I., Phong Tran, Triller, A., Darzacq, X., Dahan, M. and Bornens, M., 2011. Assessing the localization of centrosomal proteins by PALM/STORM nanoscopy. *Cytoskeleton*, 68 (11), 619-627.

Solc, R., Tunega, D., Gerzabek, M.H., Woche, S.K. and Bachmann, J., 2015. Wettability of organically coated tridymite surface - molecular dynamics study. *Pure and Applied Chemistry*, 87 (4), 405-413.

Spallino, L., Vaccaro, L., Sciortino, L., Agnello, S., Buscarino, G., Cannas, M. and Gelardi, F.M., 2014. Visible-ultraviolet vibronic emission of silica nanoparticles. *Physical Chemistry Chemical Physics*, 16 (40), 22028-22034.

Stokes G.G, 1852. On the change of refrangibility of light. *Phil Trans R Soc(London)*, 142, 463-562.

Sui, J., Tleugabulova, D. and Brennan, J.D., 2005. Direct and indirect monitoring of peptide-silica interactions using time-resolved fluorescence anisotropy. *Langmuir,* 21 (11), 4996-5001.

Szczepanik, B., 2015. Protolytic dissociation of cyano derivatives of naphthol, biphenyl and phenol in the excited state: A review. *Journal of Molecular Structure,* 1099, 209-214.

Tam, J., and Merino, D., 2015. Stochastic optical reconstruction microscopy (STORM) in comparison with stimulated emission depletion (STED) and other imaging methods. *Journal of Neurochemistry,* 135 (4), 643-658.

Tang, C., Zhu, J., Li, Z., Zhu, R., Zhou, Q., Wei, J., He, H. and Tao, Q., 2015. Surface chemistry and reactivity of SiO2 polymorphs: A comparative study on alpha-quartz and alpha-cristobalite. *Applied Surface Science,* 355, 1161-1167.

Tavares, A., Costa, A., Rocha, F. and Velosa, A., 2016. Absorbent materials in waterproofing barriers, analysis of the role of diatomaceous earth. *Construction and Building Materials,* 102, 125-132.

Tolbert, L.M., and Solntsev, K.M., 2002. Excited-state proton transfer: From constrained systems to "super" photoacids to superfast proton transfer. *Accounts of Chemical Research,* 35 (1), 19-27.

Veeranarayanan, S., Poulose, A.C., Mohamed, S., Aravind, A., Nagaoka, Y., Yoshida, Y., Maekawa, T. and Kumar, D.S., 2012. FITC Labeled Silica Nanoparticles as Efficient Cell Tags: Uptake and Photostability Study in Endothelial Cells. *Journal of Fluorescence,* 22 (2), 537-548.

Viard, M., Gallay, J., Vincent, M., Meyer, O., Robert, B. and Paternostre, M., 1997. Laurdan solvatochromism: Solvent dielectric relaxation and intramolecular excited-state reaction. *Biophysical Journal,* 73 (4), 2221-2234.

Vrieling, E., Beelen, T., Sun, Q., Hazelaar, S., van Santen, R. and Gieskes, W., 2004. Ultrasmall, small, and wide angle X-ray scattering analysis of diatom biosilica: interspecific differences in fractal properties. *Journal of Materials Chemistry,* 14 (13), 1970-1975.

Vrieling, E., Beelen, T., van Santen, R. and Gieskes, W., 2000. Nanoscale uniformity of pore architecture in diatomaceous silica: A combined small and wide angle X-ray scattering study. *Journal of Phycology,* 36 (1), 146-159.

Wang, B., Yu, Y., Pignatelli, I., Sant, G. and Bauchy, M., 2015a. Nature of radiation-induced defects in quartz. *Journal of Chemical Physics,* 143 (2), 024505.

Wang, L., Song, Q., Liu, Q., He, D. and Ouyang, J., 2015b. Plasmon-Enhanced Fluorescence-Based Core-Shell Gold Nanorods as a Near-IR Fluorescent Turn-On Sensor for the Highly Sensitive Detection of Pyrophosphate in Aqueous Solution. *Advanced Functional Materials,* 25 (45), 7017-7027.

Wang, X., Schroeder, H.C., Wiens, M., Schlossmacher, U. and Mueller, W.E.G., 2012. Biosilica: Molecular Biology, Biochemistry and Function in Demosponges as Well as its

Applied Aspects for Tissue Engineering. *Advances in Sponge Science: Physiology, Chemical and Microbial Diversity, Biotechnology,* 62, 231-271.

Wartenberg, N., Raccurt, O., Bourgeat-Lami, E., Imbert, D. and Mazzanti, M., 2013. Radioactive Europium-Chelate-Based Silica Nanoparticles as a Probe for Stability, Incorporation Efficiency and Trace Analysis. *European Journal of Inorganic Chemistry,* (9), 1493-1498.

Wu, Q., Chen, L., Huang, L., Wang, J., Liu, J., Hu, C. and Han, H., 2015. Quantum dots decorated gold nanorod as fluorescent-plasmonic dual-modal contrasts agent for cancer imaging. *Biosensors & Bioelectronics,* 74, 16-23.

Xiao, Y., Wang, Y., Luo, G. and Bai, S., 2016. Using hydrolysis of silicon tetrachloride to prepare highly dispersed precipitated nanosilica. *Chemical Engineering Journal,* 283, 1-8.

Zhou, S., Huang, W., Belton, D.J., Simmons, L.O., Perry, C.C., Wang, X. and Kaplan, D.L., 2015. Control of silicification by genetically engineered fusion proteins: Silk-silica binding peptides. *Acta Biomaterialia,* 15, 173-180.

Chapter 2: Instrumentation and general preparative methods

This chapter is an introduction of basic techniques used in the study. It consist of computational methods and experimental methods. Computational methods include identifying different protonated states by SPARC, spectral decomposition using DATAN and Gaussian functions. Experimental methods used includes absorbance spectroscopy, fluorescence spectroscopy, dynamic light scattering, zeta potential measurements fluorescence anisotropy and confocal microscopy.

2.1 Absorbance spectroscopy

When a molecule absorbs a photon the energy of the molecule increases, It is directly proportional to the concentration c of the light absorbing species in the sample. This is best explained by Beer Lamberts law (Ricci, Ditzler and Nestor 1994).

$$A = \epsilon bc \qquad (eqn\ 2.1)$$

A is absorbance normally denoted in " absorbance unit", c is the concentration and always given in units of moles per litre (M), b is the path length commonly expressed in centimetres and epsilon (ε) is called molar absorptivity has the unit ($M^{-1}cm^{-1}$) Beer's Lambert's law states that absorbance is proportional to the concentration of the absorbing species however, Beer Lambert's law fails at many instances, such as (1) In highly concentrated solutions where solute molecule influence one another as a result of their proximity (2) when non-absorbing species interact with absorbing species through light scattering (Dastidar, Bharath and Roy 2011).

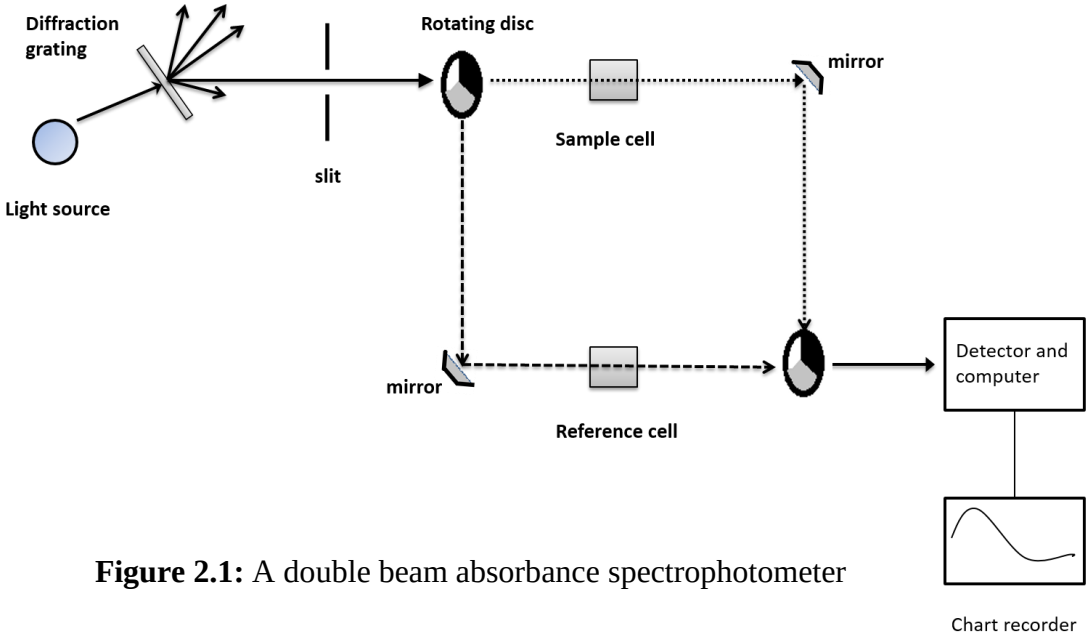

Figure 2.1: A double beam absorbance spectrophotometer

Absorption spectroscopy was carried out in a dual beam spectrometer (JASCO V-670) in 1 cm quartz cuvettes. The optical set up in the double beam spectrophotometer is described in **Figure 2.1**, It has two light source a deuterium lamp for the UV part of the spectrum and halogen lamp for the visible part. It has a wavelength range from 190 nm to 2700 nm. It has a diffraction grating which splits the lights into different wavelength. It has a rotating disc, which has three parts; a black section, mirrored section and transparent section. If the light coming from the diffraction grating hits the transparent section, it will pass through sample and bounced by a mirror on to a second rotating disc. If the original beam of light from the slit hit the mirrored section of the disc it passes through the reference material. If the light from the diffraction grating hit the black section, it will be blocked.

$$A = log_{10} \frac{I_0}{I} \qquad (eqn\ 2.2)$$

Light that passes through the sample and reference cell is detected by the detector. Light detected from the sample cell is denoted as *I* and light detected from the reference cell is denoted as I_0. Absorbance can be calculated using equation 2.2

2.2 Fluorescence spectroscopy (Tecan 2012)

Fluorescence measurements were made using a Tecan fluorescence system (Infinite M200 PRO). The system consists of one light source, excitation double monochromator, fluorescence top optics, emission double monochromatic and fluorescence detection. The optical set for Tecan as in **Figure 2.2** Fluorescence light source consists of six components (1) Flash lamp, The infinite M200 PRO utilizes high energy xenon arc discharge lamp, this lamp is used for both fluorescence and absorbance measurements. (2) condensing optics: The condenser focuses the flash light into the entrance slit of the excitation monochromater it is made up of fused silica. (3) Filter wheels, filter wheels blocks the undesired diffraction orders produced by optical gratings

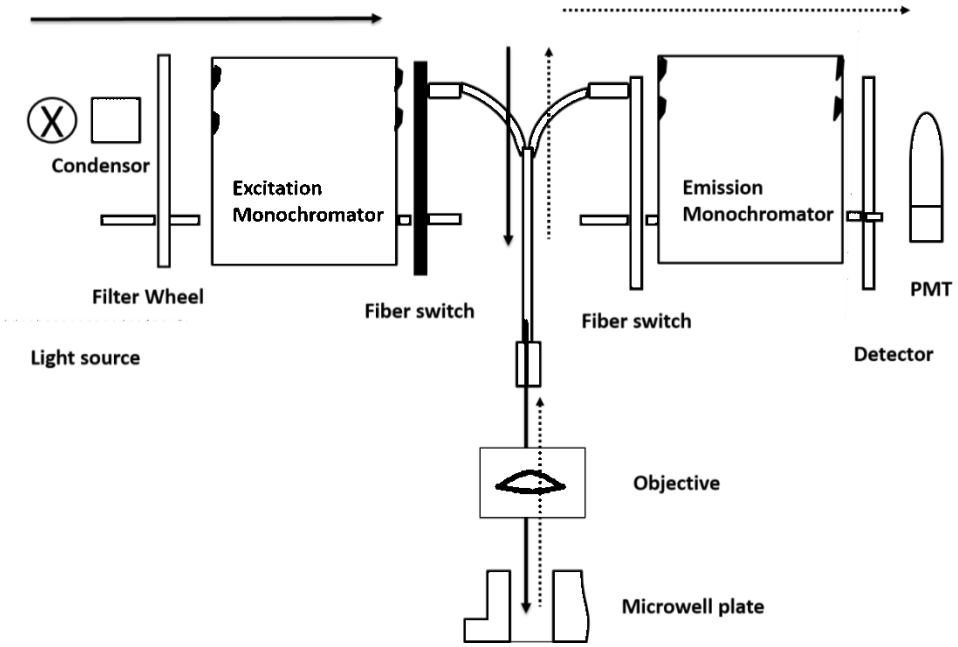

Figure 2.2: Tecan M200 Optical system for Fluorescence spectroscopy

(4), Excitation monochromator ; a monochromator is an optical instrument that enables any wavelength to be selected from a defined optical spectrum. Tecan M200 consists of a fibre optic bundle which guides the light to measuring optics. (5), Measuring optics consist of fluorescence intensity lens system (objective) which is designed to focus the excitation light into the sample (micro well plate) and also collects the fluorescence light and focus it back into the fibre bundle. (6) Tecan M200 also has a fluorescence detection system which consist of emission double monochromatic, filter wheel and PMT detector.

2.3 Fluorescence Spectral correction

Emission spectrum from 300 nm to 428 nm was calibrated using tryptophan in water, excitation wavelength used was 265 nm and emission range from 486 nm to 678 nm calibrated with coumarin 153 in methanol and using an excitation wavelength used of 400 nm. The data was plotted against corrected emission spectrum **Figure 2.3.** From the appendix1 as in of Principles of Fluorescence Spectroscopy by Joseph R.Lakowicz

(Lakowicz 2006).The wavelength range from 428 nm to 486 nm was interpolated from the measured data.

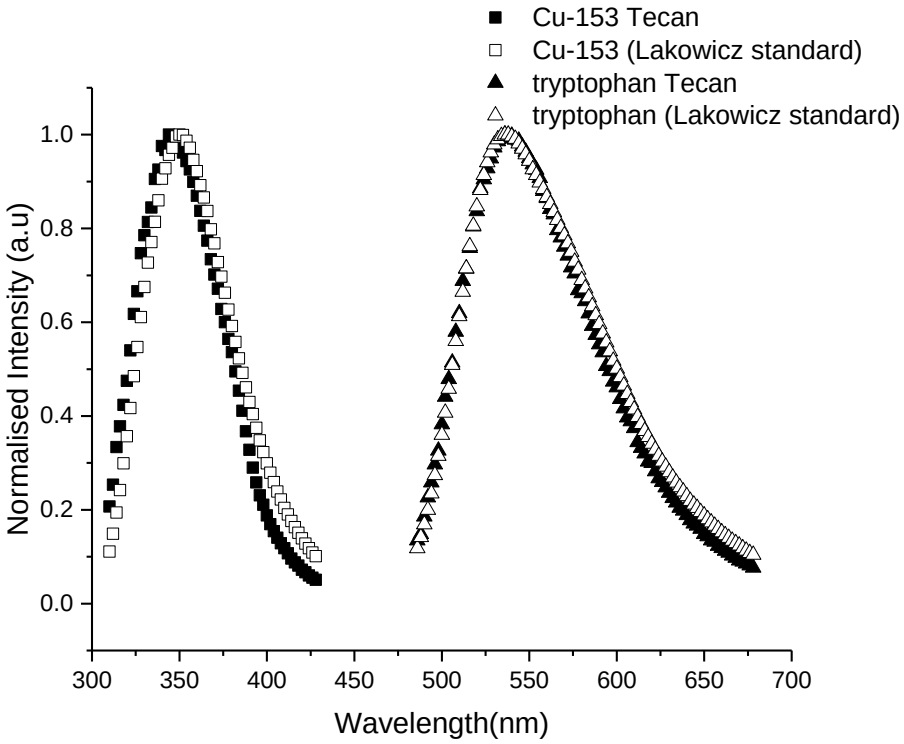

Figure 2.3: Calibration of Tecan M200 with normalized fluorescence emission from lackowicz

2.4 DATAN

DATAN fitting is an algorithm that can be used to determine the acid dissociation constant, K_a.(Scarminio and Kubista 1993). From absorbance/ fluorescence experimental data DATAN calculate all protolytic species and their concentration as a function of pH. For DATAN to analyse the data it has to assume the number of protolytic species that are contributing to the observed behaviour and this is estimated using principle component analysis (PCA). PCA predicts the number of components. In the algorithm there is an option to select the number of components under the protolytic tab. The range with which protolytic constants should be specified, typically one can select pK_a from the entire range. It is also possible to adjust the number of iteration steps to reach the specified range. DATAN determines pK_a by finding the minimum of sum of squared residues between concentrations determined by the rotation

of the principle components, spectra of PDMPO (in presence or absence of silica) at different pH values are digitized and arranged in a data matrix A, Rotation of principle components were done by orthonormal basis set by NIPALS (Scarminio and Kubista 1993).

$$A = \sum_{i=1}^{r} t_i p'_i \qquad (eqn\ 2.3)$$

The orthogonal target vectors t_i and orthonormal projection vectors p_i' are mathematical constructs that cannot be directly related to component spectra r is the number of spectroscopic components that's involved in absorbance or fluorescence. These are related by measured spectrum and concentrations determined by chemical equilibrium expressions (eqn 2.4, eqn 2.5, eqn 2.6) DATAN can be used for spectroscopic titration up to four protolytic species.

$$AH_n^{Z+} \rightleftharpoons AH_{(n-1)}^{(Z-1)+} + H+ \qquad (eqn\ 2.4)$$

$$AH_{(n-1)}^{(Z-1)+} \rightleftharpoons AH_{(n-2)}^{(Z-2)+} + H+ \qquad (eqn\ 2.5)$$

$$AH_{(n-2)}^{(Z-2)+} \rightleftharpoons AH_{(n-3)}^{(Z-3)+} + H+ \qquad (eqn\ 2.6)$$

Equilibrium constants calculated initial concentrations (eqn 2.7, eqn 2.8 and equ 2.9)

$$K_1 = \frac{\left[AH_{(n-1)}^{(z-1)+}\right][H^+]}{[AH_n^{Z+}]} \qquad (eqn\ 2.7)$$

$$K_2 = \frac{\left[AH_{(n-1)}^{(z-2)+}\right][H^+]}{\left[AH_{(n-1)}^{(z-1)}\right][H^+]} \qquad (eqn\ 2.8)$$

$$K_3 = \frac{\left[AH_{(n-1)}^{(z-3)+}\right][H^+]}{\left[AH_{(n-1)}^{(z-2)+}\right][H^+]} \qquad (eqn\ 2.9)$$

In the case of PDMPO we have three different protonated states. Spectrum which exhibit excellent agreement between measured and reproduced spectra with a distinct non negative calculated component spectra are only used for the analysis.

2.5 Gaussian fitting for fluorescence spectrum (Van Bramer 2007)

Gaussian functions are suitable to describe many spectroscopic properties of light. For example, the random noise in a signal, induced by complicated physical factors, can be simply modelled with the Gaussian distribution according to the central limit theorem from the probability theory (Van Bramer 2007). We have used Gaussian functions to fit our fluorescence emissions. Fluorescence emissions are the results of relaxation from a single vibrational level of a singlet excited state to single vibration level of ground singlet state so fluorescence emissions follow a Gaussian distributions whose width would depend on lifetime of the excited state (Vequi-Suplicy, Coutinho and Teresa Lamy 2015). In a fluorescence emission spectrum wavelength is not linear to energy so the emissions have to be converted to wavenumber or frequency to obtain a Gaussian distribution. A typical Gaussian curve can be described by equation 2.10

$$f(x) = aexp\left(-\frac{(x-b)^2}{2c^2}\right) \qquad (eqn\ 2.10)$$

Where a, b, c are arbitrary constants. The parameter a is the height of the curve, b is the position of the centre of the peak and c is the standard deviation sometimes called Gaussian RMS width. The parameter c is related to the full width at half maximum (FWHM) according to equation 2.11

$$FWHM = \sqrt{2ln2c} \qquad (eqn\ 2.11)$$

2.6 SPARC online calculator

Predictive modelling of speciation: Predictive chemical modelling of the pH dependent chemical forms of PDMPO and the associated pK_a's was performed using the web version of SPARC The SPARC computational approach is based on the combination of well-established structure activity relationships, linear free energy relationships and perturbed molecular orbital theory to estimate pK_a (Hilal, Karickhoff and Carreira 1995). The SPARC method of pK_a determination has been tested on 3685 compounds to estimate 4300 ionization pK_a's and their overall RMS deviation from measured values was 0.37. In performing SPARC calculations the molecular structure of a compound is broken into functional units called the reaction centre and perturber. The reaction centre is the smallest subunit that has the potential to ionize or lose a proton to a solvent and the perturber is the molecular structure attached to the reaction centre. The pK_a of the reaction centre is either calculated from direct measurements or from values present in the literature and is adjusted for the specific molecule using mechanistic perturbation models (Hilal, Karickhoff and Carreira 1995).

2.6 Fluorescence anisotropy (Tecan 2012)

Fluorescence anisotropy works on the extent of polarization of the fluorescence emission. In a typical homogeneous solution, a ground state fluorophore is randomly orient when subjected to polarised light. Those fluorophore whose absorption transition moment are oriented along the electric vector of incident light are preferentially excited. A significant fraction of excited molecule share the same transition moment along the electric vector of the polarized excited light. Rotational diffusion can change the direction of the transition moment and emission can be depolarized. Fluorescence emission reports the average angular displacement of the flurophore that occur between absorption and subsequent emission of a photon. This angular displacement is dependent up on the rate and the extent of rotation

diffusion during the lifetime of the excited state. The intensity of the fluorescence emissions is measured through a polarizer. When the emission polarizer is oriented parallel to the direction of polarized excitation the observed intensity is called I_{II} and when polarizer oriented perpendicular it is called $I_{\perp}$.These intensities are used to calculate the anisotropy (r) (Lakowicz 2006).

$$r = \frac{I \parallel - G * I \perp}{I \parallel + 2 * G * I \perp} \qquad (eqn\ 2.12)$$

G factor is not related to properties of the sample but is purely an experimental correction for the polarization bias of the detection system. To find out the most consistent G factor, two samples with known anisotropies, basic solution of fluorescein, pH=8 (low anisotropy) and erythrosin in water (high anisotropy), were used.

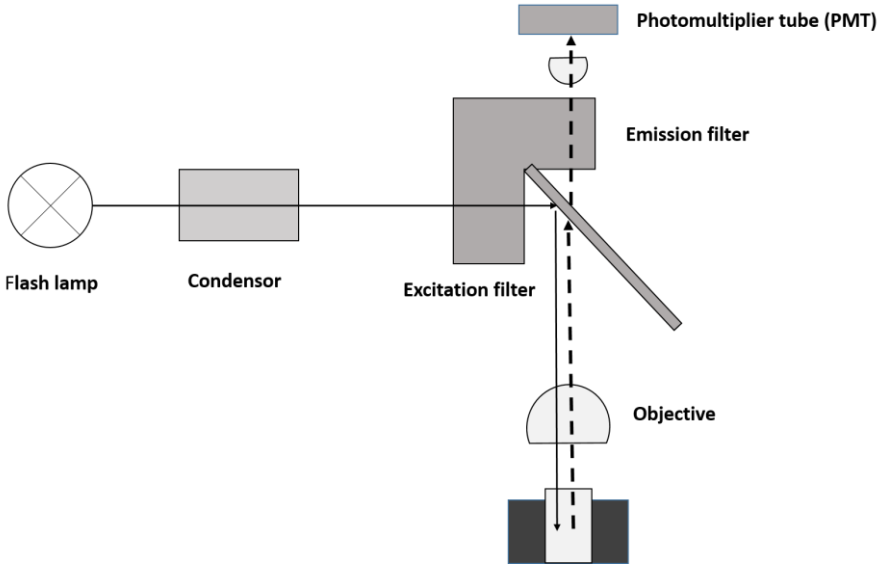

Figure 2.4: Optical setup of Tecan F200

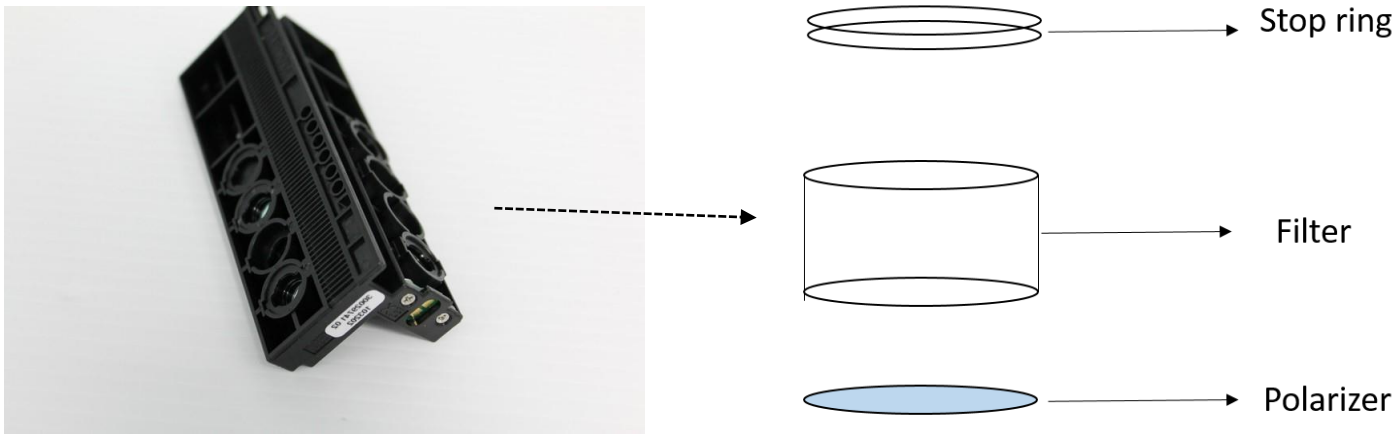

Figure 2.5: Filter slides of Tecan F200, Each filter slide consist of filter, polarizer and stop ring.

As the value of G-factor depends on the PMT voltage (gain), the test was repeated at each working PMT voltage; for example at PMT voltages of 30-50 the G-factor of 1.256 worked well while at the gain of 50-60. Once the G-factor was found, the anisotropies of all samples were calculated manually (equation 2.12) using raw parallel and perpendicular intensity. Fluorescence anisotropy was measured using a Tecan F200 and the optical set up of F200 is described in **Figure 2.4** The optical set up consists of a light source, fluorescence optics and fluorescence detection system. F200 utilises a high energy xenon arc discharge lamp with a flash frequency of 40Hz. The light source also consists of condenser which focuses the light through the entrance slit to the fluorescence optical system. The fluorescence optical system consist objective lens which collect the fluorescent light emitted from a well and focuses it through the exit slit to the detection system. The detection system consists of an emission filter and photomultiplier. For fluorescence anisotropy there are filter slides which consist of filter and polarizers for excitation and emission as in (**Figure 2.5)** each filter slide is equipped with a maximum of two different fluorescence polarization filters pairs as each anisotropy measurements required two excitation and emission filters.

2.7 Photon correlation spectroscopy

Photon correlation spectroscopy or dynamic light scattering (DLS) were used to measure particle size. This is done by first measuring the brownian motion of the particles in a sample using dynamic light scattering and interpreting the size using established theories (Malvern Instruments Ltd 2004**).** Brownian motion is defined as "the random movement of particles in liquid due to the bombardment by the molecules that surrounds them". DLS is a consequence of interaction of light with the electric field of a small particle or molecule, a photon induces an oscillating dipole in the electron cloud of particles as the dipole changes energy is radiated in all directions and this is phenomenon is called scattering of light. Rayleigh theory (Strutt 1871) and Mie theories (Gustav 1908) are the most widely used theories used for DLS measurements. Rayleigh theory is applicable to small particles with a diameter less than one tenth of the laser wavelength. In the Zetasizer the He –Ne laser lamp (633 nm) was used so this corresponds to particles less than ≈ 60 nm. The scattering produced by such small particles is isotropic (equal in all directions) and intensity of light produced is proportional to d^6 where d is the particle diameter. On the other hand Mie theory is a description on how the spherical particles of all sizes and optical properties scatter light. When the particle diameter is larger than one tenth of laser wavelength scattering changes from being isotropic to distortion towards the forward direction and scattering becomes a complex function with maxima and minima with respect to angle. Mie theory correctly explains the maxima and minima in the plots. DLS measure the speed of particles undergoing Brownian motion. Brownian motion is influenced by particle size, sample viscosity and temperature. For smaller particles there is rapid Brownian motion in comparison to larger particles. Translational diffusion coefficient (D) is used to define the velocity of Brownian motion and translational diffusion coefficient (D) can be converted to particle size using the Stokes Einstein equation (Einstein 1905).

$$d_H = \frac{kT}{3\pi\eta D} \qquad (eqn\ 2.13)$$

Where d_H is the hydrodynamic diameter, it is a hard sphere that diffuse as the same speed of the particles and it is dependent upon on size of particle, surface structure and ions in the medium. Ions in the medium and total ionic concentration affect the particle diffusion speed by changing the thickness of electrical double layer called Debye length (κ^{-1}) k is the Boltzmann's constant, T is absolute temperature and η is the viscosity of the solvent.

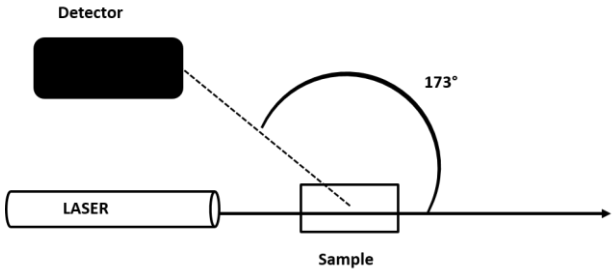

Figure 2.6: Optical set up of DLS, It consist of laser and detector at an angle 173°

2.8 Zeta potential

When nanoparticles interact with solvents the development of a net charge at the particle surface can occur distribution of ions in the surrounding interfacial region. This results in an increased concentration of counter ions, ions of opposite charge to that of the particle, close to the surface. Thus an electrical double layer exists round each particle as in **Figure 2.7.** The liquid layer surrounding the particle exists as two parts; an inner region (Stern layer) where the ions are strongly bound and an outer (diffuse) region where they are less firmly associated. Within the diffuse layer there is a notional boundary inside which the ions and particles form a stable entity. When a particle moves (e.g. due to gravity), ions within the boundary move with it. Those ions beyond the boundary stay with the bulk dispersant. The potential at this boundary (surface of hydrodynamic shear) is the zeta potential (**Figure 2.7**).

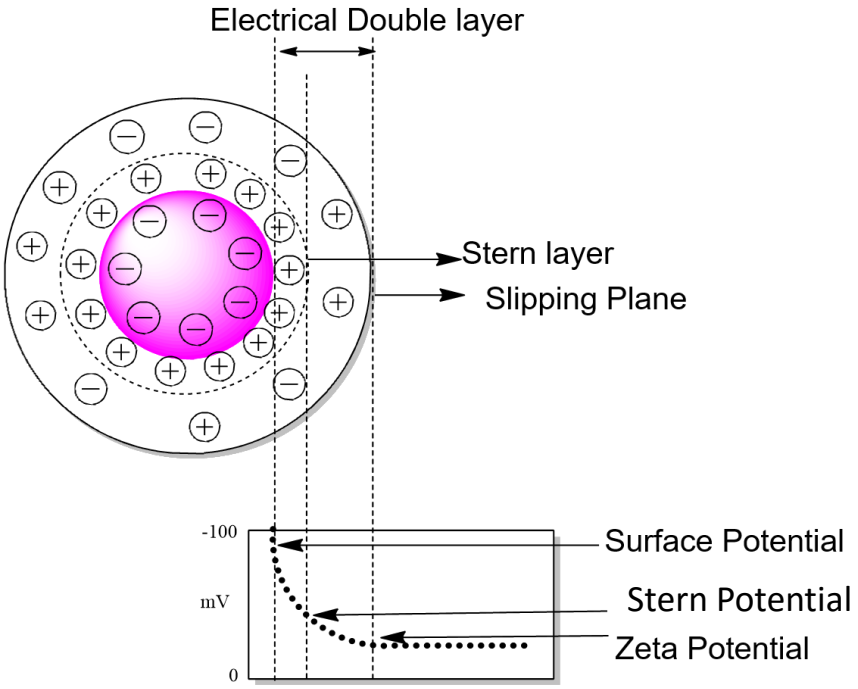

Figure 2.7: Electrical double layer around the nanoparticles

An important consequence of the existence of electrical charges on the surface of particles is that they interact with an applied electric field. These effects are collectively defined as electrokinetic effects. The velocity of the nanoparticles in a unit electric field is referred to as electrophoretic mobility. Zeta potential is related to the electrophoretic mobility by the Henry equation (Hunter 1988).

$$U_E = \frac{2\varepsilon z f(\kappa_a)}{3\eta} \qquad (eqn\ 2.14)$$

Where U_E is the electrophoretic mobility, z is the zeta potential, ε is the dielectric constant, η is viscosity and f(κa) is Henry's function. The optical set up of zeta potential measurement is explained in **Figure 2.8.**

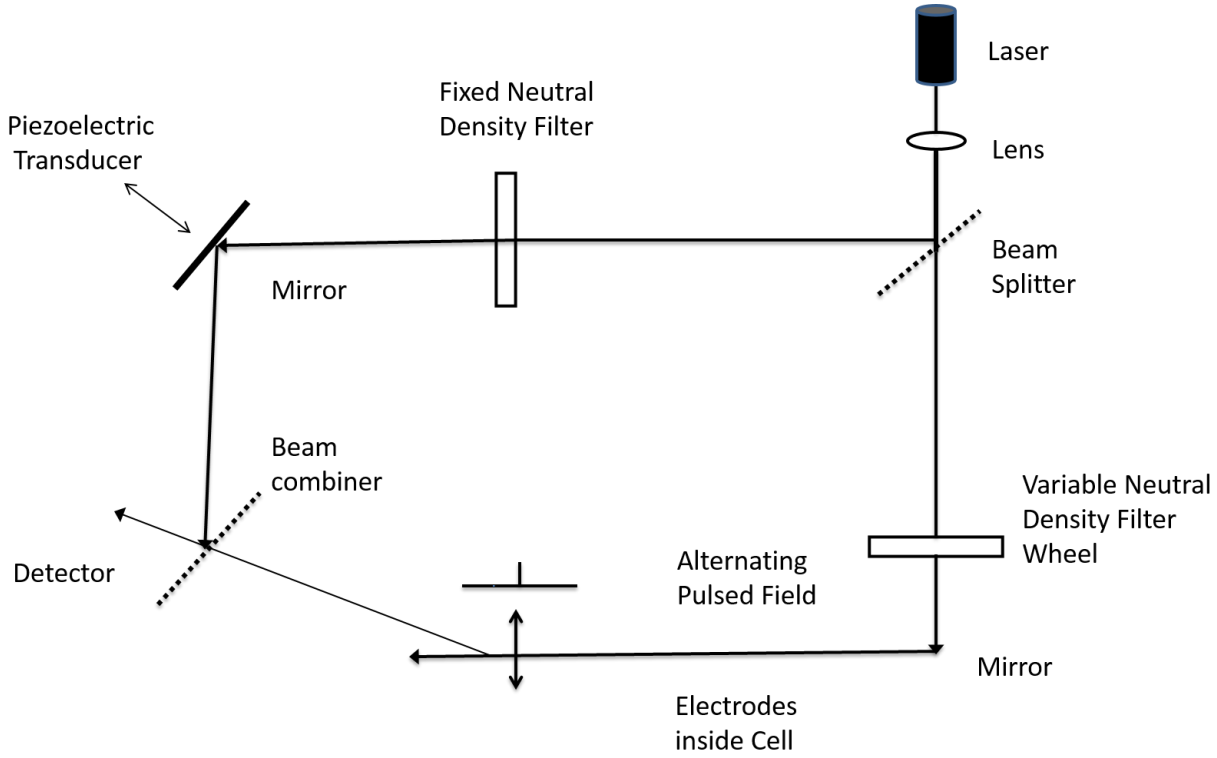

Figure 2.8 : Optical set up of zeta potential measurements

A zeta potential measurement system involves a laser which is used to provide a light source to illuminate the particles within the sample. For zeta potential measurements, this light source is divided to provide an incident and reference beam. The incident laser beam passes through the middle of the sample cell, and the scattered light at an angle of about 13^{o} is detected by detector. When an electric field is applied to the cell, any particles moving through the measurement volume will cause the intensity of light detected to fluctuate with a frequency proportional to the particle speed and this information is detected.

2.9 Confocal microscopy

Confocal microscopy is an optical sectioning technique is used to obtain physical sections with high axial resolution there by facilitating three dimensional imaging (Zemanova, et al. 2004). In a normal wide field fluorescence microscope the total volume of the specimen is uniformly and concurrently illuminated and the fluorescence emissions are collected, this

can also results in out of focus blur from above and below the specimen, which can have adverse effects on the contrast and resolution of the images obtained by the wide field fluorescence microscope (Amos and White 2003).

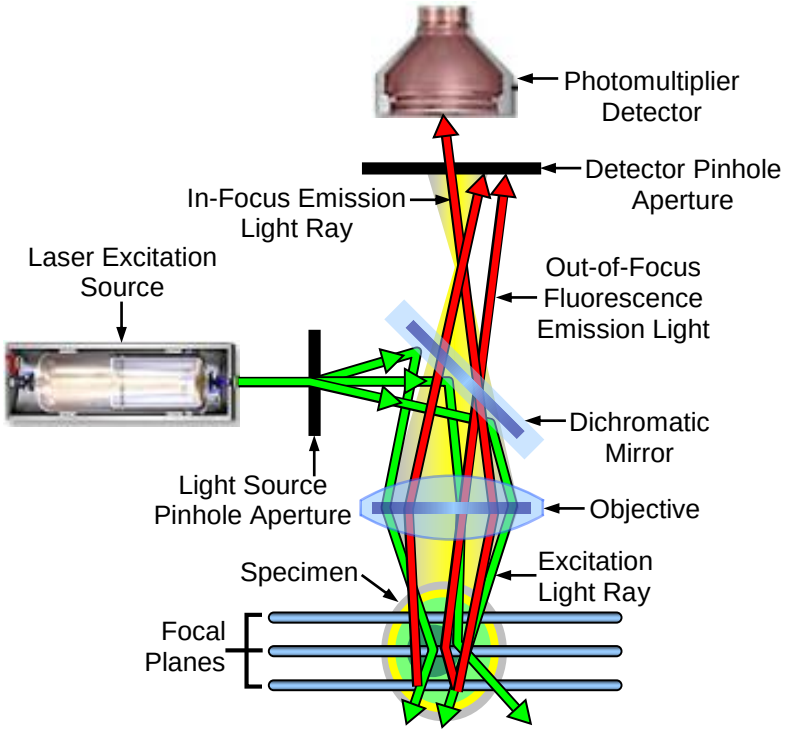

Figure 2.9: Confocal microscope optical set up

In a confocal microscope out of focus light coming from above and below the samples is eliminated by a pinhole (small aperture), as a result only fluorophores that are in focus with both illumination and detection pinholes are only observed. Major parameters which effect the confocal microscopy includes the numerical apertures (NA). The resolution of a confocal microscope depends on NA; moreover with higher NA thinner slices can be scanned and two pin hole: light coming from out of focus planes is prevented by pin hole before it reach to detector (Amos and White 2003, Foldes-Papp, Demel and Tilz 2003, Furrer and Gurny 2010).Confocal microscopy is now capable of spectral imaging. Spectral imaging merges the disciplines of microscopy and spectroscopy into a combination that enables determination the both the intensity and spectral properties of a specimen for each pixel in an image. In

traditional imaging the intensity at every pixel is known. However in spectral imaging the fluorescence emission wavelength values at each pixel location are also provided.

References

Amos, W.B., and White, J.G., 2003. How the Confocal Laser Scanning Microscope entered Biological Research. *Biology of the Cell,* 95 (6), 335-342.

Belton, D.J., Deschaume, O. and Perry, C.C., 2012. An overview of the fundamentals of the chemistry of silica with relevance to biosilicification and technological advances. *Febs Journal,* 279 (10), 1710-1720.

Coradin, T., Eglin, D. and Livage, J., 2004. The silicomolybdic acid spectrophotometric method and its application to silicate/biopolymer interaction studies. *Spectroscopy-an International Journal,* 18 (4), 567-576.

Strutt, J., 1871. On the scattering of light by small particles. *Philosophical Magazine*, 4(41), 447-454.

Dastidar, S.G., Bharath, P. and Roy, A., 2011. Rayleigh like scattering from silica-titania core-shell particles and their application in protection against harmful ultraviolet rays. *Bulletin of Materials Science,* 34 (2), 199-206.

E. Joseph Billo, 2004. Analysis of Kinetics Data. *In:* Analysis of Kinetics Data. *Excel for chemist.* second ed. Wiley-VCH, 2004, .

Einstein., A.1905 .Über einen die Erzeugung und Verwandlung des Lichtes betreffenden heuristischen Gesichtspunkt *Annalen der Physik* 17 (6): 132–148.

Foldes-Papp, Z., Demel, U. and Tilz, G.P., 2003. Laser scanning confocal fluorescence microscopy: an overview. *International Immunopharmacology,* 3 (13-14), 1715-1729.

Furrer, P., and Gurny, R., 2010. Recent advances in confocal microscopy for studying drug delivery to the eye: Concepts and pharmaceutical applications. *European Journal of Pharmaceutics and Biopharmaceutics,* 74 (1), 33-40.

Ghafari, H., Parambath, M. and Hanley, Q.S., 2012. Macromolecular binding and kinetic analysis with optically sectioned planar format assays. *The Analyst,*

Gustav.,M 1908. Beiträge zur Optik trüber Medien, speziell kolloidaler Metallösungen . *Annalen der Physik*, 330 (3), 377–445

Hilal, S.H., Karickhoff, S.W. and Carreira, L.A., 1995. A rigorous test for SPARC's chemical reactivity models: Estimation of more than 4300 ionization pK(a)s. Quantitative Structure-Activity Relationships, 14 (4).

Hunter., R. J. 1988 Zeta potential in colloid science: principles and applications. *Academic Press* London, UK:;

http://www.jascoinc.com, .

Lakowicz, J., 2006. *Principles of Fluorescence Spectroscopy.* USA: Springer.

Malvern Instruments Ltd, 2004. *Zetasizer Nano Series User Manual Zetasizer Nano Series User Manual.* 1.1st ed. England: MAN0317.

Puddu, V., and Perry, C.C., 2014. Interactions at the Silica-Peptide Interface: The Influence of Particle Size and Surface Functionality. *Langmuir,* 30 (1), 227-233.

Ricci, R.W., Ditzler, M.A. and Nestor, L.P., 1994. Discovering the Beer-Lambert Law. *Journal of Chemical Education,* 71 (11), 983-985.

Roach, P., Farrar, D. and Perry, C., 2006. Surface tailoring for controlled protein adsorption: Effect of topography at the nanometer scale and chemistry. *Journal of the American Chemical Society,* 128 (12), 3939-3945.

Scarminio., I and Kubista., M .1993. Analysis of Correlated Spectral Data. *Analytical Chemistry,* 65 (4), 409-416.

Tecan, 2012. *Instructions for use for infinte 200 PRO.* 1.2nd ed. Austria: Tecan Austria GmbH.

Van Bramer, S.E., 2007. A brief introduction to the Gaussian distribution, sample statistics, and the Student's t statistic. *Journal of Chemical Education,* 84 (7).

Vequi-Suplicy, C.C., Coutinho, K. and Teresa Lamy, M., 2015. New Insights on the Fluorescent Emission Spectra of Prodan and Laurdan. *Journal of Fluorescence,* 25 (3), 621-629.

Zemanova, L., Schenk, A., Nienhaus, G.U., Valler, M.J. and Heilker, R., 2004. Confocal optics microscopy for biochemical and cellular high-throughput screening (vol 8, pg 1085, 2003). Drug Discovery Today, 9 (1), 26-26.

Chapter 3

The nature of the silicaphilic fluorescence of PDMPO

This chapter is about the nature of the silicaphilic fluorescence of PDMPO. This chapter discusses the chemistry involved in the interaction of this fluorescent dye with silica, understanding the excited state processes of the fluorescent probe, location of the dye on silica, the effect of polarity on the fluorescent probe, and ask the following questions: how does the dye bind on silica?, why the dye bind on silica? and further used the understanding gained is silicaphilic fluorescence is used for pH determination.

Based on

M. Parambath, Q. S. Hanley, F. J. Martin-Martinez, T. Giesa, M. J. Buehler and C. C. Perry, *Phys. Chem. Chem. Phys.*, 2016, Advance Article, DOI: 10.1039/C5CP05105C

(DFT calculations were done at MIT but not included in the thesis)

3.1 Introduction

There is considerable interest in the unique fluorescence of PDMPO (2-(4-pyridyl)-5-((4-(2 dimethylaminoethylaminocarbamoyl)methoxy)phenyl) oxazole) in the presence of silica and its resulting use as a silica probe (Shimizu, et al. 2001) as in Scheme 1.

Scheme 1

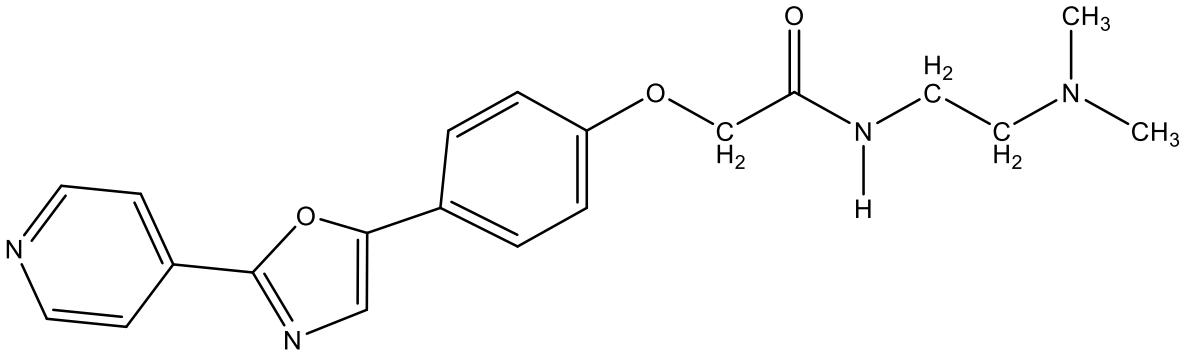

PDMPO has been widely used to study new silica deposition. Examples include: precipitation of silica in diatoms (Durkin, et al. 2012a, Hazelaar, et al. 2005), silica deposition in *Equisetum arvense* (Law and Exley 2011), observation of the skeletal growth patterns in *Polycystine radiolarians* (Law and Exley 2011) and identifying silica transporters in silicifying organisms (Ogane, et al. 2010) such as *Bolidophyceae* and *Parmale* (Ichinomiya, et al. 2011). There have been many attempts to develop probes for studying the molecular properties of silica using a variety of molecules include rhodamine B (Kucki and Fuhrmann-Lieker 2012), rhodamine 19 (Kucki and Fuhrmann-Lieker 2012), rhodamine 101 (Kucki and Fuhrmann-Lieker 2012), rhodamine 123 (Li, Chu and Lee 1989), bis(cyclopentadienyl) titanium dichloride (Perry, Moss and Williams 1990), and fluorescein coupled via 3-aminopropyl triethoxysilane (Hodson, et al. 1994) but these alternatives have a range of

problems such as low accumulation efficiency and insolubility in aqueous solution. PDMPO has proven to be a very effective tracer during biosilicification and has seen wide application in silica related studies.

PDMPO is an oxazole dye developed to study intracellular pH changes inside acidic organelles (Diwu, et al. 1999a). A further class of oxazole dyes derived from 2,5-diphenyloxazole are known to exhibit unique solvatochromic and electron transfer properties (Diwu, et al. 1997) These dyes are weakly basic amines that selectively accumulate in cellular compartments with low internal pH making them valuable tools to investigate the biosynthesis and pathogenesis of lysosomes (Hurwitz, et al. 1997). Oxazole dyes can freely permeate cell membranes and concentrate in acidic organelles and PDMPO has been used to study pH at high hydrostatic pressures (DePedro and Urayama 2009). Shimizu *et al* in 2014 first demonstrated a "silica-philic" fluorescence from PDMPO at 510 nm and noted its unique properties as a silica tracer (Shimizu, et al. 2001). Although PDMPO-silica interactions are being used by scientists (Shimizu, et al. 2001, Hazelaar, et al. 2005, Law and Exley 2011, Ogane, et al. 2010, Durkin, et al. 2012b, Ichinomiya, et al. 2010, Saxton, et al. 2012), there are gaps in our understanding. Specifically: the mechanism of the PDMPO-silica interaction is unknown; the spectroscopic details are unclear leading to difficulty selecting optimal excitation and emission wavelengths; the process creating "silica-philic" fluorescence in PDMPO is unknown and the location of PDMPO on silica is not known. While proposals have been made to use PDMPO to study silica polymerisation, experimental results to date were not specific enough to correlate PDMPO behaviour with the degree of silica oligomerization.

This study investigates the unique fluorescence of PDMPO in the presence of silica. We began by identifying the possible protonation states of PDMPO and estimated their pK_a's by

computational methods. We used these considerations to inform a set of experiments investigating the ground and excited state behaviour of PDMPO beginning in aqueous solutions, proceeding through a range of solvents, and finishing with silica materials (Stöber particles (50 nm)). These data provide a clear understanding of the silica dye interaction and provide a significant analytical framework for application of this technique in biology and chemistry.

3.2 Materials and Methods

3.2.1 Materials: PDMPO (LysoSensor™ yellow/blue DND-160, 1 mM in dimethylsulfoxide) was obtained from Life Technologies. Chemicals for preparation of citrate and phosphate buffers, ammonia solutions, tetraethoxysilane (TEOS), coumarin 153, tryptophan, HPLC grade water, were obtained from Sigma Aldrich. Other solvents (water, methanol, ethanol, acetone, acetonitrile, dimethylsulfoxide, chloroform) were purchased from Fisher Scientific. When required, solutions were prepared in HPLC grade water.

3.2.2 Predictive modelling of speciation: Predictive chemical modelling of the pH dependent chemical forms of PDMPO and the associated pK_a's was performed using the web version of SPARC (Hilal, Karickhoff and Carreira 1995). The SPARC computational approach is based on the combination of well-established structure activity relationships (J. E. Lemer and E.Grunwald 1965) linear free energy relationships (L. P. Hammett 1970) and perturbed molecular orbital theory (M. J. S. Dewar 1969) to estimate pK_a. The SPARC method of pK_a determination has been tested on 3685 compounds to estimate 4300 ionization pK_a's and their overall RMS deviation from measured values was 0.37 (Hilal, Karickhoff and Carreira 1995).

3.2.3 Absorbance spectroscopy: All spectroscopy experiments were carried out in 0.1 M phosphate at pH $\geq$ 5 and citrate pH $\leq$ 5 buffers with some experiments in the range pH 4-6 carried out in both buffers to ensure no effect of buffer identity on the fluorescence behaviour observed. To correct for small variations in concentration and some interference from DMSO the spectra were normalised relative to the isobestic point (352 nm) and analysis restricted to 250-450 nm. Absorption spectroscopy was carried out in a dual beam spectrometer (JASCO V-670) in 1 cm quartz cuvettes over a pH range 2.5-12.01 with all samples prepared in 0.1 M buffer with PDMPO added to give a concentration of 4.0×10^{-5} M.

3.2.4 Fitting pKas to spectroscopic data: The DATAN software tool developed by Kubista *et al*.,(Scarminio and Kubista 1993, Elbergali, Nygren and Kubista 1999) was used to calculate spectral profiles, concentrations and equilibrium constants by utilizing equilibrium expressions that are related to the components. In this study, all the recorded absorbance data and fluorescence data were assembled into data matrices and introduced to the DATAN programme (Elbergali, Nygren and Kubista 1999) to obtain pure spectra for the individual species, concentration profiles and acidity constants of the dye in absorbance and fluorescence modes.

3.2.5 Fluorescence spectroscopic properties of PDMPO: Fluorescence measurements were carried out in 96-well plates (Nunc Optical bottom plates (164588)) using a commercial microplate reader (M200 pro; Tecan). Corrected spectra were computed over the range 300-678 nm using standard methods (Lakowicz 2006) relative to tryptophan in water (300-428 nm with 400 nm excitation) and coumarin 153 in methanol (486-678 nm with 402 nm excitation) with interpolated values between 428 and 486 nm. The effect of acid/base on the fluorescence emission of protonated/ non-protonated states of the dye (1.0×10^{-7} M) was

studied in buffers with pH ranging from 2.3 to 14. The wavelength for excitation was chosen as 360 nm for maximum response which is close to the isobestic point (352 nm) of the $PDMPOH_2^{2+}$ to $PDMPOH^+$ transition of the dye.

3.2.6 Solvatochromic properties of PDMPO: The effect of solvent polarity on the fluorescence emission of the dye (1.0×10^{-7} M) was studied in protic solvents (water, ethanol, acetone), polar aprotic solvents (DMSO and acetonitrile), and non-polar solvents (chloroform) having a range of dielectric constants. A series of binary mixtures of ethanol and water (pH 7.0) and acetonitrile in water containing 0.1 μM PDMPO was used to measure its behaviour in protic solvents over a range of dielectric constants.

3.2.7 Fluorescence emission of PDMPO on silica: Silica nanoparticles (SNPs) were prepared using a modified Stöber process (Roach, Farrar and Perry 2006). Briefly, synthesis involved mixing two solutions (A and B) previously prepared with particle size adjusted by varying the concentration of ammonia in solution A. For 50 nm silica particles: solution A was prepared by taking 21.6 ml of 0.2 M ammonium hydroxide (NH_4OH) in distilled deionized water (ddH_2O) and adding ethanol to make up the volume to 80 ml in ethanol. Solution B was prepared by diluting 22.3 ml of TEOS in ethanol to 76.6 ml. Freshly prepared solutions were heated to 50°C, mixed then stirred at 4000 RPM for 2 hours at the same temperature before allowing them to mature at room temperature for 1 day. Ethanol was removed by rotary evaporation at 50°C, the sample centrifuged at 4000 RPM for 10 minutes and the particles washed with ethanol then distilled water and freeze dried.

Solutions containing the dye at 0.1 μM were prepared in 0.1 M buffers (pH 1.8 to 13.8). Silica nanoparticles (50 nm diameter, final concentration: 1mg/mL) were suspended in buffer

solutions, incubated for 30 minutes at 25°C on a plate shaker at 10 RPM before measuring changes in the fluorescence emission spectrum. An excitation wavelength of 360 nm was used to collect fluorescence emission spectra for all silica PDMPO interactions.

3.2.8 PDMPO-silica interactions: Experiments were conducted in 0.1 M buffer (pH 1.8 to 13.8) with PDMPO (0.1 μM) and silica particles (50 nm) at a nominal concentration of 1 mg/mL. Zeta potential and dynamic light scattering (DLS) measurements were carried out at 25°C. The hydrodynamic diameter (D_h) of Stöber particles in the presence and absence of PDMPO was calculated as an average of five independent measurements.

Concentration dependent effects of the dye were studied using a constant amount of SNP (50 nm diameter, 1mg/mL), varying the amount of dye present (0.1 μM to 800 μM). In a typical experiment (e.g. for 10 μM dye) 500 μg of SNP was added to 495 μL buffer (phosphate at pH ≥ 5 and citrate at pH ≤ 5), sonicated for 1 hour and 5 μL of 1.0 mM dye was added and shaken vigorously. Samples were left to equilibrate for 30 minutes at 25°C on a shaker at 10 RPM before performing zeta potential measurement followed immediately by fluorescence emission measurements.

The fluorescence anisotropy of the dye in combination with silica was measured using SNPs (50 nm diameter, 1mg/mL) in 0.1M Buffer (pH 1.8 to 14.0) with PDMPO (0.1 μM). Steady state anisotropies were measured using a Tecan F200 with excitation filter 360/35 nm and emission filter 540/35 nm. The PMT gain setting was 40 and the G factor 1.256.

3.2.9 pH dependent behaviour of PDMPO adsorbed on silica: Silica particles (50 nm diameter, 10mg/ ml) were used and pH measurements performed in buffer (0.1M) in the presence of 1 μM PDMPO. pH was measured before and after spectroscopic measurements.

As for other experiments, samples were left to equilibrate for 30 minutes at 25ºC on a shaker at 10 RPM. For fluorescence measurements the dye was excited at 360 nm.

3.2.10 Fitting peak positions and relative areas: Spectra were decomposed by least squares minimisation of a two component Gaussian model after conversion to wavenumber. Parameters fitted were: peak position (μ), peak width (σ), and scale (conversion factor to arbitrary fluorescence units).

3.3 Results

3.3.1 Computational speciation studies

To understand the effect of pH on the ground states of PDMPO, pK_as were estimated computationally to provide an interpretive framework for subsequent UV-vis spectroscopic studies. The possible species are represented in **Scheme 2.** Although convention gives that the first proton lost from a compound gives rise to pK_1, in this study we chose to omit the first two acidity constants from our discussions of the dye as they have no physical meaning in normal aqueous solutions. The SPARC computation predicted one neutral and four protonated states. Of these, three species are important above pH 1.2 (highlighted; **Scheme 2)**; these are $PDMPOH_2^{2+}$ (predicted pK_{a1} 4.87, protonation of the pyridine group and terminal amine), $PDMPOH^+$ (predicted pK_{a2} 6.78, protonation of terminal amine), and the neutral species, PDMPO.

3.3.2 Absorbance properties of PDMPO

The absorption spectra of PDMPO were measured in buffered solutions and normalised to an estimated isobestic point of 352 nm (**Figure 3.1.a**). DATAN analysis recovered only two of

the species predicted by SPARC (nominally $PDMPOH_2^{2+}$, $PDMPOH^+$) (**Figure 3.1.b**) with their concentrations and associated pK_a (**Figure 3.1.c**). The recovered pK_a (4.20) was in reasonable agreement with SPARC predictions (4.87) and previous reports (Diwu, et al. 1999b). The absence of a pK_a for $PDMPOH^+$/PDMPO indicated the absorption spectra are dominated by protonation of the pyridine group and the protonation state of the amine side chain has negligible effect. This was confirmed in the raw data (**Figure 3.1.d)** which showed no change in the absorbance at 331 nm above pH 6. This analysis left two species (**Figure 3.1.b)** with λ_{max} values at 382 nm ($\varepsilon = 3.84\times10^4$ M^{-1} cm^{-1}) and 331 nm ($\varepsilon = 1.67\times10^4$ M^{-1} cm^{-1}). Although protonation of the amine side chain has no role in the absorbance behaviour of the dye, it can affect the binding interaction of the dye with silica . For clarity, the recovered species with λ_{max} at 331 nm will be referred to as $PDMPOH^+$, however, at high pH significant amounts of the neutral species will be present. Attempts were made to determine the ground state pK_a of PDMPO in the presence of silica. These measurements were unfeasible due to the requirement for low concentrations of the dye and the high scattering of the nanoparticulate solutions.

Scheme 2

Chemical species identified by SPARC and their estimated pK_as. Highlighted species are important in aqueous solution; the others are destroyed by acid hydrolysis.

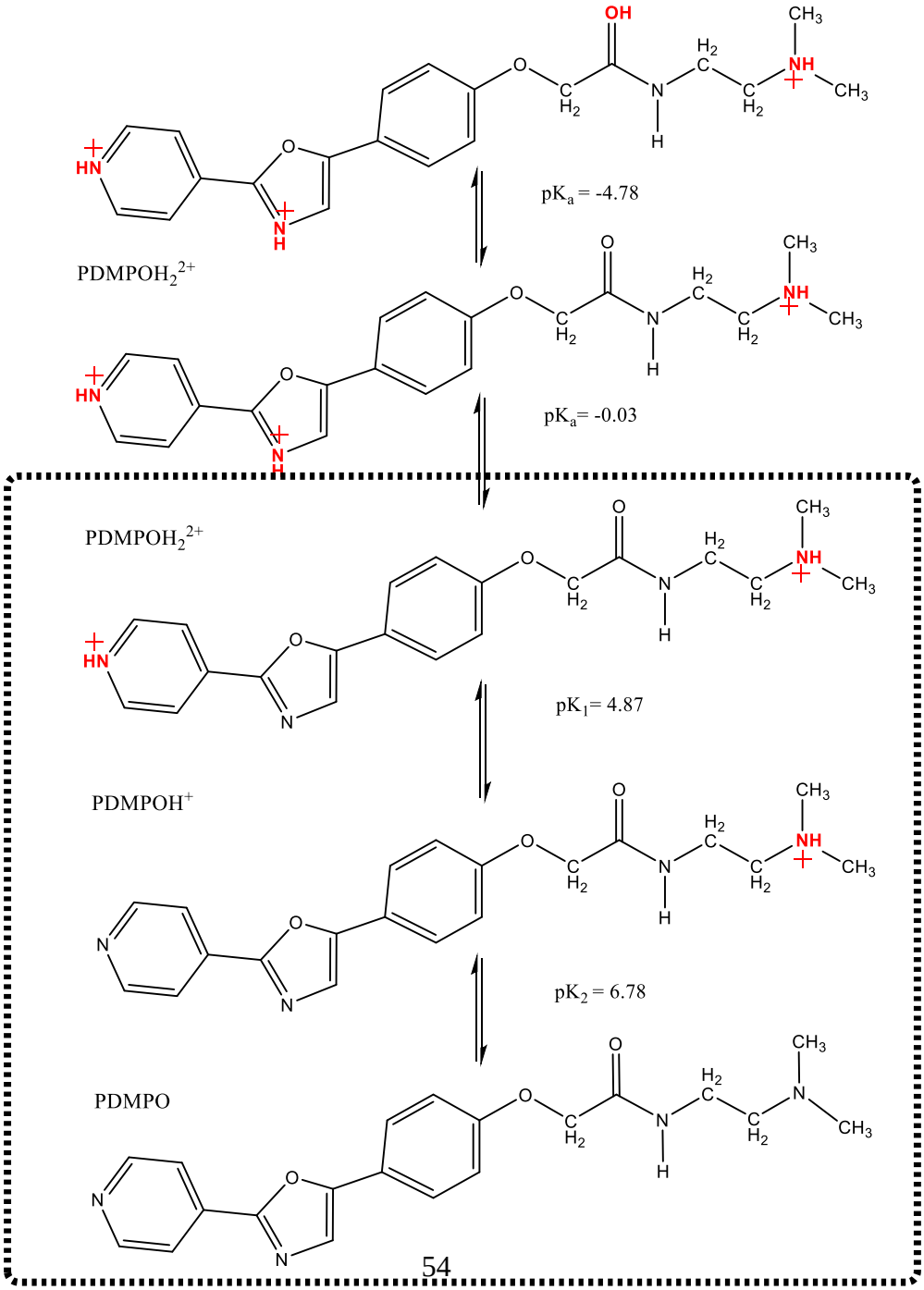

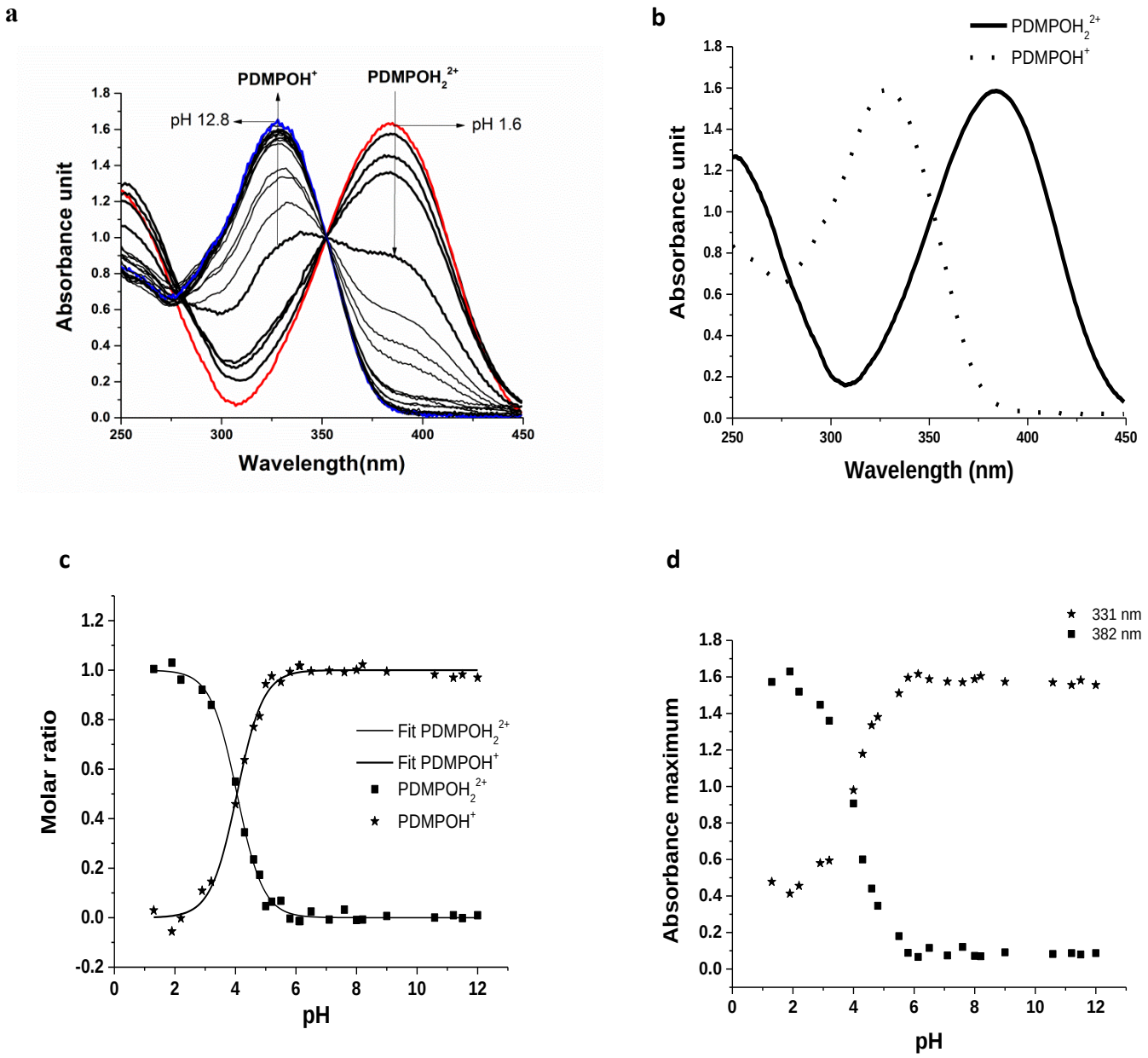

Figure 3.1: Absorption spectra of PDMPO (40 µM) in 0.1 M buffers: (a) spectra recorded over the range pH 1.6 to 12.8, red spectrum obtained from pH 1.6 buffer and blue spectrum obtained from pH 12.8 buffer (b) spectra of $PDMPOH_2^{2+}$ and $PDMPOH^+$ recovered by DATAN analysis; (c) calculated mole ratio of $PDMPOH_2^{2+}$ and $PDMPOH^+$ compared to those predicted by the resulting K_a; (d) absorbance at 331 nm (nominally $PDMPOH^+$) and 382 nm ($PDMPOH_2^{2+}$) above pH 6 there is no change in absorbance at 331 nm.

3.3.3 Fluorescence spectroscopic properties of PDMPO in aqueous solutions

Emission spectra of PDMPO in buffered aqueous solutions revealed pH dependent behaviour (**Figure 3.2.a**) with two distinct peaks over the pH range studied. DATAN analysis of the spectra (**Figures 3.2.b and 3.2.c**) suggested 3 forms with estimated excited state pK_a^*s of 4.2 and 13.7. The ground state pK_{a1} and first excited state pK_a^* appear to be the same (4.20) however, work with similar dyes in this class[26] indicates they undergo excited state proton transfer from water to $PDMPOH^{+*}$. The "species" dominating between 4.2 and 13.7 (**Figure 3.2.c**) is a rate determined mixture of the protonated and deprotonated pyridine forms with a yield dependent on $[H_2O]$. As the pH approaches pK_w, the concentration of water decreases significantly due to formation of hydroxide ion and proton transfer becomes less favourable. The second recovered pK_a^* (13.7) is within experimental uncertainty of pK_w leaving the actual pK_a^* ($PDMPOH_2^{2+*}$/ $PDMPOH^{+*}$) unobservable more than 9.5 pK_a units away from the corresponding ground states. Similar to the absorbance behaviour, there was no evidence the ammonium group on the side chain influences the excited state and the recovered species with a peak at 454 nm will be referred to as $PDMPOH^{+*}$. This analysis leaves two excited state forms, $PDMPOH_2^{2+*}$ (protonated pyridine group; $\lambda_{max,em}$ = 544 nm) and $PDMPOH^{+*}$(neutral pyridine group; $\lambda_{max,em}$ = 454 nm), which exists in three pH regions: i) pH < 4.2 (dominated by $PDMPOH_2^{2+*}$); pH 4.2-13.7 ($PDMPOH^{+*}$ and $PDMPOH_2^{2+*}$ in a kinetically defined ratio); and pH >13.7 (dominated by $PDMPOH^{+*}$) (**Scheme 2**). The reasons for the slight blue shift in the emission maxima between pH 4.2 and 13.7 are unclear. we ascribe to pKw rather than the actual ($PDMPOH_2^{2+*}$/ $PDMPOH^{+*}$) which is unobservable.

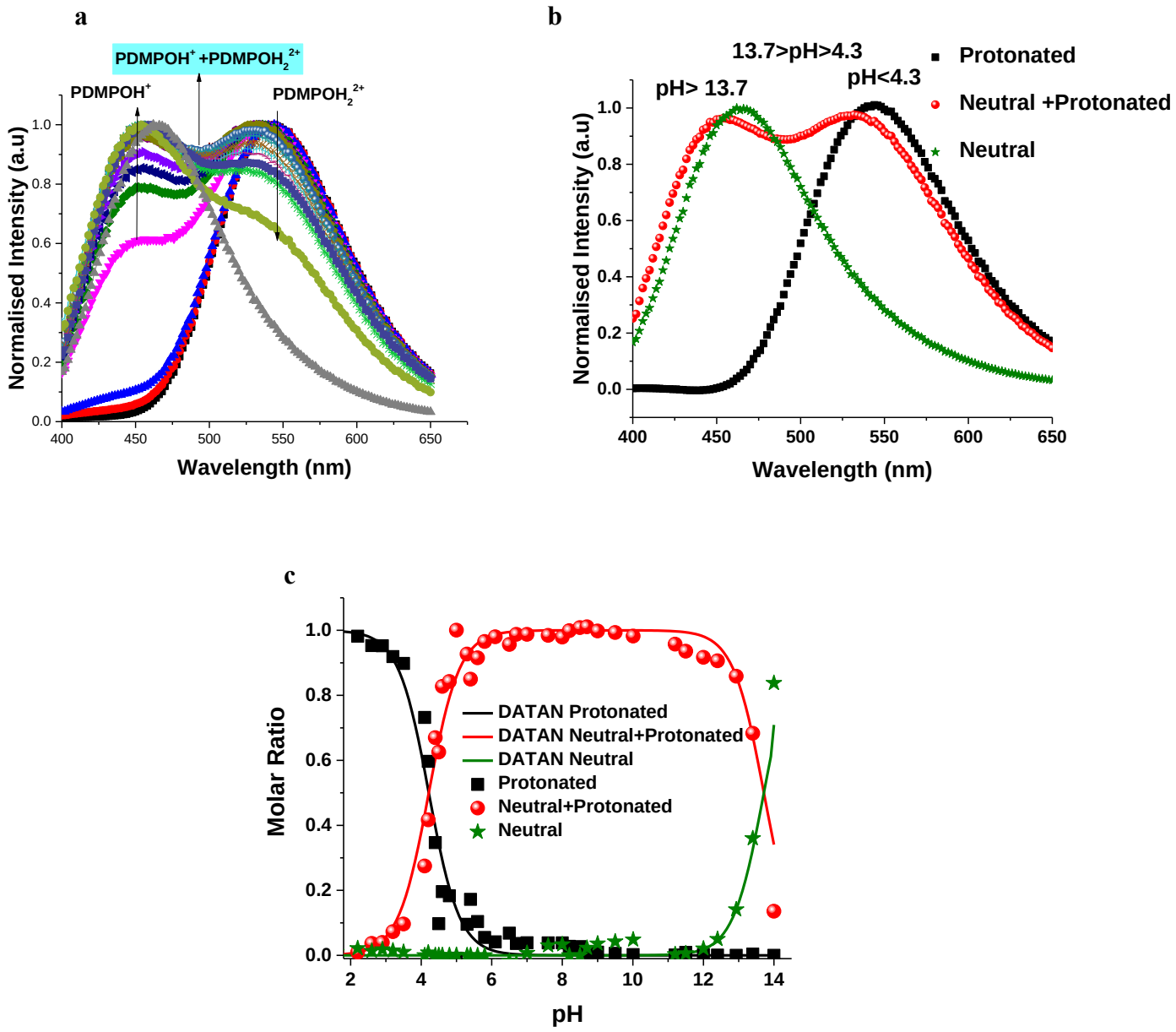

Figure 3.2: (a) Fluorescence emission of PDMPO from pH 2.3 to 14.0 using 360 nm excitation (b) Spectra recovered from DATAN analysis suggested two forms, $PDMPOH_2^{2+*}$ and $PDMPOH^{+*}$ with the behaviour between pH 4.2 and 13.7 due to excited state dynamics in the presence of water (see text for details) (c) Calculated molar ratios returned by DATAN suggest two pK_a^*s (4.2 and 13.7). The first of these corresponds to the point where ground state $PDMPOH^+$ first appears while the second, pK_w, masks pK_{a1}^* which is at least 9.5 pK_a units greater than pK_{a1} (see text for details).

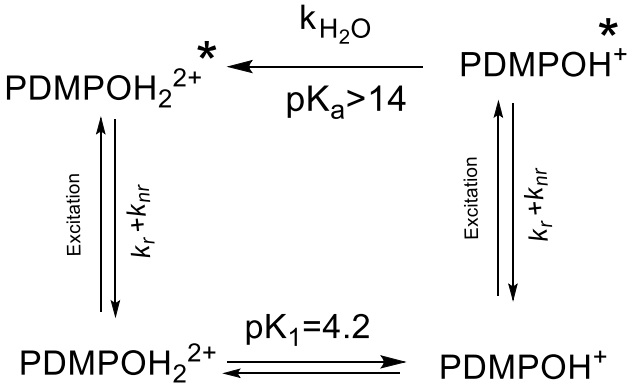

Scheme 3: Excited state behaviour of $PDMPOH_2^{2+}$* and $PDMPOH^{+*}$ in aqueous solution. Excitation of $PDMPOH^+$ leads to competition for $PDMPOH^{+}$* between extraction of a proton from water (represented by k_{H2O}) and direct deactivation of the excited state (represented by the sum of the radiative (k_r) and non-radiative (k_{nr}) rate constants). The mixed form (pH 4.2 to 13.7) results from competition kinetics between direct return to ground state $PDMPOH^+$ and excited state proton transfer from water to $PDMPOH^{+*}$ forming $PDMPOH_2^{2+*}$ followed by return to the ground state. A constant ratio is observed due to a constant value for $k_{H2O}[H_2O]$.

To estimate pK_a^*s ($PDMPOH_2^{2+*}$/ $PDMPOH^{+*}$) we applied the Förster equation (Lakowicz, 2006) which gave a value of 12.6. We believe our pH dependent spectroscopic determination is more definitive and better matches the expectations from work on similar molecules (Charier, et al. 2006) response which also found near 14.

3.3.4 PDMPO fluorescence in the presence of silica

In contrast to aqueous phase fluorescence, DATAN analysis of PDMPO (**Figure 3.3 a-c**) in the presence of 50 nm silica particles retrieved similar spectroscopic species (**Figure 3.3.a**) but with a single pK_a (10.4) (**Figure 3.3.b and 3.3.c**) which we ascribe to pK_{a1}^*. The photoinduced proton transfer observed without silica particles is absent indicating the excited

states do not have access to water in this environment. However, the spectra of both $PDMPOH_2^{2+*}$ and $PDMPOH^{+*}$ forms exhibit a marked pH dependent silica mediated chromaticity (**Figure 3.3.a**). The protonated pyridinium form ($PDMPOH_2^{2+*}$; $\lambda_{max,em}$ >500 nm) undergoes a blue shift as pH is increased up to pH ca. 9.3. The neutral pyridinium form ($PDMPOH^{+*}$; $\lambda_{max,em}$ < 460 nm) undergoes a red shift as pH is increased from ca. 9.7 to 14.

Further insight into the PDMPO-silica interaction was obtained by measuring the fluorescence anisotropy of PDMPO on silica particles from pH 2-14 (**Figure 3.3.d**). From pH 2.6-5.2, fluorescence anisotropy increases consistent with the ground state pK_{a1} (4.2). It reaches a plateau between pH 5.2 and 8.2 indicating rotational diffusion more consistent with a larger particle. Above 8.2, the anisotropy decreases but remains slightly above that of the free dye up to pH 14. This high pH transition on silica is consistent with the work of Ong *et al* (Ong, Zhao and Eisenthal 1992) who observed a high pH species using second harmonic generation methods. These data imply that at the high and low pH regimes there is single point binding of PDMPO via the side chain amine group giving the fluorogenic portion of the molecule the ability to undergo rotational diffusion. At intermediate pH the pyridine group is protonated and a transition to two point binding on the silica surface occurs resulting in hindered rotation. Under the experimental conditions used there is no evidence (**Figure 3.3c**) that PDMPO is released from the surface, as there is no sign of the kinetically defined intermediate forms observed in aqueous solution (**Figure 3.2c**).

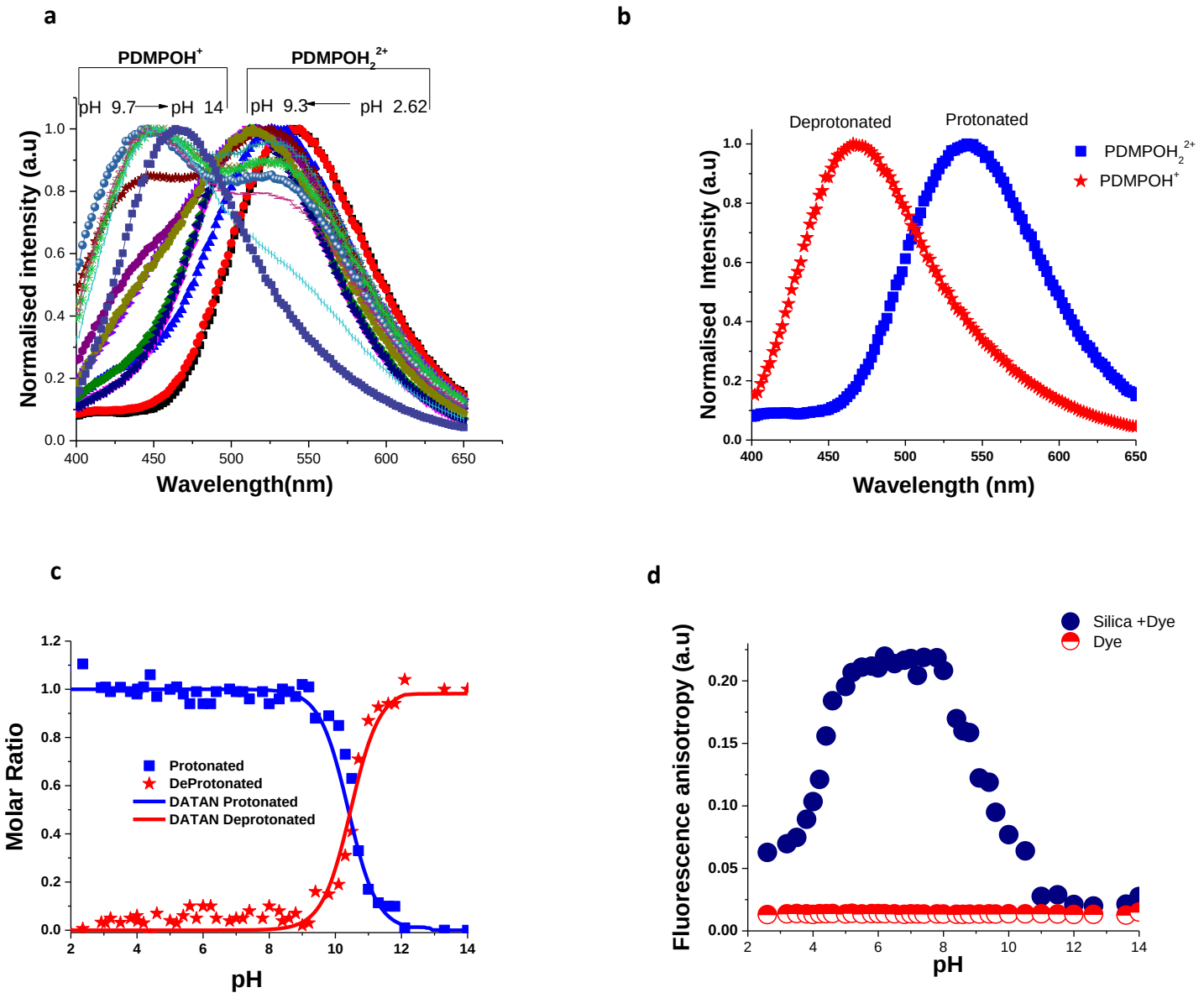

Figure 3.3: PDMPO fluorescence over the range pH 2.6 to 14.0 in the presence of 50 nm silica particles with excitation at 360 nm: (a) fluorescence emission spectra of PDMPO in the presence of silica; (b) calculated pure fluorescence spectra of $PDMPOH_2^{2+*}$ and $PDMPOH^{+*}$ in the presence of silica from DATAN; (c) calculated molar ratio (recovered pK_{a1}^{*} = 10.4); (d) pH dependent fluorescence anisotropy of PDMPO in the presence and absence of 50 nm silica particles.

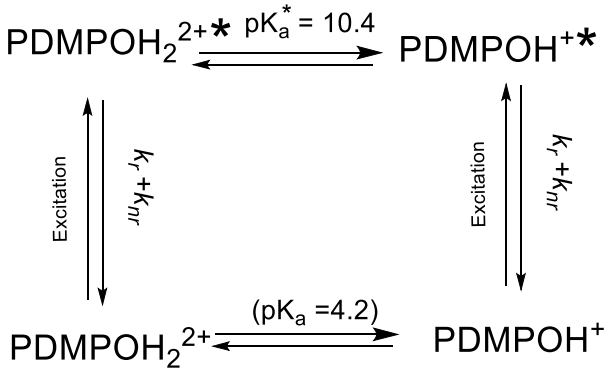

Scheme 4: Excited state behaviour of PDMPO in the presence of silica. In the presence of silica, the excited state pK_a^* is clearly visible and there is no evidence for excited state proton transfer from water. The ground state pK_a in the figure estimated at (4.2) is assumed from the behaviour in the absence of SNPs.

To further understand PDMPO interactions with 50 nm diameter silica nanoparticles, the surface charge (ζ) and hydrodynamic diameter (D_h) of the particles were measured before and after interaction with the 0.1 μM PDMPO (over a wide range of pH (1.0-12.0)) (**Figure 3.4.a, 3.4.b)**. The hydrodynamic diameter of the silica particles did not change significantly following interaction/adsorption of PDMPO over the pH range studied (**Figure 3.4.a)** implying that the dye does not extend beyond the Stern layer of the silica nanoparticles. Addition of PDMPO did result in partial neutralization of the particles between pH 4.0 and 9.5. This region coincides with the high anisotropy region suggesting that the first point of attachment via the amine residue is to both neutral silanol and siloxide groups while the second point of attachment via protonated pyridine brings a charge into the Stern-layer.

Further, PDMPO was added to 50 nm silica particles at neutral pH at a concentration of 1 mg/mL and the concentration of PDMPO adjusted over the range 0.1 to 800 μM (**Figure 3.4.c**). Increasing the PDMPO concentration resulted in the appearance of fluorescence consistent with aqueous PDMPO (unbound) and saturation of ζ. This indicates that when

PDMPO fluorescence is used with silica the concentration should be as low as possible (0.1-5 μM) to maximise silicaphilic emission and minimize neutralization of the charge on the silica particles. Under ideal conditions, the amount of PDMPO should be ≤ 10% of the quantity required for full monolayer formation.

.

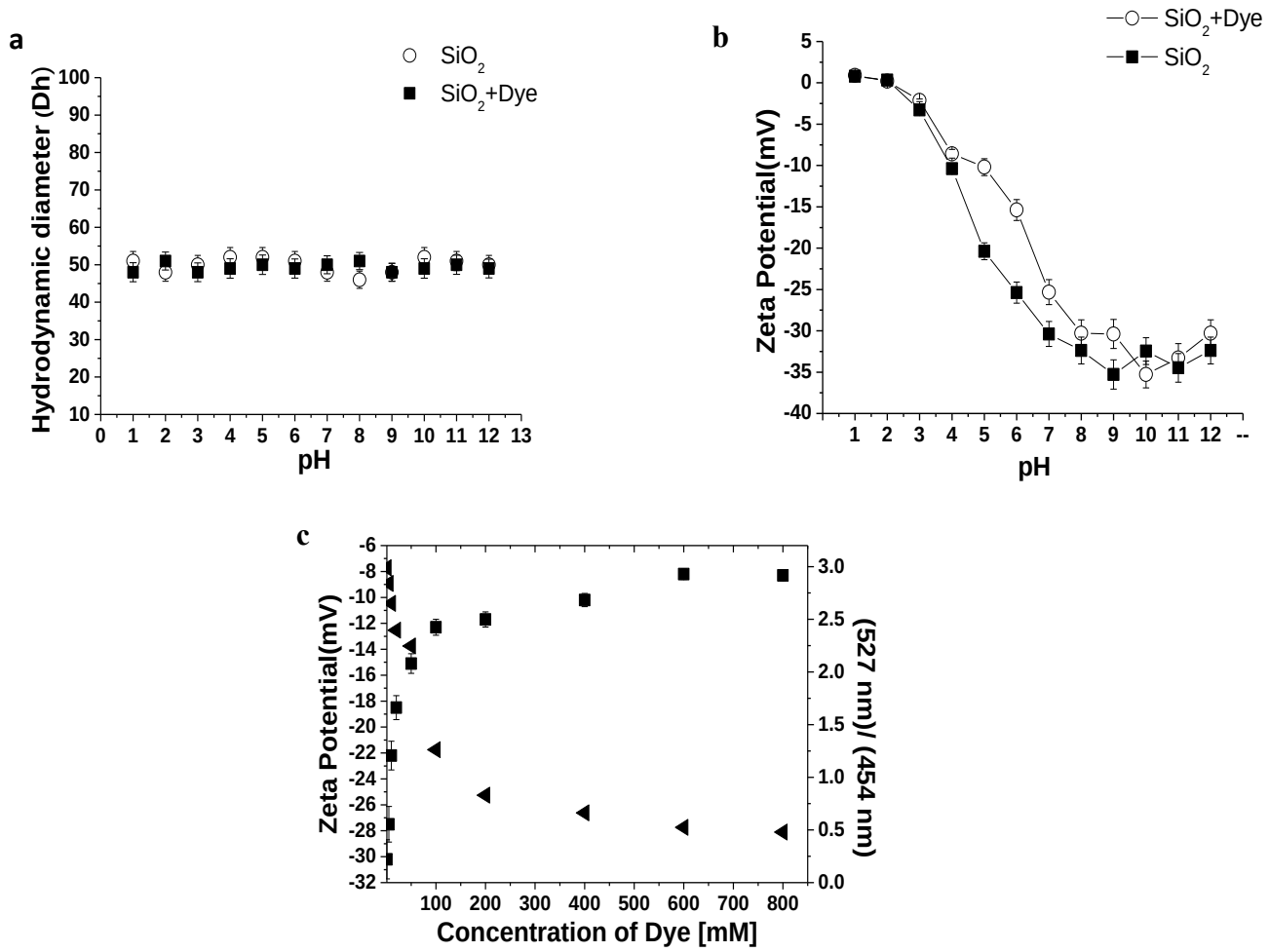

Figure 3.4: (a) Effect of pH on the hydrodynamic diameter (D_h) of Stöber particles with and without addition of PDMPO. (b) Effect of silica PDMPO interactions on zeta potential in the pH range 1.0 to 12.0 (c) Dose dependent decrease in emission ratio 527 nm/454 nm upon dye saturation on SNP surface (50 nm) (■) and dose dependent decrease in zeta potential with increase in PDMPO concentration at pH 7.02 for SNP of diameter 50 nm and concentration 1mg/mL (◄). The zeta potential of the silica (50 nm) alone was -30 mV

3.3.5 Solvent Effects on PDMPO fluorescence

Although the spectra recovered by DATAN on silica and in the aqueous phase were nearly identical, there are pH dependent shifts in $\lambda_{max,em}$ of the two key forms of PDMPO on silica. These were most noticeable at low and intermediate pH. To understand this behaviour, PDMPO was studied in a range of solvents and solvent mixtures (**Figure 3.5**). PDMPO exhibited positive solvatochromism with the position of the neutral peak shifting over the range from 418 nm (chloroform, ε_r = 4.8) to 454 nm (water, ε_r = 80.7) (**Figure 3.5.a**). The position of the peak gives an estimate of the local dielectric constant (**Figure 3.5.b**) which when applied to 50 nm silica particles suggests the dielectric constant within the Stern layer surrounding the particles is close to that of water.

Measurement of the spectroscopic response in water-acetonitrile and water-ethanol mixtures allowed us to assess the effects of dielectric constant on the form having a positively charged pyridine group and the distribution of neutral and positively charged pyridine forms as the availability of protons from water decreases. The yield of the neutral $PDMPOH^{+*}$ forms increased as the percentage of water decreased, even at pH 3.0. These data confirm the interpretation presented in Scheme 3 and indicate that PDMPO is more sensitive to solvent than other fluorescent probes (Loving, Sainlos and Imperiali 2010) .

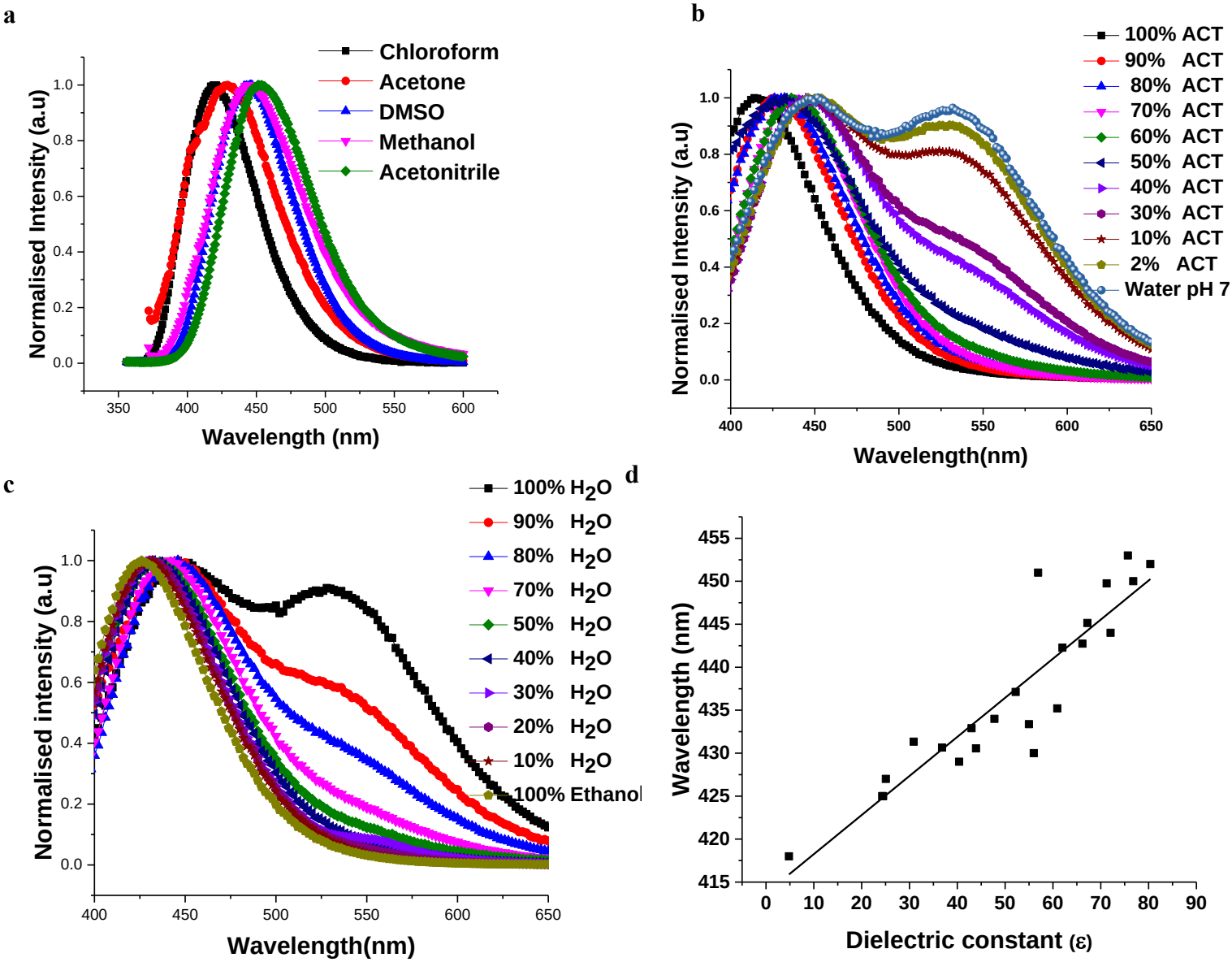

Figure 3.5: PDMPO Solvatochromism: (a) corrected emission spectra of neutral PDMPO in chloroform, acetone, DMSO, methanol and acetonitrile. Solvatochromism of PDMPO as the composition of solvent varied from 0 to 100% (v/v) for acetonitrile (b) and ethanol (c) and peak position with solution dielectric constant for these solutions (d).

3.3.6 Indirect determination of pH using PDMPO-silica interactions.

The data in **Figure 3.3.a and 3.3c** suggest that below pH 8 PDMPO fluorescence cannot be used to monitor pH in the presence of silica as there is no applicable pK_a^*. However, chromatic and ratiometric indicators (**Figure 3.6**) show strong correlation with bulk pH in the presence of silica particles suspended in solution over the pH range 3-13. The silica mediated shifts in PDMPO fluorescence emission maxima (**Figure 3.6.a**) arising from pH we ascribe to changes in dielectric constant at the silica surface. This makes PDMPO chromaticity a proxy for bulk pH which extends the range over which this dye can sensibly be used to monitor pH (**Figure 3.6**). The chromatic effects mask changes in the emission ratio during DATAN analysis (**Figure 3.6.b**). There is a continuous change in the ratio of the two forms over the entire range studied. At the lowest pH, the basic form is not present and the ratio is affected by the Raman band of water which appears near the most shifted wavelengths for the basic form of the dye. Above pH 3-4 (the most useful pH's for silica studies) the behaviour of the ratio of the two forms appears to be mediated by silica in a way that affects both the ground and excited state. The dye alone shows more typical pH dependent behaviour with rapid changes consistent with the ground state pK_a (4.2). As the pH increases, the ratio for the free dye is nearly constant until pK_w is approached. The region is not seen in the silica bound dye. The free and silica bound forms coincide above pH 11. There is short plateau near pH 10 for the silica bound dye which is believed to be due to the excited state pK_a. Sigma values from $PDMPOH^+$ and wavelength shift for $PDMPOH_2^{2+}$ can also be used as a rough pH indicators (Supplementary information). PDMPO is thus a unique molecule for interrogating pH and surface behaviour in the presence of silica. This response extends well beyond the range expected based on pK_as in the absence of chromaticity.

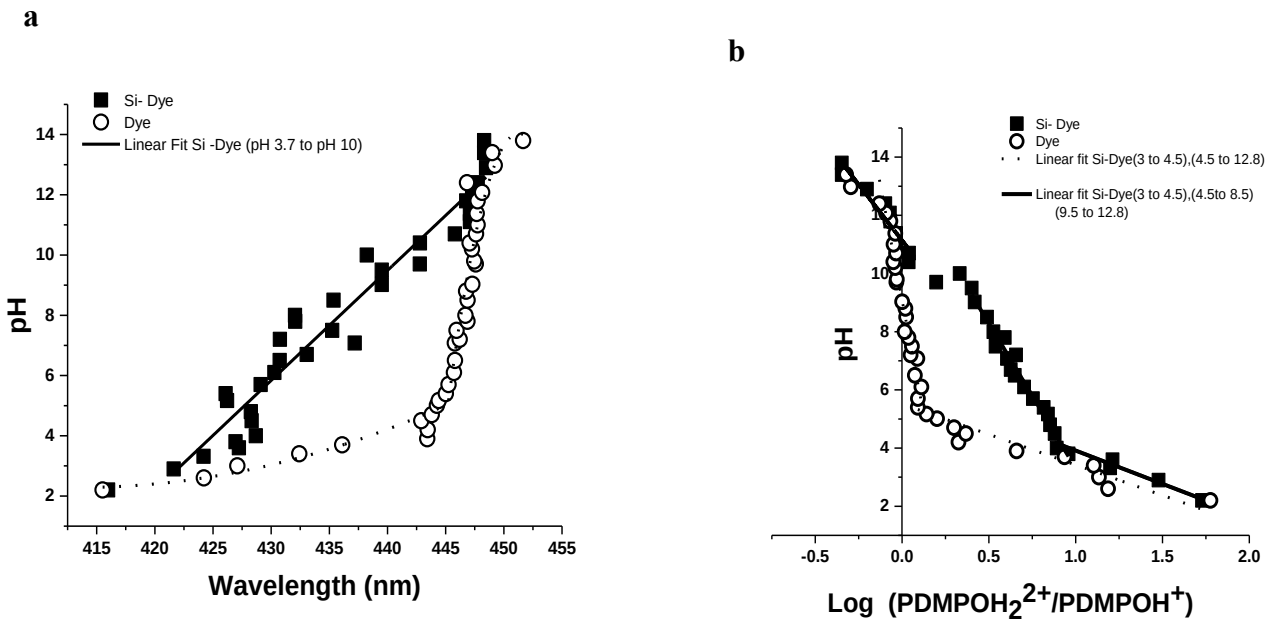

Figure 3.6: Chromatic and ratiometric effects of pH on PDMPO in the presence (■) and absence (○) of silica nanoparticles: (a) chromatic shift in $PDMPOH^{+*}$ in the presence of silica allows estimation of pH and (b) ratiometric (log ($PDMPOH_2^{+2*}$/$PDMPOH^{+*}$) estimation of pH in the presence of silica. Solid lines indicate useful regions for estimation of pH. Dotted lines are to guide the eye.

3.4 Discussion and Conclusions:

3.4.1 Nature of PDMPO absorbance and fluorescence

PDMPO is a probably the most common fluorescent dye used today to monitor silica deposition during biomineralization and track the movement of lysosomes inside living cells. Nonetheless, the spectroscopic properties of the dye have been poorly understood until now. This study represents a significant advance in our understanding of both the aqueous and the silicaphilic fluorescence of PDMPO. The behaviour of PDMPO is similar to that of the

fluorescent dyes 4 PYPO, 4-PYMPO, 4-PYMPOM, 2-PYMPO, 2-QUIMPO, 2- PYMPO-CO_2Me, and 2-PYMPO-CH_2OH.(Charier, et al. 2006) Photophysical properties of PDMPO most closely resemble that of the 4-PYMPO series, with pK_{a1} 4.2 and 4.3 for PDMPO (current study) and PYMPO respectively.(Charier, et al. 2006) We have shown for the first time that the fluorescence behaviour of the dye in aqueous solution above pH 4.2 involves photoinduced proton transfer from water to PDMPO which is disrupted when PDMPO binds to silica. While photoinduced proton transfer has been reported in the 4-PYMPO series of dyes, the disruption of this proton transfer by silica particles in aqueous solution has not. The extensive chromaticity of PDMPO in the presence and absence of silica has not been previously documented nor has this been used previously as a proxy for bulk solution pH over the pH range 3-13. Similar chromaticity and/or disruption of photoinduced proton transfer in the presence of silica has not been reported for 4-PYMPO and related dyes, however, many will exhibit similar behaviour and screening related compounds for desirable silicaphilic fluorescence is likely to be fruitful.

3.4.2 What is the nature of the silicaphilic behaviour of PDMPO?

In the presence of silica, pK^*_{a1} shifts 6.2 pK_a units and the photoinduced proton transfer observed in aqueous solution is disrupted. This indicates stabilisation of $PDMPOH^+$ through interaction with the silica surface and the absence of reactive water within its 'local' environment suggesting PDMPO does not extend beyond the Stern layer. PDMPO does not change the hydrodynamic diameter of the particles at any pH giving further evidence PDMPO is located within the Stern layer. This provides a model (**Figure. 3.7**) similar to ones arising from experiments investigating the interaction of cationic particles with large unilamellar vesicles (LUV) (de Sousa Neto, Hawe and Tabak 2013). Since the silicaphilic response of the dye reports on the surface of the silica particles themselves, the concentration

of the dye is critical. We suggest that dye concentrations be less than 10% of surface coverage to minimise fluorescence emission from the bulk solution.

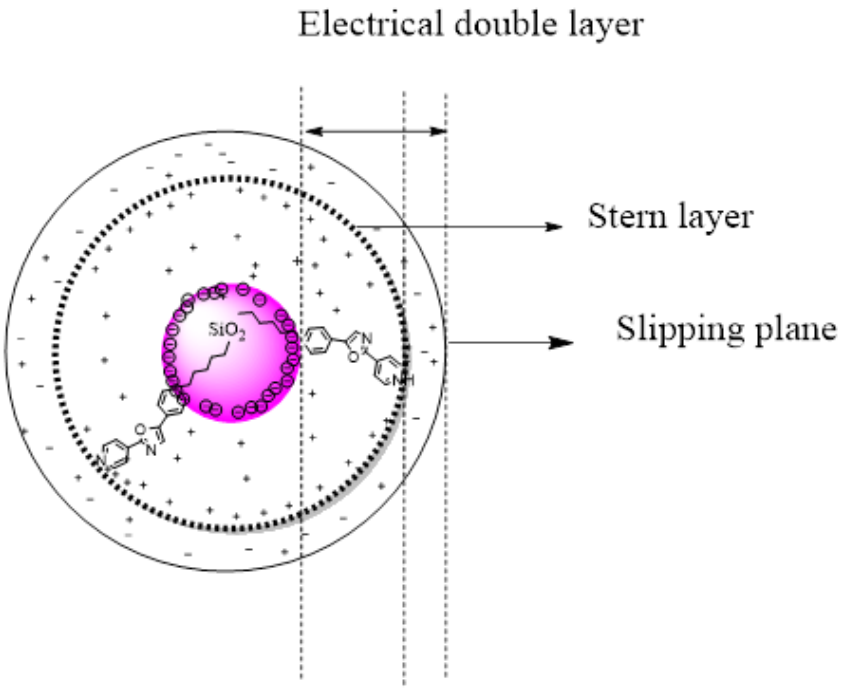

Figure 3.7: Preferential location of PDMPO in the Stern layer

Data from the (**Figure 3.2.b**) is interesting, we have observed a blue shift. This blue shift can be understood using Lippert Mataga equations which demonstrate the change can be due to the perturbations to the structure in the solvent shell. However, interpretation in this way requires abrupt step changes to the solvent and structure around pKa1 and pKa* which is what we observe, but this is physically unrealistic. In general, solvatochromism is understood using the Lippert Mataga equation (eqn 3.1)(Mataga 1956)

$$\bar{\nu}_A - \bar{\nu}_F = \frac{2}{hc}\left(\left(\frac{\varepsilon-1}{2\varepsilon+1}\right) - \left(\frac{n^2-1}{2n^2+1}\right)\right)\left(\frac{(\mu_E-\mu_G)^2}{a^3}\right) \qquad \text{(eqn 3.1)}$$

The principal factors which affect whether a blue shift or a red shift are observed are the dielectric constant of the solution (ε), the refractive index of the solvent(s) (n), the radius of the cavity where the fluorophore resides (a), the ground (μ_G) and excited (μ_E) state dipole moments and where $\bar{\nu}_A - \bar{\nu}_F$ is the energy difference between the ground state and the excited state.

The issue is that in our interpretation, there should be no difference between the species in isolation (less than pH 4.3 and greater than pH 13.7) and when mixed at intermediate pH (pH 4.3 – 13.7). A slight blue shift is observed for the mixture. We wouldn't anticipate step changes to arise from a combination of refractive index, dielectric constant, dipole moments, and cavity radius at pH 4.3 to lead to a chromatic shift that remains constant until 13.7 when a step change in the reverse direction occurs. A relaxation effect associated with proton transfer is likely but we do not think we have sufficient evidence to prove this is the case as opposed to some limitation in the quality of the data or the analysis.

3.4.3 How does the dye bind to silica?

The silicaphilic behaviour of PDMPO gives considerable insight into PDMPO-silica interactions. The fluorescence anisotropy data suggest that at all pH values below ca. 12 the molecule is attached to the surface via either single point (low anisotropy) or multipoint modes (high anisotropy). Studies of electrostatically vs tethered covalently bound dyes have shown the importance of electrostatic interactions in influencing the anisotropy of fluorophores on the silica surface (Yip et al 2012). Our results confirm this while also making clear the role of pH in influencing the charge states of the silica-dye that control this interaction. We observed increases in the fluorescence anisotropy of PDMPO on silica above the pKa1 which can only be explained by a change in the interaction resulting in more restrictive binding. We rationalise this with a two point binding model of PDMPO on silica (**Figure 3.8**) PDMPO is able to partially neutralize the surface charge of silica particles but only within a specific pH range (4.0-9.5) and this range coincides with the region of high fluorescence anisotropy. This indicates the pyridinium form is stabilised by interaction with negatively charged silica resulting in a proton being taken from the bulk solution. This proton

is shared between a siloxide group and the pyridinium moiety on PDMPO leading to 2 point binding of PDMPO, loss of rotational diffusion (high anisotropy), and partial neutralisation of the silica surface. These considerations suggest a model for pH dependent binding of PDMPO (**Fig 3.8**). All the data reported here were taken at pH values above the point of zero charge for silica (ca. 2) and therefore all silica samples carry silanol and siloxide groups with their relative proportions changing with pH. In all cases, adsorption of the dye can be attributed to electrostatic interaction mediated by protons between negatively charged silica surfaces and the dye. As the dye is held in close proximity to the silica surface, it is highly sensitive to pH dependent changes in local dielectric constant which gives rise to the observed shifts in emission maxima.

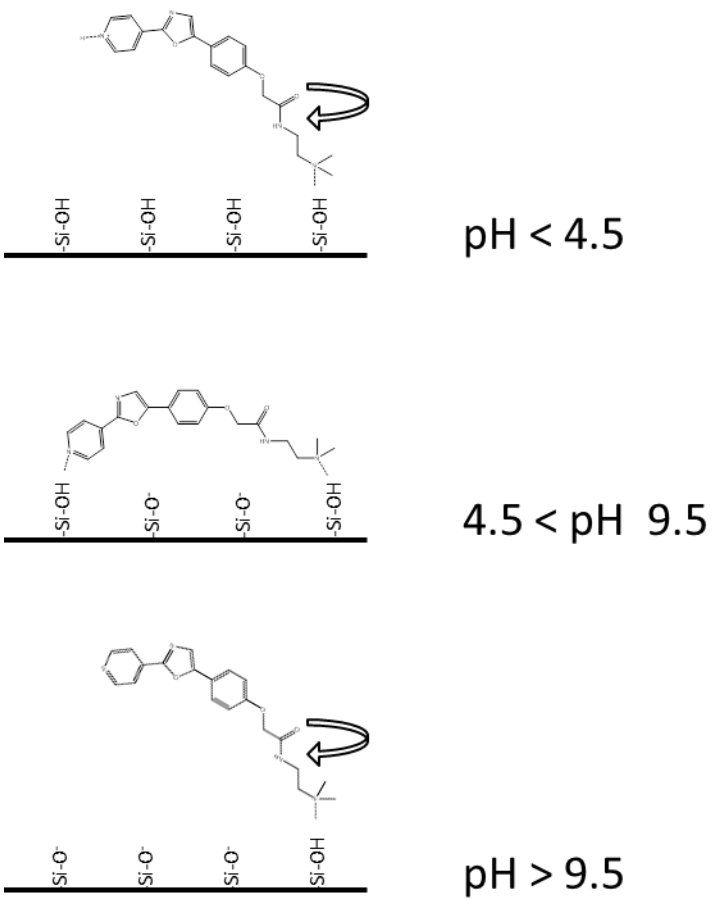

Figure 3.8 pH dependent binding of PDMPO on silica surface the arrow represents depolarising motion.

3.4.4 PDMPO-silica interactions: an indirect measure of solution pH

The data presented in **Fig 3.6** show that PDMPO interacting with silica can be used as a probe of bulk pH over a wide pH range (ca. 3-13). However, the relevant ground and excited state pK_as (4.2 and 10.4) are insufficient to cover such a wide range of pH. Outside of these regions, the chromatic behaviour serves as a proxy for pH. It is clear that the presence of silica is critical and the data show that there is a relationship between pH and local dielectric constant when silica is present. Unpicking the various contributions to the observed behaviour remains to be done.

3.4.5 Future work and application of PDMPO-Silica interactions

PDMPO has been widely used in vivo to study new silica deposition. Examples include: precipitation of silica in diatoms silica deposition in *Equisetum arvense* identifying silica transporters in silicifying organisms such as *Bolidophyceae* and Parmales. The more detailed understanding provided by the current study opens up many new applications. The ability to directly report on pH within biological organelles over an unprecedented range with a single dye will allow us to monitor the formation of silica more effectively, both in vitro and in vivoA more detailed understanding of the behaviour of PDMPO and its interaction with silica opens up many new applications. The ability to directly report on pH within biological organelles over an unprecedented range with a single dye will allow us to monitor the formation of silica, both *in vitro* and *in vivo*. This will extend our knowledge of the fundamentals of silica formation in the laboratory and in organisms, such as diatoms, where it has never before been possible to follow silica formation in the silica deposition vesicle. It will also allow us to probe individual silica structures within composites of mixed silica structures produced by silicifying organisms including single celled organisms such as diatoms and multicellular plants and animals such as sponges. PDMPO may also be used more widely to quantitatively investigate biophysical interactions of silica at solid liquid interfaces, colloid stabilization, the assembly of silica thin films and to study electrostatic interactions between polyelectrolytes on thin films made of silica.

3.5 References

Charier, S., Ruel, O., Baudin, J.B., Alcor, D., Allemand, J.F., Meglio, A., Jullien, L. and Valeur, B., 2006. Photophysics of a series of efficient fluorescent pH probes for dual-emission-wavelength measurements in aqueous solutions. *Chemistry-a European Journal,* 12 (4), 1097-1113.

de Sousa Neto, D., Hawe, A. and Tabak, M., 2013. Interaction of meso-tetrakis (4-N-methylpyridyl) porphyrin in its free base and as a Zn(II) derivative with large unilamellar phospholipid vesicles. *European Biophysics Journal with Biophysics Letters,* 42 (4), 267-279.

DePedro, H.M., and Urayama, P., 2009. Using LysoSensor Yellow/Blue DND-160 to sense acidic pH under high hydrostatic pressures. *Analytical Biochemistry,* 384 (2), 359-361.

Diwu, Z., Lu, Y.X., Zhang, C.L., Klaubert, D.H. and Haugland, R.P., 1997. Fluorescent molecular probes .2. The synthesis, spectral properties and use of fluorescent solvatochromic Dapoxyl(TM) dyes. *Photochemistry and Photobiology,* 66 (4), 424-431.

Diwu, Z.J., Chen, C.S., Zhang, C.L., Klaubert, D.H. and Haugland, R.P., 1999a. A novel acidotropic pH indicator and its potential application in labeling acidic organelles of live cells. *Chemistry & Biology,* 6 (7), 411-418.

Diwu, Z.J., Chen, C.S., Zhang, C.L., Klaubert, D.H. and Haugland, R.P., 1999b. A novel acidotropic pH indicator and its potential application in labeling acidic organelles of live cells. *Chemistry & Biology,* 6 (7), 411-418.

Durkin, C.A., Marchetti, A., Bender, S.J., Truong, T., Morales, R., Mock, T. and Armbrust, E.V., 2012a. Frustule-related gene transcription and the influence of diatom community composition on silica precipitation in an iron-limited environment. *Limnology and Oceanography,* 57 (6), 1619-1633.

Durkin, C.A., Marchetti, A., Bender, S.J., Truong, T., Morales, R., Mock, T. and Armbrust, E.V., 2012b. Frustule-related gene transcription and the influence of diatom community composition on silica precipitation in an iron-limited environment. *Limnology and Oceanography,* 57 (6), 1619-1633.

Elbergali, A., Nygren, J. and Kubista, M., 1999. An automated procedure to predict the number of components in spectroscopic data. *Analytica Chimica Acta,* 379 (1-2), 143-158.

Hazelaar, S., van der Strate, H.J., Gieskes, W.W.C. and Vrieling, E.G., 2005. Monitoring rapid valve formation in the pennate diatom Navicula salinarum (Bacillariophyceae). *Journal of Phycology,* 41 (2), 354-358.

Hilal, S.H., Karickhoff, S.W. and Carreira, L.A., 1995. A rigorous test for SPARC's chemical reactivity models: Estimation of more than 4300 ionization pK(a)s. *Quantitative Structure-Activity Relationships,* 14 (4).

Hodson, M.J., Smith, R.J., Vanblaaderen, A., Crafton, T. and Oneill, C.H., 1994. Detecting Plant Silica Fibers in Animal Tissue by Confocal Fluorescence Microscopy. *Annals of Occupational Hygiene,* 38 (2), 149-160.

Hurwitz, S., Terashima, M., Mizunuma, N. and Slapak, C., 1997. Vesicular anthracycline accumulation in Doxorubicin-selected U-937 cells: Participation of lysosomes. *Blood,* 89 (10), 3745-3754.

Ichinomiya, M., Gomi, Y., Nakamachi, M., Ota, T. and Kobari, T., 2010. Temporal patterns in silica deposition among siliceous plankton during the spring bloom in the Oyashio region. *Deep-Sea Research Part Ii-Topical Studies in Oceanography,* 57 (17-18), 1665-1670.

Ichinomiya, M., Yoshikawa, S., Kamiya, M., Ohki, K., Takaichi, S. and Kuwata, A., 2011. Isolation and Characterization of Parmales (Heterokonta/heterokontophyta/stramenopiles) from the Oyashio Region, Western North Pacific. *Journal of Phycology,* 47 (1), 144-151.

J. E. Lemer and E.Grunwald, 1965. *Rates of Equilibria of Organic Reactions.* New York, NY: John Wiley & Sons.

Kucki, M., and Fuhrmann-Lieker, T., 2012. Staining diatoms with rhodamine dyes: control of emission colour in photonic biocomposites. *Journal of the Royal Society Interface,* 9 (69), 727-733.

L. P. Hammett, 1970. *Physical Organic Chemistry.* New York: McGraw Hill,.

Lakowicz, J., 2006. *Principles of Fluorescence Spectroscopy.* USA: Springer.

Law, C., and Exley, C., 2011. New insight into silica deposition in horsetail (Equisetum arvense). *Bmc Plant Biology,* 11, 112.

Li, C.W., Chu, S. and Lee, M., 1989. Characterizing the Silica Deposition Vesicle of Diatoms. *Protoplasma,* 151 (2-3), 158-163.

Loving, G.S., Sainlos, M. and Imperiali, B., 2010. Monitoring protein interactions and dynamics with solvatochromic fluorophores. *Trends in Biotechnology,* 28 (2), 73-83.

Mataga., K.M.N. Kaifu Y.,1956 Bul*l Chem Soc Jpn, ,* 29, 465-470.

M. J. S. Dewar, 1969. *The Molecular Orbital Theory of Organic Chemistry.* New York: McGraw Hill.

Ogane, K., Tuji, A., Suzuki, N., Matsuoka, A., Kurihara, T. and Hori, R.S., 2010. Direct observation of the skeletal growth patterns of polycystine radiolarians using a fluorescent marker. *Marine Micropaleontology,* 77 (3-4), 137-144.

Ong, S.W., Zhao, X.L. and Eisenthal, K.B., 1992. Polarization of Water-Molecules at a Charged Interface - 2nd Harmonic Studies of the Silica Water Interface. *Chemical Physics Letters,* 191 (3-4), 327-335.

Perry,C., Moss,E.. and Williams,R ., 1990. A Staining Agent for Biological Silica. *Proceedings of the Royal Society B-Biological Sciences,* 241 (1300), 47-50.

Roach, P., Farrar, D. and Perry, C., 2006. Surface tailoring for controlled protein adsorption: Effect of topography at the nanometer scale and chemistry. *Journal of the American Chemical Society,* 128 (12), 3939-3945.

Saxton, M.A., D'souza, N.A., Bourbonniere, R.A., McKay, R.M.L. and Wilhelm, S.W., 2012. Seasonal Si:C ratios in Lake Erie diatoms - Evidence of an active winter diatom community. *Journal of Great Lakes Research,* 38 (2), 206-211.

Scarminio, I., and Kubista, M., 1993. Analysis of Correlated Spectral Data. *Analytical Chemistry,* 65 (4), 409-416.

Shimizu, K., Del Amo, Y., Brzezinski, M.A., Stucky, G.D. and Morse, D.E., 2001. A novel fluorescent silica tracer for biological silicification studies. *Chemistry & Biology,* 8 (11), 1051-1060.

Yip,P., Karolin,J., Birch.., S.J.D., 2012. Fluorescence anisotropy metrology of electrostatically and covalently labelled silica nanoparticles. *Measurement Science and Technology,* 23(8),084003

Chapter 4 :

Applications of silicaphilic fluorescence of PDMPO in studying silica surface acidity, silica condensation and invivo biosilicification

This chapter explores the applications of silicaphilic fluorescence of PDMPO to understand the surface acidity silica surfaces and translating spectroscopic knowledge into imaging applications using confocal microscopy. Estimates the charge of the biosilica deposited in living organisms such as Equisetum arvense and Nitzschia stellata. Finally, the application of silicaphilic fluorescence in studying silica condensation are all described.

4.1 Introduction

The maintenance of surface charge density on silica surface is fundamental in many cellular process. Examples include silica deposition (Ikuma, et al. 2014), silica condensation (Cho, et al. 2014), agglomeration kinetics or adsorption of solutes (Wisniewska, et al. 2015), establishment of electrochemical gradients (Sola and Chiari 2015), adaptive response to environmental pH variation (Kroutil, et al. 2015) and other silica surface dependent phenomena. The quantification of *in vivo* and *in vitro* surface charge density on silica surface is not easy, however, if properly done it can be extremely useful in understanding biosilicification and nanoprocess involved at the silica water interface. Surface charge density is rapidly altered by surface area (Prakash, et al. 2015), pH (Ovanesyan, et al. 2016), size of the surface (Barisik, et al. 2014), ionic strength (Salis, et al. 2016, Brown, Bossa and May 2015) and the presence of counter ions (Brown, Bossa and May 2015). For all these reasons, surface charge determination must be consistent to ensure reproducibility and reliability.

When silica is dispersed in a aqueous media, a cloud of oppositely charged ions normally surrounds the silica surface forming an electrical double layer (EDL). Surface properties of silica are determined by this electrical double layer however properties of the EDL depends on the surface charge density (σ_0), surface potential (ψ_0) and the surface ionisable groups on silica (Makino and Ohshima 2010). Zeta potential (ζ) is the most widely used method to calculate surface charge density (Malvern Instruments Ltd 2004). Zeta potential is the potential difference between the dispersion medium and the stationary layer of fluid attached to the dispersed particle. Whereas, surface charge density is the amount of electric charge per

unit area. However there are many of theoretical methods developed to interpolate surface charge from zeta potential using the Grahame equation (Grahame 1947).

In this study a ratiometric probe PDMPO was introduced which upon interacting with silica emits a unique fluorescence and it is located in Stern layer of silica surface (Parambath et al 2015, chapter 3). To explore the potential dye as an alternative indicator for surface charge density measurements by studying the relationship between zeta potential values and fluorescent emission ratios. Employing spectroscopic methods along with confocal approaches for quantification of surface charge density for both *in vivo* and *in vitro* studies. The utility of this approach is demonstrated using silica nano particles with different sizes having different surface charge densities. There are many methods to characterize biogenic or bio-inspired silica formation including ^{29}Si Solid state NMR, infrared spectroscopy, electron microscopy, physisorption and porosimetry (Iler 1979). For biological silicas we have observed many structural particulate arrangement. Different extents of dehydration on silica surfaces has been established Perry *et al* in 1990 using bis(cytopentadienyl) titanium dichloride (Perry C.C 1990). Nevertheless the dynamics of the polymerization process are much more difficult to understand. ^{29}Si solution NMR studies provides information about silica polymerization (Belton, Deschaume and Perry 2012) but this technique demands high concentrations of silica and abundance of NMR-active ^{29}Si isotope which do not represents the silica precursors in natural system. The silicomolybdic acid assay (SMA) (Peryy and Lu. 1991) is another method commonly used to titrate monosilicic acid $Si(OH)_4$ in aqueous environments. However, these techniques have limitations. (1), SMA cannot be used to titrate oligomers larger than disilicic acid (2), phosphate ions interact with silicomolybdic acid to form phosphomolybdic polyacid which absorb at same wavelength (400 nm) as that of silicomolydic acid (Coradin, Eglin and Livage 2004); (3), The limit of detection of yellow silicomolybdic is the order of 10^{-4}mol l^{-1} and (4) SMA cannot be used in *in vivo* conditions.

PDMPO based silica analysis along with the established techniques of SMA and ^{29}Si solution NMR provides will provide an in-depth understanding of oligomerisation.

As far we are aware this is the first attempt to study surface charge density on the silica surface using a ratiometric fluorescent pH probe. We have also utilized the spectral imaging capability of confocal microscope to study effect of hydration. This new approach has allowed us to probe individual silica structures within a composite of mixed silica structures produced by silicifying plants specifically *Equisetum arvense* and *Nitzschia stellata*. Our approach is also fruitful in investigating silica condensation rates and factors affecting the degree of silica condensation.

4.2 Materials and Experimental method

4.2.1 Materials: PDMPO (LysoSensor™ yellow/blue DND-160, 1 mM in dimethylsulfoxide) was obtained from Life Technologies. Chemicals for preparation of citrate and phosphate buffers, ammonia solutions, tetraethoxysilane (TEOS), coumarin 153, HPLC grade water, guanidine hydrochloride were obtained from Sigma Aldrich. Plant material *Equisetum arvense* and Diatoms (*Nitzschia stellate*) were gift from Dr Dave Belton.

4.2.2 Silica PDMPO interaction: Silica nanoparticles (SNPs) were prepared using a modified Stöber process (Roach, Farrar and Perry 2006). Briefly, synthesis involved mixing two solutions (A and B) previously prepared with particle size adjusted by varying the concentration of ammonia in solution A.

For silica particles: solution A was prepared by taking 21.6 mL of 0.1- 0.5 M ammonium hydroxide (NH_4OH), varied to obtain different sized silica nanoparticles in distilled deionized water (ddH_2O) and adding ethanol to make up the volume to 80 mL. Solution B was prepared by diluting 22.3 mL of TEOS in ethanol to 76.6 mL. Freshly prepared solutions

were heated to 50°C, mixed then stirred at 4000 RPM for 2 hours at the same temperature before allowing them to mature at room temperature for 1 day. Ethanol was removed by rotary evaporation at 50°C, the sample centrifuged at 4000 RPM (169.936 G) for 10 minutes and the particles washed with ethanol then distilled water and freeze dried.

Silica nanoparticles of size (22 nm), (30 nm), (50 nm), (77 nm) and (133nm) were used to study the effect of PDMPO adsorption on silica nanoparticles. Experiments were conducted in 0.1 M buffer (pH 2.2 to 13.8) with PDMPO (0.1 μM) and silica particles at a nominal concentration of 1 mg/mL. Solutions containing the dye at 0.1 μM were prepared in 0.1 M buffers (pH 2.2 to 13.8) (phosphate buffer at pH $\geqslant$ 5 and citrate buffer pH $\leqslant$ 5 buffers) with some experiments in the range pH 4-6 carried out in both buffers to ensure no effect of buffer identity on the fluorescence behaviour observed.

4.2.3 Fluorescence spectroscopy: Silica nanoparticles of size (22 nm, 30 nm, 50 nm, 77 nm, 133 nm diameter, final concentration: 1mg/mL) after confirming the size by dynamic light scattering (Appendix 2.1) were suspended in buffer solutions, incubated for 30 minutes at 25°C on a plate shaker at 10 RPM before measuring changes in the fluorescence emission spectra. An excitation wavelength of 360 nm was used to collect fluorescence emission spectra in the range between 400 nm to 600nm for all silica PDMPO interactions. Fluorescence measurements were carried out in 96-well plates (Nunc Optical bottom plates (164588) using a commercial microplate reader (M200 pro; Tecan). The wavelength for excitation was chosen as 360 nm for maximum response which is close to the isobestic point (352 nm) of the $PDMPOH_2^{2+}$ to $PDMPOH^+$ transition of the dye.

4.2.4 Fitting pKas to spectroscopic data: The DATAN software tool developed by Kubista *et al*.(Scarminio and Kubista 1993, Elbergali, Nygren and Kubista 1999) was used to calculate spectral profiles and molar concentrations. In this study, all the recorded

fluorescence data were assembled into data matrices and introduced to the DATAN programme (Elbergali, Nygren and Kubista 1999) to obtain pure spectra for the individual species, concentration profiles and acidity constants of the dye in fluorescence modes.

4.2.5 pH dependent behaviour of PDMPO adsorbed on silica: Silica particles (22 nm, 35 nm, 50 nm, 77 nm, 133 nm) were used and pH measurements performed in buffer (0.1M) in the presence of 1 μM PDMPO. The pH was measured before and after spectroscopic measurements. As for other experiments, samples were left to equilibrate for 30 minutes at 25^{o}C on a shaker at 10 RPM. For fluorescence emission measurements the PDMPO was excited at 360 nm and for confocal measurements PDMPO was excited at 405 nm (405 nm was chosen due to the instrumental constraints).

4.2.6 Fitting peak positions and relative areas: Spectra were decomposed by least squares minimisation of a two component Gaussian model after conversion to wavenumber. Parameters fitted were: peak position (μ), peak width (σ), and scale (conversion factor to arbitrary fluorescence units).

4.2.7 Fluorescence anisotropy : The fluorescence anisotropy of the dye in combination with silica was measured using SNPs (15 nm, 30 nm, 50 nm, 77 nm, 133 nm) in 0.1M Buffer (pH 1.8 to 13.8) with PDMPO (0.1 μM). Steady state anisotropies were measured using a Tecan F200 with excitation filter 360/35 nm and emission filter 540/35 nm. The PMT gain setting was 40 and the G factor 1.256.

4.2.8 Zeta potential and dynamic light scattering (DLS) measurements: Zeta potential and DLS measurements were performed using a MALVERN nanos Zetasizer. Experiments were carried out at 25^{o}C. Clear disposable zeta cell (DTS1060C) were used to make measurements. The hydrodynamic diameter (D_h) of Stöber particles in the presence and absence of PDMPO was calculated as an average of five independent measurements.

4.2.9 Confocal imaging on silica particles: Experiments were conducted in 0.1M phosphate buffer (pH 7.1) with PDMPO (0.1 μM) and silica particles (22 nm, 35 nm, 50 nm, 77 nm, 133 nm) at a nominal concentration of 1 mg/mL. Samples were left to equilibrate for 30 minutes at 25^{o}C on a shaker at 10 RPM before imaging. Imaging was performed on Leica SP5, Maximum intensity at the z position was determined and the z maximum was used for wavelength scans. A wavelength of 405 nm was used to excite the silica nanoparticles coated with PDMPO. Confocal parameters used were numerical aperture (0.5 NA) with objectives (20 ×) used at pinhole size of 63 μm. Fluorescence emissions were calculated and spectra were decomposed by the least squares minimisation of a two component Gaussian model after conversion to wavenumber. Parameters fitted were: peak position (μ), peak width (σ), and scale (conversion factor to arbitrary fluorescence units). Ratios of the scale where used for determine surface charge/pH.

4.2.10 Effect of charge neutralization on silica surface using guanidine hydrochloride (GHCl)

1 mg/mL of of 50 nm SNP (+/- 5 nm) was weighed and transferred to phosphate buffer 0.1M, pH 7.01, A typical sample contain 1mg/mL of SNP (50 nm), dose dependent concentration of GHCl (0 to 80 mM), 0.1μM of PDMPO, with the final volume was kept constant as 1000μL and incubated for 30 min, From each sample aliquots 200 μL was air dried for two hours followed by collection of fluorescence emission by SP5 confocal microscope by exciting at 405 nm. Each of the stock aliquots without PDMPO (1mg/mL of SNP (50 nm) and dose dependent concentration of GHCl (0 to 80 mM)) were subjected to zeta potential measurements.

4.2.11 Charge estimation on biological samples

Biological samples from node, internodes of *Equisetum arvense* and *Nitzschia stellata* were acid treated and dried (Samples were dried at room temperature and lightly ground with a

pestle and mortar followed by treatment with a mixture of concentrated nitric and sulphuric acids (4:1 by volume) heated at 100^{o}C for at least 24 h to remove the organic cell wall components. These samples are then treated with PDMPO. Experiments were conducted in 0.1M Phosphate buffer (pH 7.1) with PDMPO (1.0 µM). A nominal concentration of 1 mg/mL of acid treated biological samples (*Equisetum arvense*, *Nitzschia stellate)* was used for imaging.

a **b**

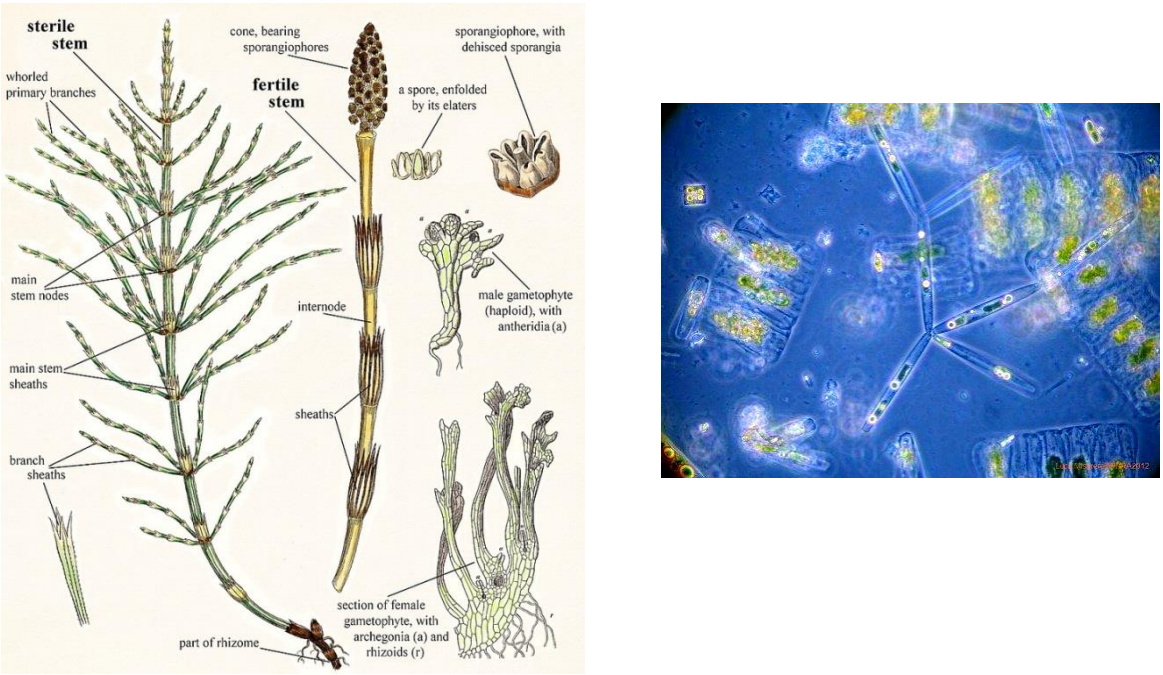

Figure 4.1: Biological samples used to study charge estimation (a)Plant sample used for the study is *Equisetum arvense* (b) Diatoms from Antarctica *Nitzschia stellate* was also used to study charge estimation.

Fluorescence imaging were performed after 60 minutes of incubation on shaker at 10 RPM at 25^{o}C. Maximum intensity on *z* position was monitored, the maximum was then used for wavelength scan. 405 nm was used to excite the acid treated samples. Different region of interest were selected and spectral imaging was performed. Spectra were decomposed by least squares minimisation of a two component Gaussian model after conversion to

wavenumber. Parameters fitted were: peak position (μ), peak width (σ), and scale (conversion factor to arbitrary fluorescence units). Ratios of the scale where used for determine surface charge. The morphology of the samples was determined by scanning electron microscopy (SEM) (JEOL JSM-840A, 20 kV). Samples were attached to aluminium stubs using double-sided carbon adhesive tape and carbon coated (Edwards, sputter coater S150B).

4.2.12 Monitoring silica condensation using PDMPO

Monitoring silica condensation was performed by evaluating the surface acidity of silica using fluorescent emission ratios. Kinetic analysis of silica condensation was performed using TEOS (tetraethyl orthosilicate) as the precursor. To study the effect of TEOS the concentration was varied over different TEOS concentrations which first hydrolysed (10 mM HCl) and then the pH was raised to 7.08 using a buffered system (Phosphate buffer pH 7.08, 0.1 M) to carrying out silica condensation. Fluorescence emissions were monitored at 511 and 440 after exciting at 360 nm. Due to experimental constraints fluorescence emissions can only collected after 5sec of condensation time due to the fast rate of silica aggregations.

To study the effect of different pH conditions on silica condensation. A concentration of 40 mM of prehydrolysed precursor using 10 mM HCl was added to condensation system of pH 5.07, pH 5.70, pH 6.24, pH 6.57, pH 7.08. Which was followed by addition of 1μM of PDMPO. Fluorescence emission from the condensation system was monitored a in every 30 sec for 5.5 hours. Pseudo first order rate constants were calculated according to Yuan at al. (Yuan, Lin and Yang 2011, Dale T, J and Rebek, J 2005). The pseudo-first-order rate constant k' was calculated according

$$In\left[\left(\frac{F_{max}-F_t}{F_{max}}\right)\right]=-k't \qquad (eqn\ 4.1)$$

Where F_{max} and F_t is fluorescent emission ratio at when reaction is completed and emission ratio at time t and k' pseudo first order rate constant.

4.2.13 Monitoring silica condensation using molybdic assay

The blue silicomolybdic assay solution A is made of 20 g ammonium molybdate tetrahydrate and 60 mL concentrated hydrochloric acid in deionized water. Solution B was prepared by adding oxalic acid (20 g), 4-methylaminophenol sulphate (6.67 g), anhydrous sodium sulfite (4 g), deionised water (500 mL) and concentrated sulphuric acid (100 mL) to a 1 litre volumetric flask and completed with deionised water. In a typical experiment, 1 mL of the unknown concentration silicic acid solution was sampled and diluted to 16 mL with deionised water. To this was added 1.5 mL of solution A. After 10 minutes, 7.5 mL of solution B was added to the assay solution. The blue colour was left to develop over 2 hours at room temperature before measuring the optical density at λ = 810 nm using tecan M200. To study the effect of silica condensation. Hydrolysed precursor was added to a condensation system at pH 7.08. At an interval of 30 sec 1 mL from the condensation system was sampled and diluted to 16 mL with deionised water and 1.5 mL of solution A is added, after 10 minutes then 7.5 mL of solution B was added to the assay solution and left for two hours at room temperature and optical density measured at 810 nm.

4.3 Results and Discussion

4.3.1 Determination of surface acidity or surface pH on silica surface using PDMPO

To study the effect of surface acidity on the interactions occurring between dye upon silica particles, a set of pristine silica spheres ranging between 22 and 133 nm nanometre (22 nm, 30 nm, 50 nm, 77 nm, 133 nm) were used for investigations, size of the particles were confirmed by dynamic light scattering (**Appendix 2.1**). Silica PDMPO interaction was conducted at a single pH (7.08) where strong fluorescence emissions from $PDMPOH_2^{2+}$ was typically observed (**Figure 4.2.a**). It is known from the literature (Iler 1979) that silica particle size can significantly increase the surface acidity of particles greater than ca. 10 nm with the zeta potential of the particles increasing as particle size was increased up to 133nm as in the **Figure 4.2.b** This behaviour was matched by an increase in emission ratio ($PDMPOH_2^{2+}/PDMPOH^+$) with increase in particle size, as in (**Figure 4.2.a, 4.2.b)** There is a inverse correlation between the enhancement of fluorescence

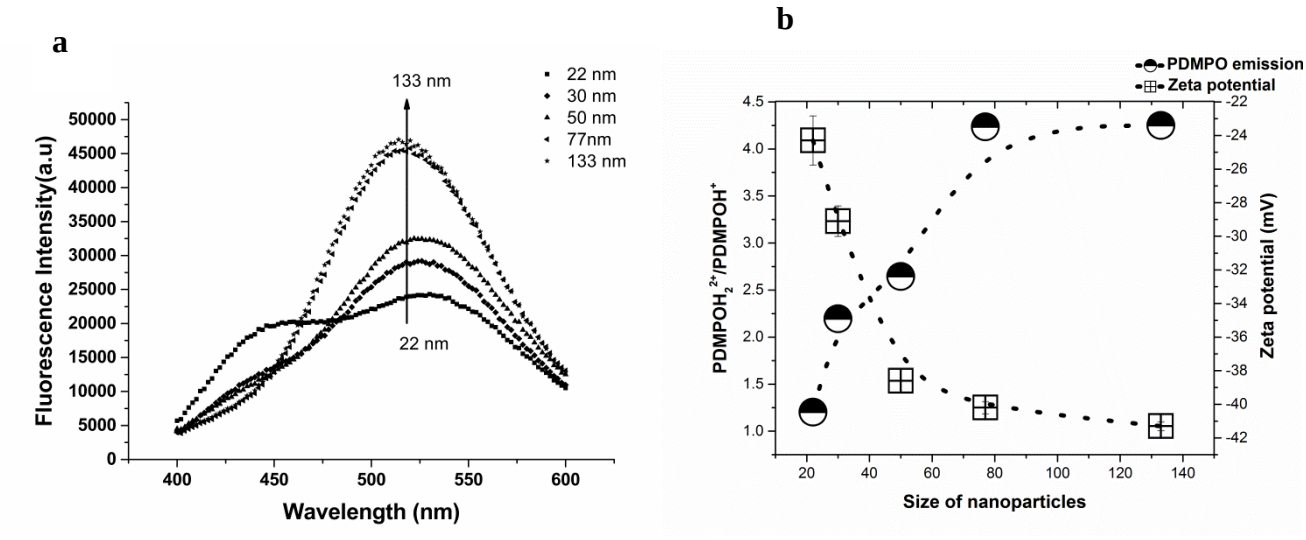

Figure 4.2: Effect of silica particle (22nm -133 nm) on dye adsorption and particle surface charge (zeta potential) (a) Fluorescence emission increases with increase in size of silica particles (b) Increase in fluorescence emission ratio (with increase in size of silica nanoparticle and Zeta potential measurement on SNPs.

as measured by the ratio from $PDMPOH_2^{2+}/PDMPOH^+$ and increases in zeta potential measurements (surface acidity) on different sized silica particles, **Figure 4.2.b** suggesting that this dye can be used to study the surface acidity of silica. Enhancement of fluorescence ratio ($PDMPOH_2^{2+}/PDMPOH^+$) with increases in particle size, particularly for the two largest particle sizes (77 and 133nm) suggest that fluorescence emission in the presence of SNP rises from $PDMPOH_2^{2+}$

4.3.2 pK_a prediction on different sized silica particles.

To further understand the shift in fluorescence emission spectrum on silica particles with increase in size of particles, the fluorescence emission spectrum of PDMPO in the presence of different size silica nanoparticles (22 nm, 30 nm, 50 nm, 77 nm and 133 nm) were collected followed by DATAN analysis. Molar ratios were retrieved from fluorescence emission spectra from (pH 2- pH 14) with different pK_a* figure 4.2 a-e. PDMPO on the smaller sized particles have lower pK_a* value compared to higher sized particles. pK_a* value of 9.60, 10.20, 10.50, 11.40, 11.44 was retrieved for 22nm, 30 nm, 50 nm, 77 nm and 133 nm particles respectively (**Figure 4.3 a-e**). There is a size dependent increase in the pK_a* value of PDMPO upon interaction with silica (**Figure 4.3.e**).

Surface charge on the different silica particles was monitored using zeta potential measurements (**Figure 4.4.a**). The increase of surface charge of particles increases with increase in particle size has already been demonstrated by Puddu and Perry (Puddu and Perry 2014). To further understand the silica PDMPO interaction the fluorescence anisotropy of PDMPO on silica particles from pH 2 – pH 14 was measured. There was a size dependent increase in fluorescence anisotropy with increases in size of the silica particles(**Figure 4.4.b**).

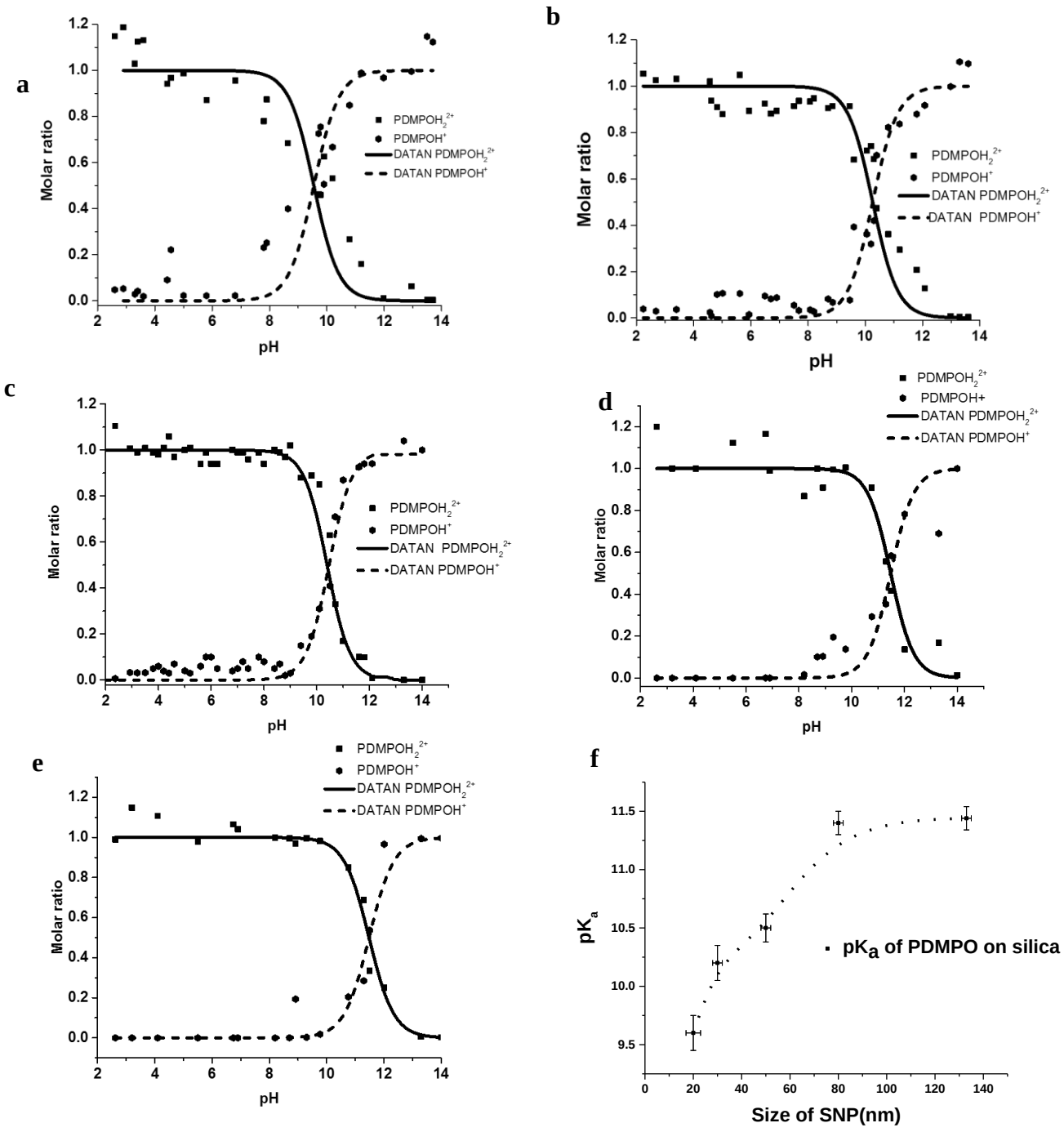

Figure 4.3: DATAN analysis on fluorescence emission spectrum upon silica PDMPO interaction (pH 2 to pH 14) after exciting at 360 nm.(a) 22 nm (b) 30 nm (c)50 nm (d) 77 nm (e) 133 nm diameter of the particles (f) Effect of silica size on pK_a value on silica.

Zeta potential measurements from (**Figure 4.4.a**) shows that surface charge densities of silica nanoparticles is size dependent. pH dependent surface charge is expected. As the concentration of H^+ ions decreases with increased pH, more negatively charged SiO^- are formed from the surface Si-OH functional groups resulting in higher negative surface charge density. Overall **Figure 4.4.a** indicates that there is a size dependent effect on the surface charge on silica which is affecting the shift in pK_a values of PDMPO as observed in **Figure 4.3.f.**

a

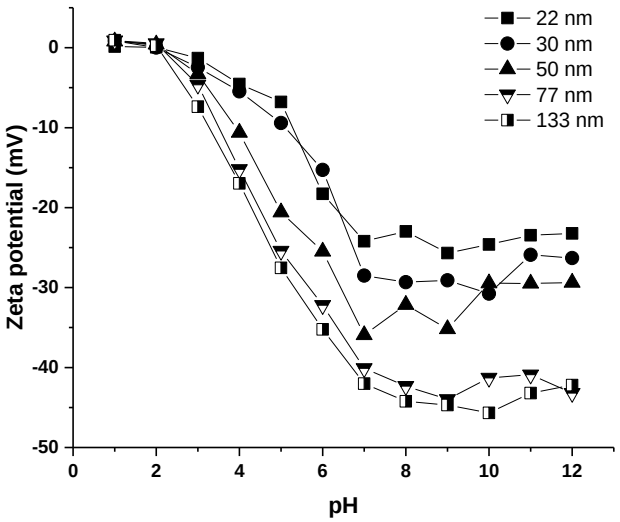

b

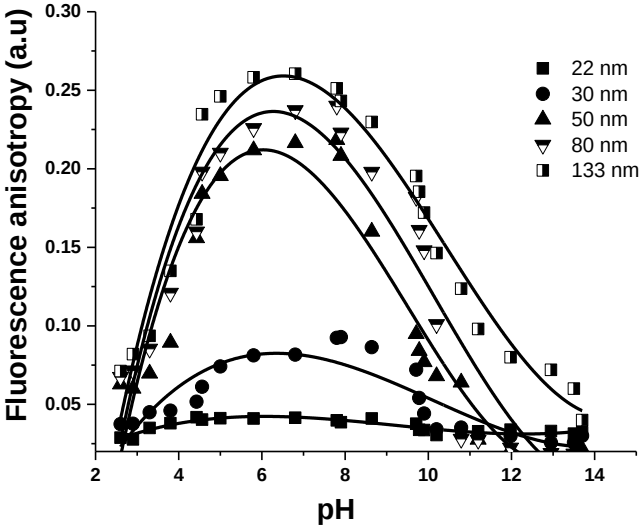

Figure 4.4: Silica PDMPO interaction on different sized silica particles (a) zeta potential measurements on different sized silica particles (22 nm, 30 nm, 50nm, 80 nm and 133nm) (b) effect of fluorescence anisotropy on different sized silica particles

Fluorescence anisotropy values from (**Figure 4.4.b**) depict that regardless of the size of particle fluorescence anisotropy increases consistent with the ground state pK_{a1} (4.2). It reaches a plateau between pH 5.2 and 8.2 indicating rotational diffusion. Above 8.2, the anisotropy decreases but remains slightly above that of the free dye up to pH 14. At a high pH above 10 there is shift in fluorescence anisotropy with size. However data also imply

that bigger sized particles (133 nm) have higher binding interaction than smaller particles (22 nm). Larger sizes particles (133 nm) have higher surface charge compared to smaller sized particles there by have an higher electrostatic interaction with the side chain amine group of PDMPO giving fluorogenic portion of the molecule the ability to undergo hindered rotational diffusion there by exhibiting an enhanced fluorescence anisotropy upon binding with silica.

4.3.3 Charge determination on silica particles using confocal spectral imaging

Confocal microscopy has the capability to perform spectral imaging. Confocal microscopy can be integrated with the silicaphilic fluorescence of PDMPO to determine surface charge density on silica surfaces. Moreover, the current generation of confocal microscopes generally have laser excitation and the capability to simultaneously detect fluorescence emissions (Borlinghaus 2006). Popular excitation sources at lower wavelength are the 405 nm diode and an argon ion laser that emits at 488 nm. The Isobestic point of PDMPO is 360 nm. To adapt it to 405 nm excitation wavelength, we studied the effects of change in excitation wavelength on particulate solution.

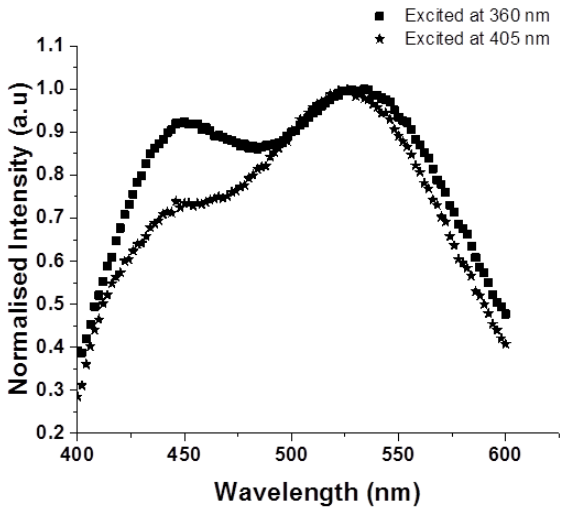

Figure 4.5: Effect of change in emission spectrum upon change in excitation wavelength (excitation wavelength changed from 360 nm to 405 nm) on PDMPO at pH 7

When the excitation wavelength is shifted to 405 nm there is partial excitation of the double protonated species compared to the single protonated species; there is a 22 % reduction in fluorescence intensity of the single protonated species (**Figure 4.5**). However, these constraints do not restrict the dye in its utility to be used as a ratiometric probe. Similar fluorescence behaviour observed for aromatic flurophores are denoted as a red edge effect (Demchenko 2002). The red edge effect depends on excitation wavelength and existence of an excited state distribution of fluorophores on their interaction energy with the environment and a slow rate of dielectric relaxation (Demchenko 2002).

4.3.4 Estimation of charge on silica using confocal spectral imaging

Confocal spectral imaging on different sized particles 22 nm, 30 nm, 50 nm, 77 nm and 133 nm particles at maximum Z position (**Figure 4.6 a, c, e, g, i**) was followed by collection of fluorescence emission from confocal microscopy which is then decomposed by least squares minimisation into two component Gaussian model after conversion to frequency (**Figure 4.6 b, d, f, h, j**). Emission ratios of the scale were compared with zeta potential values (**Figure 4.6 i**). It is known from the **Figure 4.6 k** that silica particle size can have size dependent effect on fluorescence emission from PDMPO and this can be monitored quantitatively and qualitatively using confocal imaging and confocal spectral imaging. As the size of particles increases there is increases in surface charge and fluorescence emissions shifts from $PDMPOH^{+}$ to $PDMPOH_2^{2+}$. Emission ratio is calculated and plotted against zeta potential values as in **Figure 4.8.**

To further understand the effect of surface charge on silica upon fluorescence emission, charge neutralization experiments were carried out on silica nanoparticles (50 nm) we are proposed of using a chaotropic agent such as guanidine hydrochloride (GHCl). GHCl in

aqueous solution disrupts the hydrogen bonding between water molecules and effect the stability of PDMPO on the silica surface.

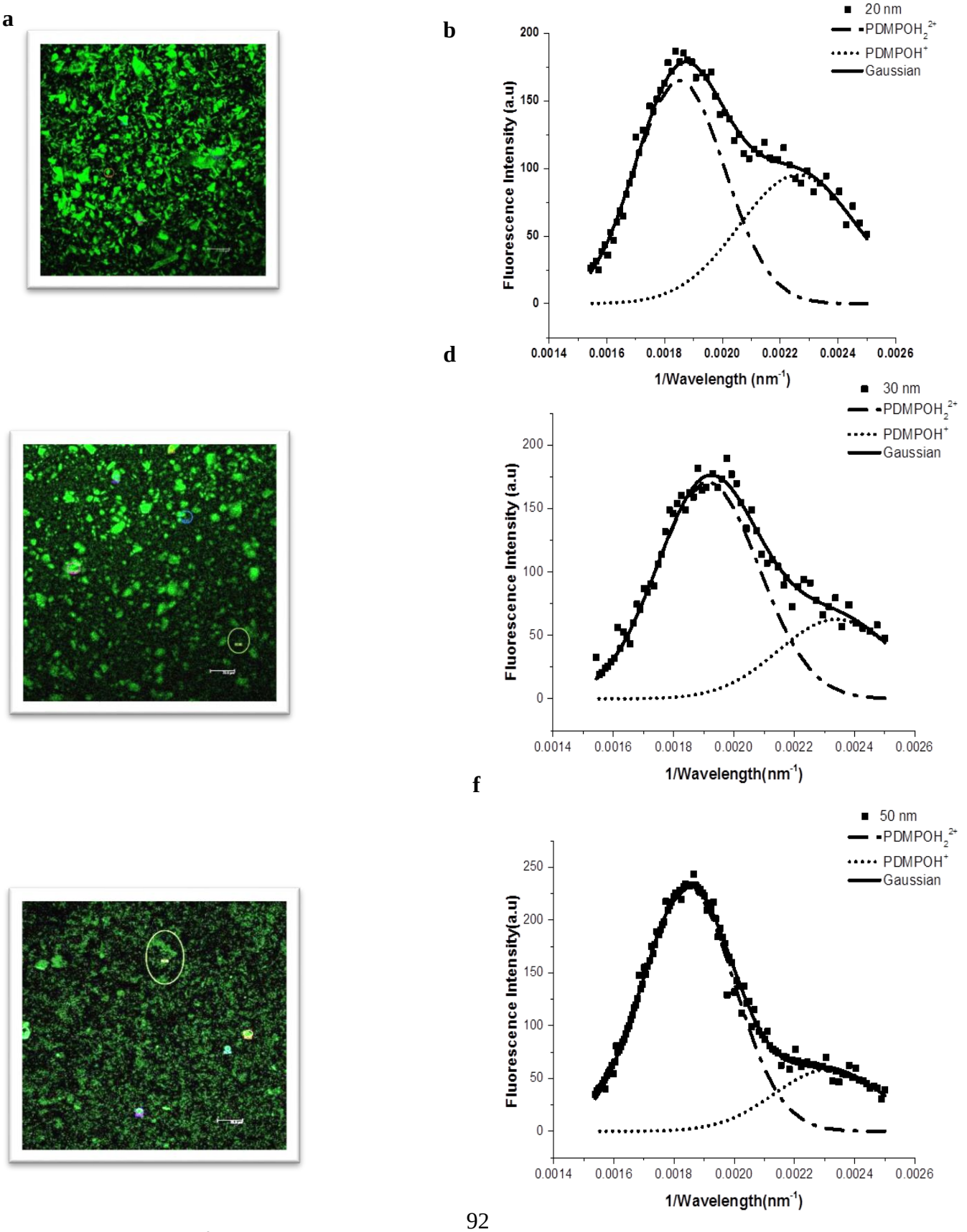

See next page for legends

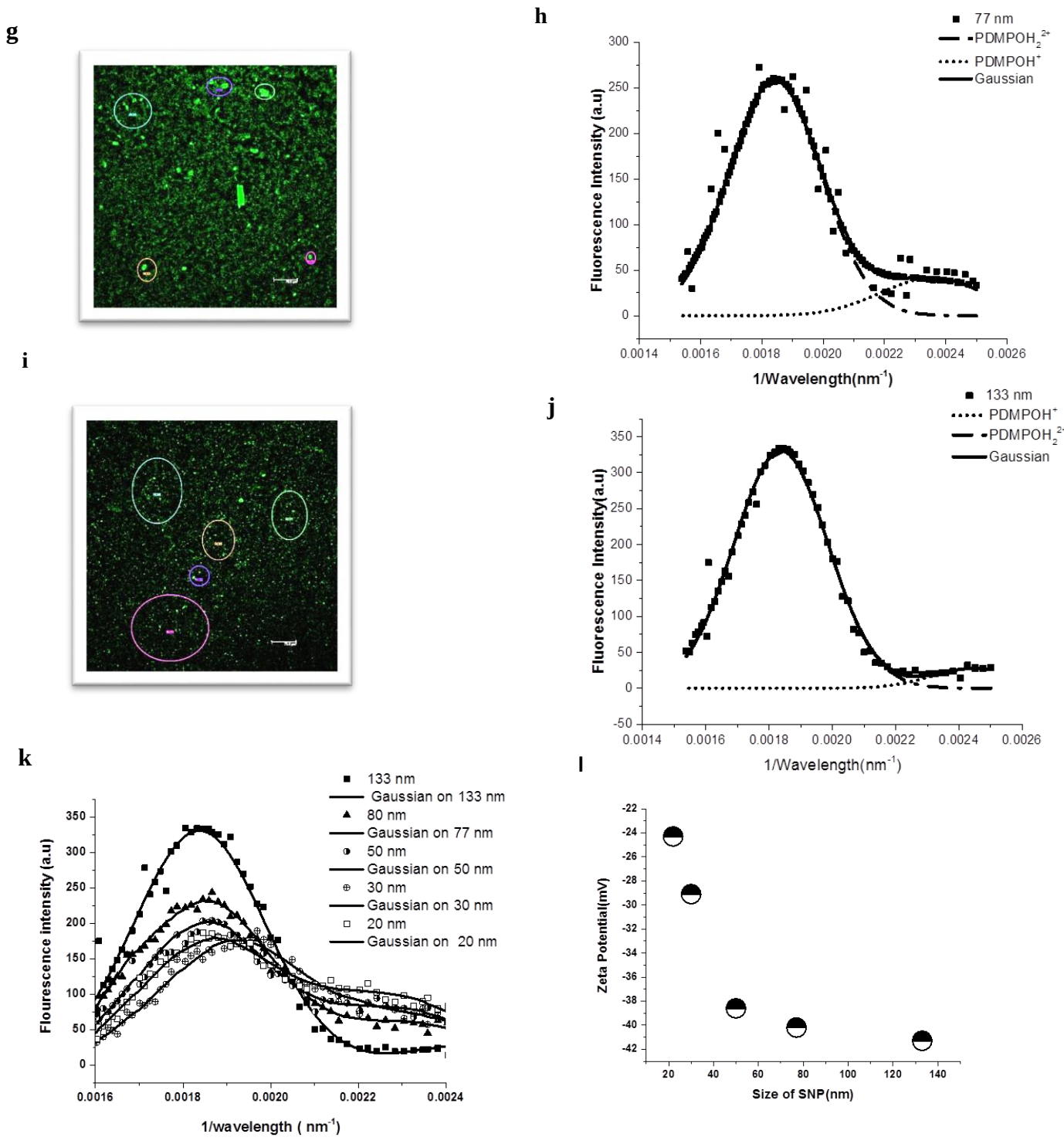

Figure 4.6: Confocal imaging of silica nano particles excited at 405 nm (left panel) and fluorescence spectrum decomposition into two Gaussian models (right panel) (a and b) 20 nm particles, (c and d) 30 nm particles, (e and f) 50 nm particles, (g and h) 77 nm particles

and (I and j) 133 nm particles. (k) A comparative plot of all the spectrum (l) Zeta potential values of 22 nm,30 nm,50 nm,77 nm and 133 nm at pH 7.2

At neutral pH GHCl is protonated to gunidinium cation which is highly stable mono cation as its pK_a of 13.6. To study the effect of charge neutralization silica nanoparticle (50 nm) a dose dependent study on SNP using GHL concentration of 10 mM to 80 mM was performed. Confocal imaging at different doses were performed (**Figure 4.7 a, c, e, g, i, k**). was followed by collection of fluorescence emission from confocal microscopy which is then decomposed by least squares minimisation into two component Gaussian model after conversion to wavenumber **(Figure 4.7 b, d, f, h, j, l**) A dose dependent shift in fluorescence from $PDMOH_2^{2+}$ to $PDMPOH^+$ was observed. Zeta potential is an indirect measurement of surface charge density. Zeta potential values were measured upon dose dependent increases GHCl (**Figure 4.6.m**). There was linear correlation between zeta potential and emission ratio (**Figure 4.8**). This proves that the emission ratio can be used to measure surface charge density. Silica surface was subjected to partial neutralization using GHCl which is a monocation, A dose dependent increases in GHCl concentration from 0 mM to 50 mM show partial neutralization of silica surface, this partial neutralization is reflected both in zeta potential measurements and fluorescence measurements.

a

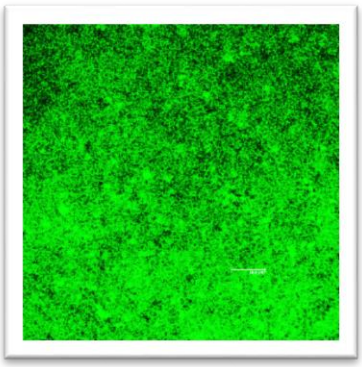

b

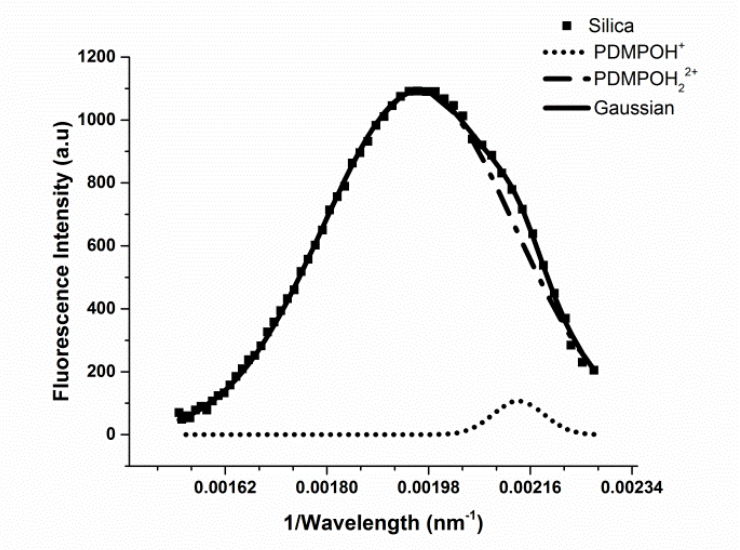

Figure 4.7 title and legend page 97

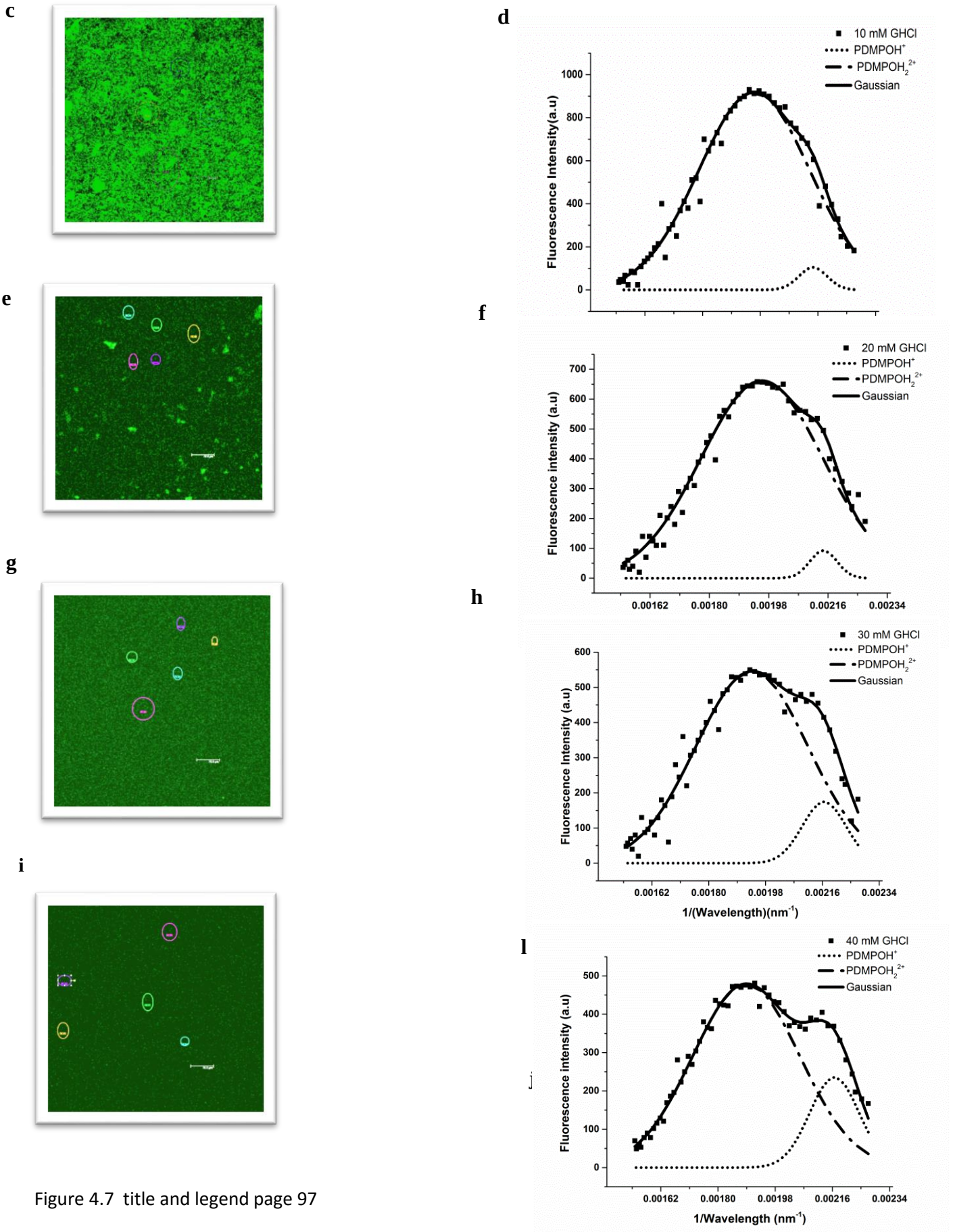

Figure 4.7 title and legend page 97

k

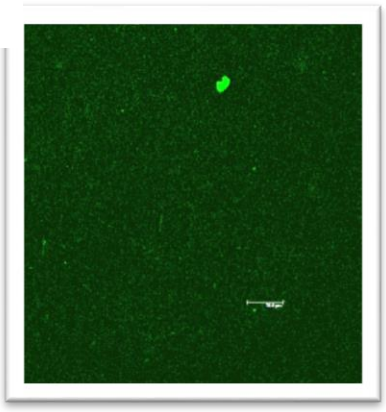

L

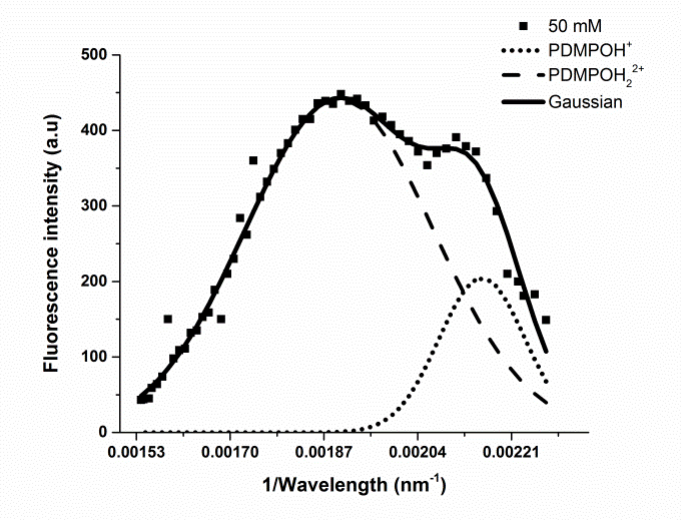

m

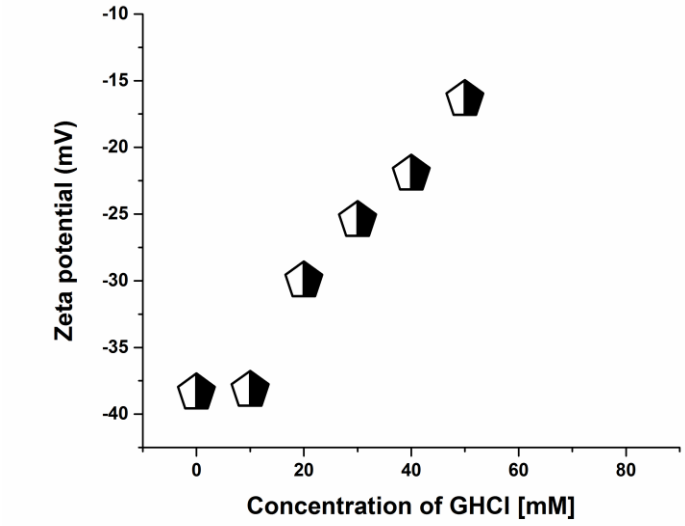

Figure 4.7: Fluorescence emission on silica nanoparticles (50 nm) upon charge neutralization using GHCl. Confocal imaging of silica nano particles excited at 405 nm and fluorescence spectrum decomposition into two Gaussian models (right panel). (a and b) silica (50 nm), (c and d) 10 mM GHCl , (e and f) 20 mM GHCl, (g and h) 30 mM GHCl,(i and j), 40 mM GHCI, (k and l) 50 mM GHCI, (m) Zeta potential values on SNP upon dose dependent increases in GHCl concentration

4.3.4 Charge estimation on silica using fluorescent emission ratio

Data from different sized silica particles and charge neutralisation experiments on silica particles were used to plot the relation between fluorescence emission ratio and zeta potential. Linear correlation between zeta potential and emission ratio from **Figure 4.8** was further used to estimate the charge on biosilicas found in nature.

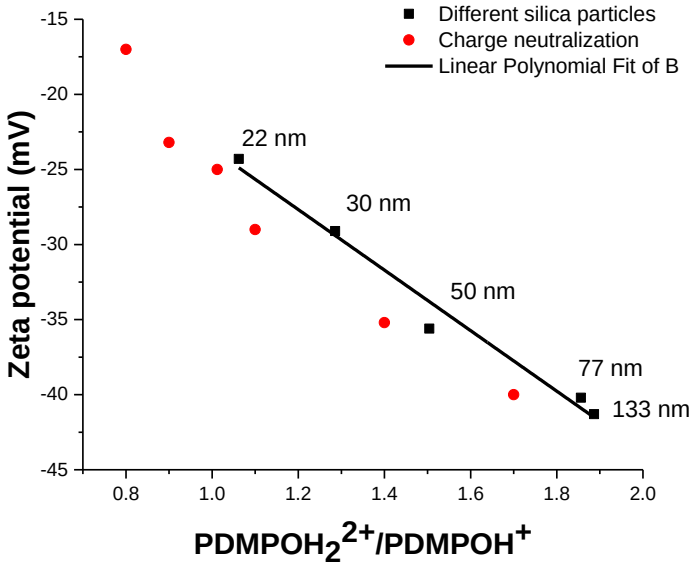

Figure 4.8 : Titration plot of the fluorescence emission ratio ($PDMPOH_2^{2+}/PDMPOH^+$) plotted against zeta potential values from **Figure 4.6 (a-l)** and **Figure 4.7 (a-m)**

Confocal spectral imaging has the capability to create a complete fluorescence emission spectrum of the specimen at every pixel location where this capability is utilised to select fluorescent emissions ratios of different nano structures on biosilica which can be used to determine charge on the individual structures. Surface morphological studies were performed on the nodes of stem of *Equisetum arvense.* Stem nodes have shallow grooves flanked by narrow ridges. Fluorescence emission data (Appendix 2.2) was collected from

three regions of interest on the upper part of ridges **(Figure 4.9.a)** and three region of interest in the lower part of ridges **(Figure 4.9.a).** Morphological characterisation of stem nodes are done using SEM (**Figure 4.9.b).** Upper part of ridges have more accumulation of the dye compared to lower portion however emission ratio indicate that lower portion ridge have higher fluorescence signal from $PDMPOH_2^{2+}$ compared to $PDMPOH^+$ (**Figure 4.9.c**). Emission ratio after Gaussian decomposition (appendix 4.2) is further used to estimate the zeta potential using **Figure 4.8** and upper part of ridge is estimated to have of charge of - 35 mV and lower part of ridge is estimated to have a charge above -45 mV. An unpaired T test was performed on the upper ridges and lower ridges. The two-tailed P value was calculated as 0.0004 which by conventional criteria is considered to be extremely statistically significant.

We have observed that the basal and distal portions of the branches were morphologically very similar but were quite distinct from the other parts of the plant. The epidermal cells in the region of the groove flanks were surmounted by regular clusters of conical pilulae in the form of star-shaped rosettes or clusters that were often seen to fuse to form bars. The remainder of the epidermal cells were covered by a random dispersion of bead-like pilulae as observed it is denoted as nodal plane. We collected fluorescence emission from three region of interest on the star shaped pilulae (**Figure 4.10.a.,** Appendix 2.2) and three region of interest in the nodal plane (**Figure 4.10. a**).

a

b

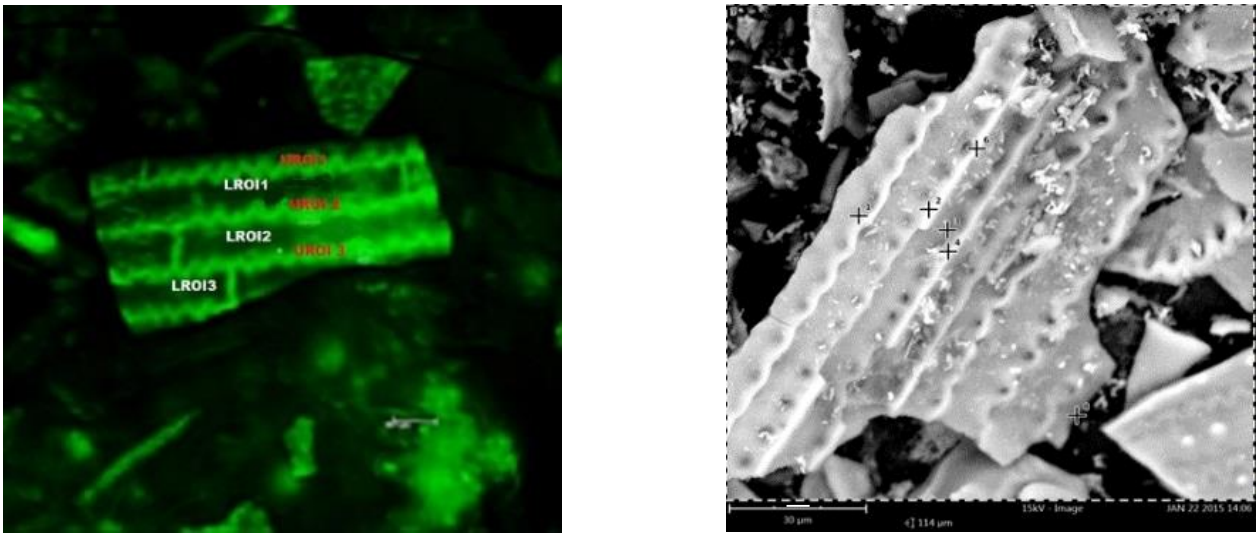

c

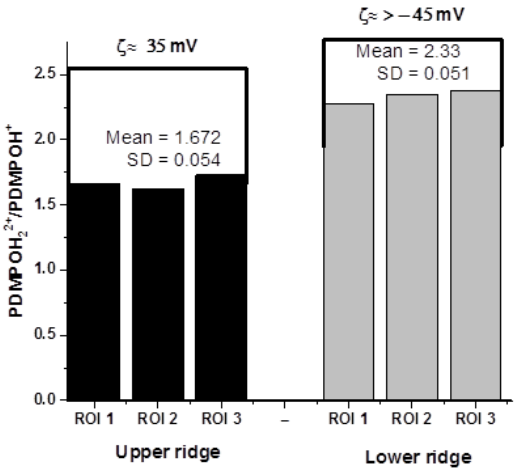

Figure 4.9: Charge estimation on the upper and lower ridges using PDMPO.(a) Confocal imaging of nodes of *Equisetum arvense* at upper and lower ridge. Six region of interest was selected three upper ridge region of interest (UROI) and three lower ridge region of interest (LROI) (b) SEM images of *Equisetum arvense* plant nodes showing two distinct upper ridge and lower ridge.(c) charge estimation is done using the emission ratios using **Figure 4.8** and zeta potential value estimated at upper ridge is – 35 mV and lower ridge is -45 mV.

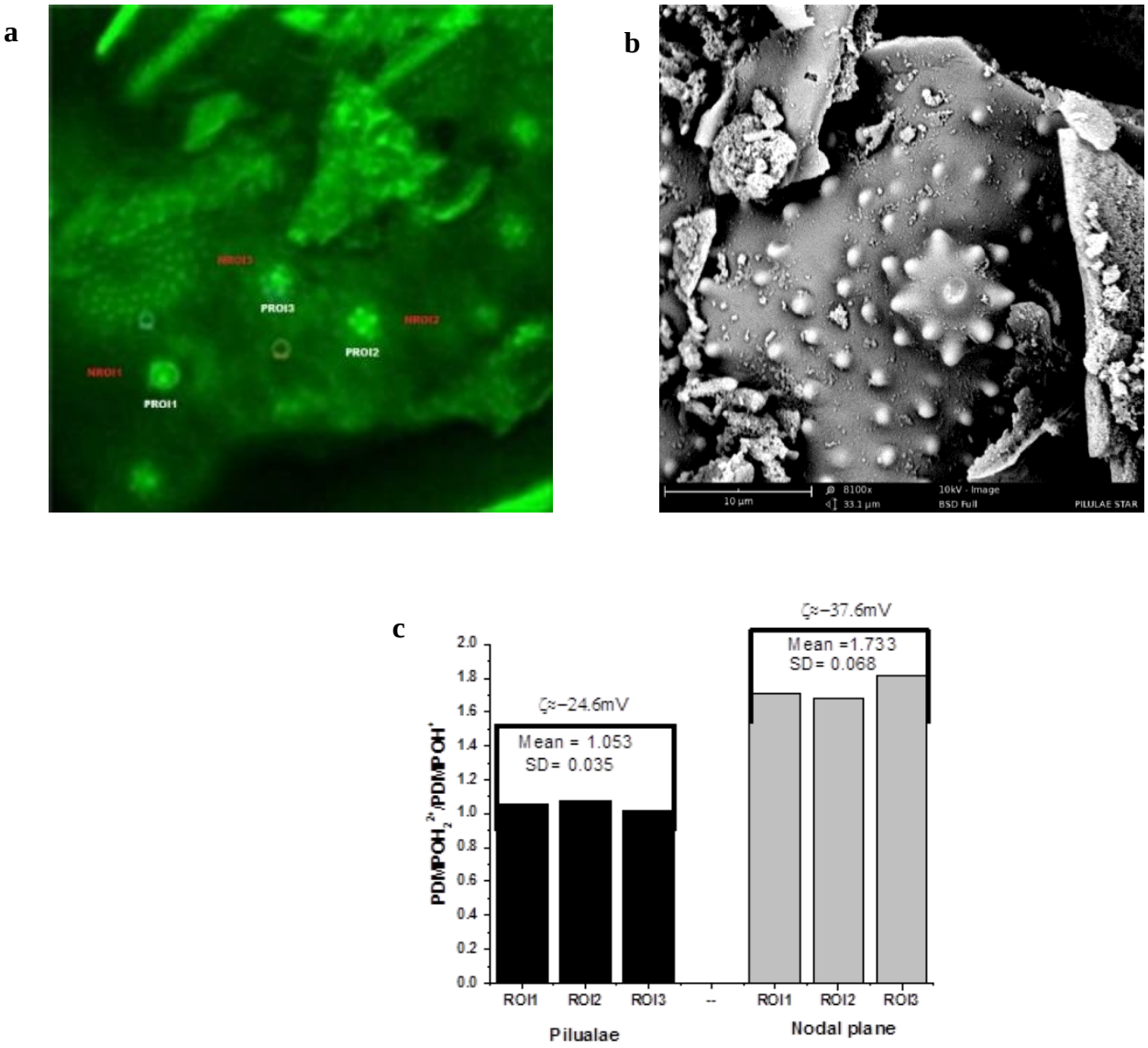

Figure 4.10: Charge estimation on the star-shaped rosettes and nodal plane using PDMPO.(a) confocal imaging of nodes of star-shaped rosettes and nodal plane of *Equisetum arvense*. Six region of interest was selected three star-shaped pilualae of interest (PROI) and three nodal region of interest(NROI); (b), SEM images *of Equisetum arvense* plant nodes showing star-shaped rosettes and nodal plane; (c) Zeta potential value estimated at star shaped pilualae is -24.6 mV and lower ridge is -37.6 mV

Fluorescent emissions from the nodal plane and star shaped clusters is dominated from emissions from $PDMPOH_2^{2+}$ compared to $PDMPOH^+$, However emission ratio demonstrate that higher value is obtained for nodal plane compared to star shaped clusters. Charge estimation using **Figure 4.8** predicts a zeta potential of -24.6 mV and -37.6 mV for the star shaped pilulae and nodal plane respectively. An unpaired T test was performed on the star shaped rosettes and nodal planes. The two-tailed P value was calculated as 0.0006 and the mean of pilulae minus nodal plane equals -0.69367 by conventional criteria is considered to be extremely statistically significant. In the basal portions of plants we observed distinct ridge and groove pattern with stomata aligned in double offset rows running along the groove flank in distinct depressions formed by adjacent epidermal cells and topped by convex mammillae encrusted, they are covered by rows of pilulae which become elongated and dumb bell shaped towards the stomatal opening. We collected fluorescence emission from three region of interest on the convex stomata **(Figure 4.11.a,** Appendix 2.4**)** and three region of interest in the nodal plane **(Figure 4.11.a).** Charge estimation using **Figure 4.8** predicts a zeta potential of -25.3 mV and -45. mV for the star shaped pilulae and nodal plane respectively with a two-tailed P value equals 0.0005. *Nitzschia stellate* are diatoms isolated from Antarctica, they are linear diatoms which taper towards the poles. It has apical axis and transapical axis. We collected fluorescence emissions from apical axis and transapical axis (**Figure 4.12.a,** Appendix 2.5). Morphological studies using SEM demonstrate rod shaped structure of the diatoms (**Figure 4.12.b**) Zeta potential values estimated -26.01 mV and -41 mV for transapical and apical region respectively**(Figure 4 a.12.c)** with a two-tailed P value equals 0.0011.

a **b**

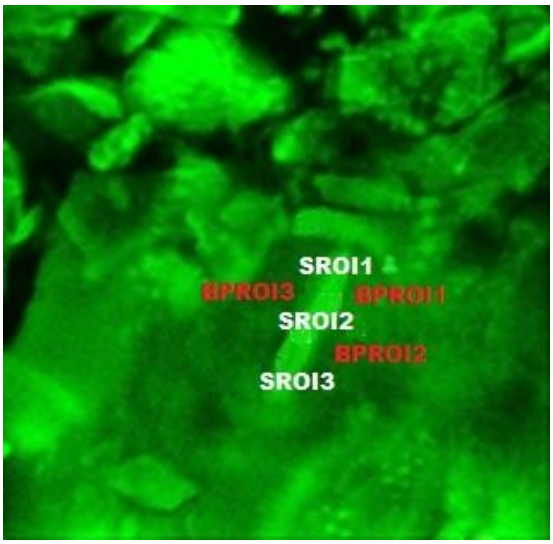

c

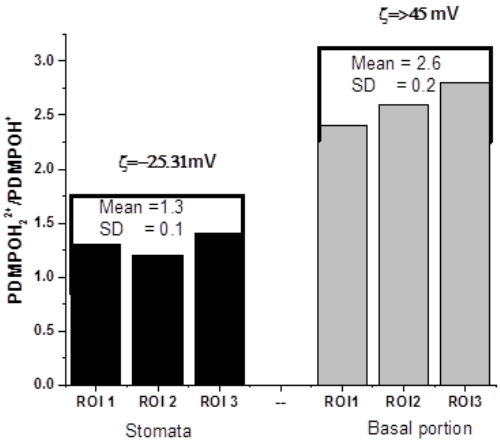

Figure 4.11: Charge estimation on the stomata and basal plane using PDMPO.(a) Confocal imaging on the stomata and basal plane of *Equisetum arvense*. Six region of interest was selected three convex stomata star star-shaped pilualae of interest (SROI) and three nodal region of interest(BPROI) (b) SEM images of *Equisetum arvense* shows a convex shaped stomata in the basal portion (c) Zeta potential value estimated as -25.34 mV and -45 mV for stomata and basal portion respectively .

a

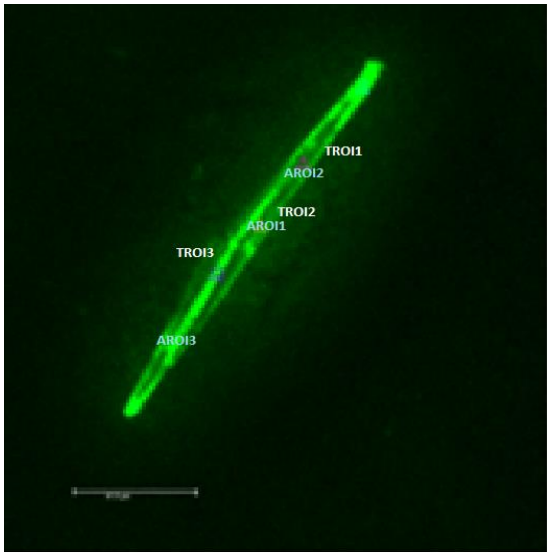

b

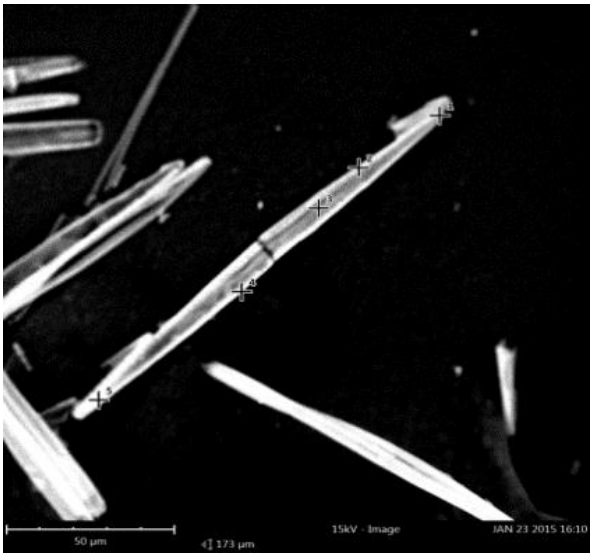

c

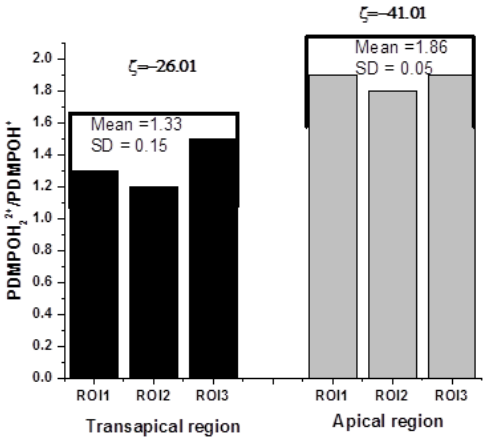

Figure 4.12: Charge estimation on apical and trans apical axis on the *Nitzschia stellate* using PDMPO (a) Confocal imaging on the apical and transapical axis of *Nitzschia stellate* Six region of interest was selected three long apical axis (AROI) and three transapical region of intrest(TROI); (b) SEM images on apical and trans apical axis on the *Nitzschia stellate*;

(c) Zeta potential value estimated as -26.01 mV and -41.01 mV for on apical and trans apical axis on the Nitzschia stellate

4.3.5 Monitoring silica condensation using PDMPO

Fluorescence emission at different stages of silica condensation after hydrolysis was monitored. The change in fluorescence emission as a function of time was monitored at different concentrations of TEOS (10 mM, 20 mM, 40 mM, 80mM, 160mM) after it was hydrolysed in 10 mM HCl and pH raised (pH 7.08) using a buffered system to carry out silica condensation. PDMPO was added to the condensation system and fluorescence emissions were monitored at 522 nm ($PDMPOH_2^{2+}$) and 440 nm ($PDMPOH^+$) after exciting at 360 nm. After addition of TEOS to the buffering system pH 7.08 there was a rapid increases in the fluorescence emission was noted (**Figure 4.13.a**) A supersaturated solution of monosilicic acid at neutral pH spontaneously polymerize into oligo and polymeric silicic acid, silica sol and finally silica gel. There is an increases in fluorescence emission at 522 nm on silica polymerisation which suggests that fluorescence emission is typical of that of $PDMPOH_2^{2+}$ and emission is due to the presence of polymeric forms of silicic acid. Experimental results from **Figure 4.13.a** shows that there is a dose dependent increase in the rate of silica condensation with increases in the concentration of TEOS. We also monitored the effect of pH on silica condensation with phosphate buffer at varied pH (pH 5.07, pH 5.5, pH 6.24, pH 6.5 and pH 7.08). Silica polymerisation is a pH dependent reaction with rate of condensation maximal at neutral pH (**Figure 4.13.b**). The experimental results shows that a maximum conversion ($PDMPOH_2^{2+}$ to $PDMPOH^+$) occurs at neutral pH 7.08 (**Figure 4.13.b**). At biologically relevant neutral pH (7.08) and near neutral pH 6.50 the rate of silica condensation follow a pseudo first order rate law for first 350 sec with a pseudo first order rate constant 0.003 sec^{-1} and 0.0018 sec^{-1} for pH 7.08 and pH 6.50 respectively.

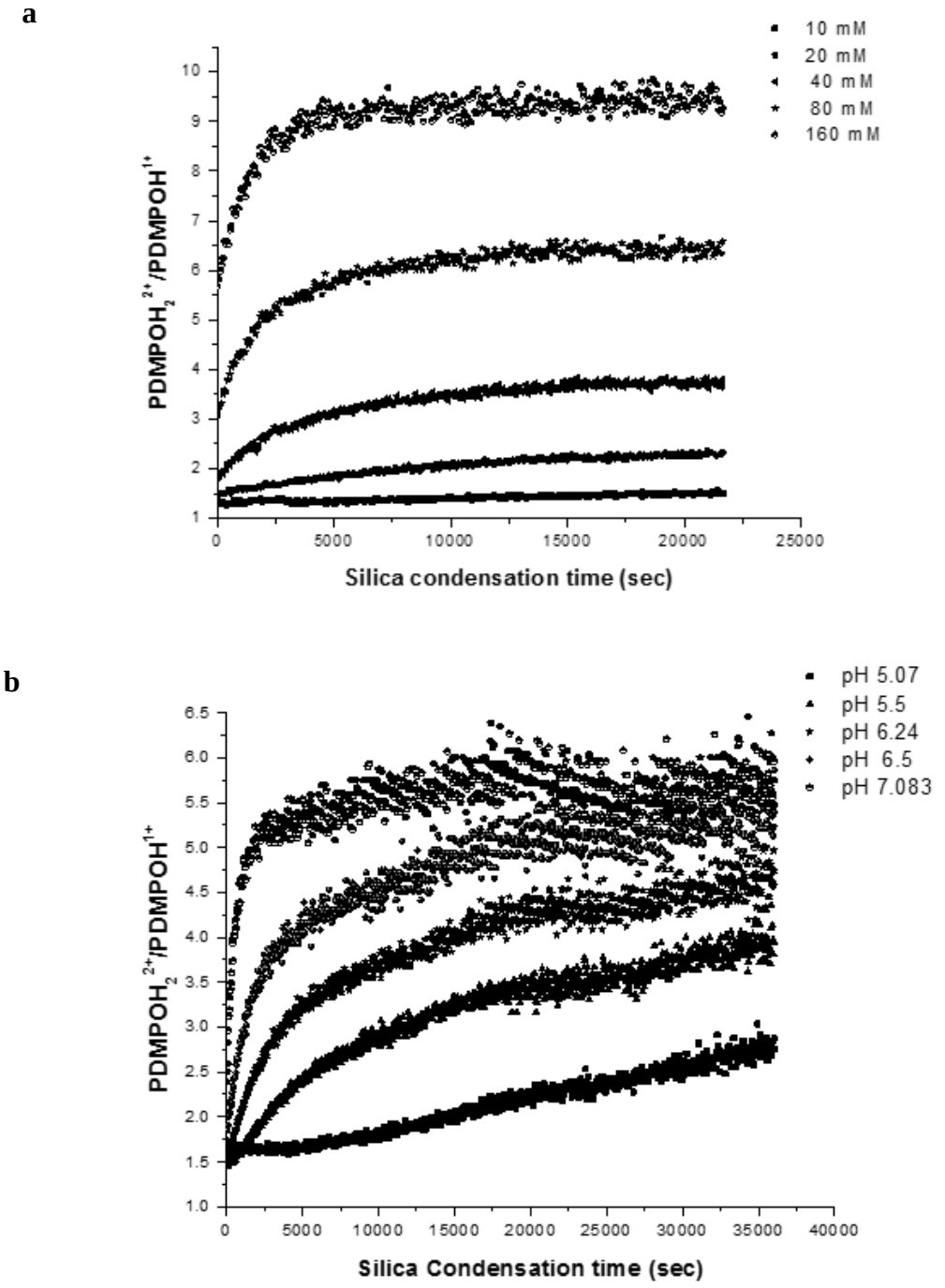

Figure 4.13 (a) PDMPO emission in the presence of different TEOS concentrations. (b) PDMPO emission in the presence of different TEOS concentrations (10 mM, 20 mM, 40 mM, 80 mM, 160 mM at pH 7.08) (b) A 40 μM TEOS solution after hydrolysis pH was

raised to 7.08, 6.50, 6.24, 5.50, 5.07 using a buffered system to carrying out silica condensation and fluorescence emissions were monitored.

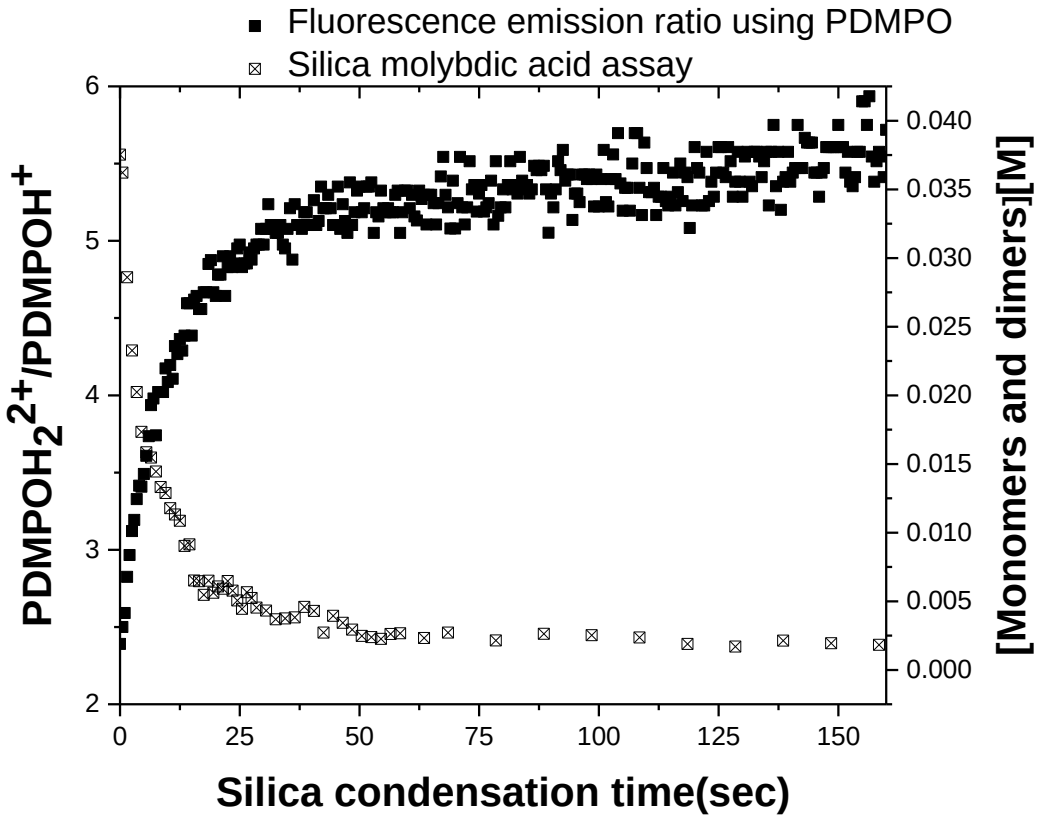

Figure 4.14. Comparative study in monitoring silica condensation using PDMPO based fluorescent method and absorbance based molybdenum blue method.

A simultaneous study on silica condensation using the molybdenum blue method was performed at 40 mM TEOS concentration (**Figure 4.14**). The molybdenum blue method determines the concentration of monomers and dimers of silicic acid. In the first 360 secs there was rapid increases in fluorescence emissions from $PDMPOH_2^{2+}$ and molybdate reactive silica in the solution drops indicating silica polymerization. The fluorescence intensity increase is slightly slower than the Si-OH polymerization process, suggesting an increases in surface acidity on silica surface upon silica condensation. However two methods

cannot be compared directly as PDMPO based silica condensation is based on formation of polymeric silica which is a product of silica condensation and emission ratio observed is due the change in the surface charge density on the silica surface during silica condensation whereas molybdenum blue method determines reduction in concentration of monomers and dimers of silicic acid during silica condensation.

4.4 Discussion

4.4.1 How it works

We are demonstrating a simple fluorescent spectroscopic method for measurement of surface charge density on silica particles using fluorescent emissions ratios of $PDMPOH_2^{2+}$ and $PDMPOH^+$. There is size dependent and ion dependent change in surface charge potential on silica surface. PDMPO is distributed in the electrical double layer. Depending upon the strength of the double layer there is change in fluorescence emissions from the protonated and deprotonated state of the dye. When there was a change in surface charge either by the change in morphology of silica nanostructure or by the presence of other cations there was a corresponding change fluorescence emission ratio. The fluorescent emission ratio could be used as proxy method to calculate zeta potential over the dynamic range between -15 mV to -40 mV.

4.4.2 Advantages of the method

Confocal spectral imaging of silica PDMPO interaction merges two well established technologies. Confocal spectrum imaging on silica particles create a complete fluorescence emission spectrum of the specimen at every pixel location. However in conventional confocal imaging they have the problems of quantitatively determining amount of dye binding on silica. In this approach we are using PDMPO to easily distinguish between fluorescence emission arising from unbound PDMPO and fluorescence emissions arising from silica

PDMPO interaction by monitoring the wavelength shift which is explained in our previous study (Parambath *et al.* 2016, chapter 3 of this thesis). Another issue of using conventional fluorescence imaging is the diameter of the specimen in the Z axis. The diameter of the specimen can range from nanometres like parts of ridges on silica cell wall to microns like the basal portion of stem of the Equisetum resulting in higher fluorescence detected from thick parts of the specimen compared to thin parts, these kind of data lead to misinterpretation of data. In our ratio metric approach these problems are solved by using ratios which reduce the signal to noise ratio during confocal imaging.

4.4.3 Why do different silica nanostructures have different charge..?

Biological organisms, particularly plants and diatoms, deposit silica. Silica deposition in plants are believed to be amorphous silica and there are at least three types of silica deposition. The first silica associated with cell wall, the second those inside the cell lumen such as root intracellular space and the third is extra cellular deposits. These silica layers provide structural support, defence against predators a means of removing toxic quantities of silicic acid from the plants. Change in pH, membrane filtration and transpiration was considered as the cause of silica precipitation and aggregation. Different structural components of silica formed at different time intervals during plant development. At the early stage of development, that is within the seven days of after emergence of inflorescence, thin sheet and silica particles are formed. By 24 days globular materials are formed and fibrillary material are formed. It has been observed that different nanostructures formed in nature have different levels of dehydration (Perry et al 1990). Our recent theoretical and experimental framework of PDMPO to probe surface charge equips us to understand how silica production is controlled and its variation in surface chemistry, It can be used to validate inter particle and particulate polymer interaction. The results presented in **Figures 4.9 to 4.12** clearly shows the difference in surface charge density on the different anatomical

regions of *Equisetum arvense* and the *Nitzschia stellate.* The change in the surface charge density at the ultrastructure of silica motif for a particular anatomical region could relate and control the overall micromorphology of biosilica. Understanding the zeta potential values on ultrastructure of biosilica can give circumstantial evidence for the involvement of silica motifs in water transport and other biochemical activities. The ability of the dye to facilitate *in-vivo* studies make this method very useful compared to complimentary methods like zeta potential measurements using light scattering and potentiometric methods. Biosilicifying organisms like bacteria, algae, plants insects are able to extract silica precursors from the environment and transport them to specific deposition sites where they undergo silica condensation. Most established technique in silica condensation studies, particularly the molybdenum blue method is not fruitful in studying real time analysis of silica condensation in biosilicifying organisims. Our method based on silica PDMPO interaction can give very good insight about the silica condensation in biosilicifying organisims. Developing an empirical model between molybdenum reactive silica and PDMPO dependent surface charge could become very powerful tool in the area of biosilicification.

4.5 References

Barisik, M., *et al..*, 2014. Size Dependent Surface Charge Properties of Silica Nanoparticles. *Journal of Physical Chemistry C,* 118 (4), 1836-1842.

Belton, D.J., Deschaume, O. and Perry, C.C., 2012. An overview of the fundamentals of the chemistry of silica with relevance to biosilicification and technological advances. *Febs Journal,* 279 (10), 1710-1720.

Borlinghaus., R., 2006. True confocal resonant scanning: a better solution for high-speed multifluorescence optical sectioning. *Nature Methods,* Supplement , 24-25.

Brown, M.A., Bossa, G.V. and May, S., 2015. Emergence of a Stern Layer from the Incorporation of Hydration Interactions into the Gouy-Chapman Model of the Electrical Double Layer. *Langmuir,* 31 (42), 11477-11483.

Cho, G.S., *et al..*, 2014. Characterization of surface charge and zeta potential of colloidal silica prepared by various methods. *Korean Journal of Chemical Engineering,* 31 (11), 2088-2093.

Coradin, T., Eglin, D. and Livage, J., 2004. The silicomolybdic acid spectrophotometric method and its application to silicate/biopolymer interaction studies. *Spectroscopy-an International Journal,* 18 (4), 567-576.

Demchenko, A.P., 2002. The red-edge effects: 30 years of exploration. *Luminescence,* 17 (1), 19-42.

Dale., T. Rebek., J . 2006. Fluorescent sensors for organophosphorus nerve agent mimics. *J Am Chem SoC, 12;128(14):4500-1.*

Elbergali, A., Nygren, J. and Kubista, M., 1999. An automated procedure to predict the number of components in spectroscopic data. *Analytica Chimica Acta,* 379 (1-2), 143-158.

Grahame, D.C., 1947. The electrical double layer and the theory of electrocapillarity. *Chemical Reviews,* 41 (3), 441-501.

Ikuma, K., et al., 2014. Deposition of nanoparticles onto polysaccharide-coated surfaces: implications for nanoparticle-biofilm interactions. *Environmental Science-Nano,* 1 (2), 117-122.

Kroutil, O., et al., 2015. Computer Simulations of Quartz (101)-Water Interface over a Range of pH Values. *Journal of Physical Chemistry C,* 119 (17), 9274-9286.

M.Parambath, Q. S. Hanley, F. J. Martin-Martinez, T. Giesa, M. J. Buehler and C. C. Perry, 2016. The nature of the silicaphilic fluorescence of PDMPO. *Phys. Chem. Chem. Phys,* .

Makino, K. and Ohshima, H., 2010. Electrophoretic Mobility of a Colloidal Particle with Constant Surface Charge Density. *Langmuir,* 26 (23), 18016-18019.

Malvern Instruments Ltd, 2004. *Zetasizer Nano Series User Manual Zetasizer Nano Series User Manual.* 1.1st ed. England: MAN0317.

Ovanesyan, Z., et al., 2016. Ion-ion correlation, solvent excluded volume and pH effects on physicochemical properties of spherical oxide nanoparticles. *Journal of Colloid and Interface Science,* 462, 325-333.

Perry, C.C., Moss, E. and Williams, R., 1990. A staining agent for biological silica. Proceedings of the Royal Society B-Biological Sciences, 241 (1300), 47-50

Perry, C.C., and Lu., Y . 1992. Preparation of silicas from silicon complexes: role of cellulose in polymerisation and aggregation Control, 241 (1300), 47-50..

Prakash, S., et al., 2015. Electrokinetic transport in silica nanochannels with asymmetric surface charge. *Microfluidics and Nanofluidics,* 19 (6), 1455-1464.

Puddu, V. and Perry, C.C., 2014. Interactions at the Silica-Peptide Interface: The Influence of Particle Size and Surface Functionality. *Langmuir,* 30 (1), 227-233.

Ralph K. Iler, 1979. *The Chemistry ot Silica.* , New York: John Wiley and Sons.

Roach, P., Farrar, D. and Perry, C., 2006. Surface tailoring for controlled protein adsorption: Effect of topography at the nanometer scale and chemistry. *Journal of the American Chemical Society,* 128 (12), 3939-3945.

Salis, A., et al., 2016. Effect of electrolytes on proteins physisorption on ordered mesoporous silica materials. *Colloids and Surfaces.B, Biointerfaces,* 137, 77-90.

Scarminio, I. and Kubista, M., 1993. Analysis of Correlated Spectral Data. *Analytical Chemistry,* 65 (4), 409-416.

Sola, L. and Chiari, M., 2015. Tuning capillary surface properties by charged polymeric coatings. *Journal of Chromatography A,* 1414, 173-181.

Wisniewska, M., et al., 2015. Adsorption mechanism of poly(vinyl alcohol) at the mixed oxide CuxOy-SiO2/aqueous solution interface. *Applied Surface Science,* 356, 905-910.

Yuan, L., Lin, W. and Yang, Y., 2011. A ratiometric fluorescent probe for specific detection of cysteine over homocysteine and glutathione based on the drastic distinction in the kinetic profiles. *Chemical Communications,* 47 (22), 6275-6277.

Chapter 5

An optical interrogation method to study silica-biomolecule interaction

This chapter explores a newly developed optical interrogation method using confocal microscopy to study silica biomolecule interactions using PDMPO silicaphilic fluorescence. This technique is further used to screen silica binding interactions using aminoacids, polyamines and peptides.

5.1. Introduction

Silica binding interactions are of great interest in chemistry, biochemistry, biophysics and have wide applications ranging from protein adsorption (Hyun, et al. 2002) and cell adhesion, biomaterials (Hickman, et al. 2012), to the selective response to biosensors (Monton, Forsberg and Brennan 2012). Binding studies on silica are now done using surface plasmon resonance spectroscopy (SPR) (Liu, Peng and Li 2014), quartz crystal microbalance (QCM) (Jachimska, et al. 2016, Vashist and Vashist 2011), calorimetry (Wang, et al. 2013) and fluorescence based techniques (Schaeferling 2012). Fluorescence based techniques are widely accepted due to their high sensitivity, diverse selection of fluorescent probes, ease of operation and numerous readout modes. Most of the fluorescence based techniques require fluorescent labelling of the analyte. Fluorescent labelling is achieved either intrinsically or extrinsically. A weak intrinsic fluorescence from silica is achieved due to oxidation on the silica surface (Spallino, et al. 2014), however weak fluorescence limits the potential as an analytical probe. Extrinsic probes are either fluorophores encapsulated in silica spheres or fluorescent dyes covalently grafted onto the surface of silica, Neither approachs is not fruitful to study silica biomolecule interaction (Veeranarayanan, et al. 2012). Dye encapsulation cannot be used to study surface phenomena while covalent grafting can induce perturbations induced by the surface characteristics . For studying silica biomolecule interactions on a silica surface, a noncovalently associated probe is desired and there are limited noncovalent associated fluorescent tracers available for silica. However our improved understanding of the silicaphilic nature of a noncovalent associated fluorescent probe PDMPO as a silica

tracer (Chapter 3, (Parambath, et al. 2015)) equipped us to use this molecule for quantitative understanding on silica binding interactions. Major fluorescence based techniques that are widely used for binding interactions include fluorescence polarization (FP) (Reindl, Strebhardt and Berg 2008), fluorescence resonance energy transfer (FRET) (Ishikawa-Ankerhold, Ankerhold and Drummen 2012), flowcytometry based assays (FC) (Dennis, et al. 2008), fluorescence correlation spectroscopy (FCS) (Yirdaw and Mchaourab 2012) and total internal reflection fluorescence (TIRF) (Matveeva, et al. 2004). Fluorescence polarization measurements provides data on molecular orientation and the mobility processes that modulate them and polarization is a general property of the fluorescent molecules. FP is of restricted utility for interactions between two large molecules and limits of detection tend to be higher than for fluorescence intensity methods (Böhlen, et al. 1974) while FRET methods are limited by factors like fluorophore orientation and FRET pair labelling (Ishikawa-Ankerhold, Ankerhold and Drummen 2012). FCS demands complex instrumentation whereas FC and TIRF require immobilisation (Dennis, et al. 2008b).

An optical sectioning technique (OST) is the process by which one can produce images of different focal planes within a thick sample. Major traditional methods in OST includes computational optical sectioning microscopy, two-photon excitation microscopy, second harmonic generation imaging microscopy, STED, 4Pi and structured illumination. Computational optical sectioning microscopy use a wide field microscope to collect the two dimensional image of the specimen and computational methods are used to remove out of focus light followed by generation of optical slices (Conchello and Lichtman 2005). Two-photon excitation microscopy requires simultaneous absorption of two long wavelength photons by a fluorescent molecule thereby the combined energy induces an excited state. The combined energy is equal to the normal one photon excitation (Esposito, et al. 2004). Second harmonic generation imaging microscopy uses a nonlinear optical process in which photons

with the same frequency interacting with a nonlinear material are effectively combined to generate new photons with twice the energy, and therefore twice the frequency and half the wavelength of the initial photons (Kristensen and Pedersen 2004, Sergeyev, et al. 2015) Stimulated emission depletion (STED) microscopy creates super-resolution images by the selective deactivation of fluorophores, engineering the shape of the point spread function, and thus enhancing the achievable resolution for a given system(Peuschel, et al. 2015). 4Pi microscopy can be a laser scanning microscopic technique extended by having two precisely aligned identical objective lenses increase the effectiveness to achieve a z-resolution down to 80 nm (Hell, et al. 1994). Structured illumination microscopy works by the interaction of a high frequency three-dimensionally modulated illumination pattern with high frequency variations in the sample fluorescence caused by very small structures (Gustafsson 2005). In our study we are developing confocal laser scanning microscopy (CSLM) to screen silicaphilic substrates involved in biosilicification and silica binding interactions. Optical sectioning methods using CSLM have been used for immunoassays (Ghafari, et al. 2009) and receptor ligand interaction studies (Ghafari, Parambath and Hanley 2012). However, no studies have applied CSLM to screen silicaphilic substrates or to study surface interactions utilizing the silicaphilic nature of PDMPO.

Screening of silicaphilic substrates for biosilicification and silica binding interactions are performed using an optical sectioning planar format assay technique called a planar format assay (OSPFA). Confocal microscopy was used for interrogations the planar format assay. Confocal microscopy is an optical sectioning technique used to obtain physical sections with high axial resolution thereby facilitating three dimensional imaging. The invention of the confocal microscope is usually attributed to Marvin Minsky, who produced a working microscope in 1955 (Marvin Minsky 1957). In a normal wide field fluorescence microscope, the total volume of the specimen is uniformly and simultaneously illuminated and

fluorescence emissions are collected. This can also results in out of focus blur from above and below the specimen which can have adverse effects on the contrast with low signal to noise ratio and with high background fluorescence. In a confocal microscope out of focus light coming from above and below the samples focal plane are eliminated by a pinhole (small aperture). As a result only the part of specimen which in focus with both illumination and detection pinholes is observed. Parameters affecting the confocal microscopy include numerical aperture (NA and (two) the size of pinhole.

The silicaphilic fluorescence of PDMPO was coimbined with a optical sectioned planar format assay (OSPFA) format to provide a new approach to study molecular binding on silica. This methodology can be widely used as a complimentary technique to other techniques such as fluorescence polarisation studies, QCM (quartz crystal microbalance) and SPR (surface plasmon resonance spectroscopy) to study silica binding interactions.

5.2 Materials and methods

PDMPO (LysoSensor™ yellow/blue DND-160, 1 mM in dimethyl sulfoxide) was obtained from Life Technologies, aniline hydrochloride, ammonium persulfate, glutaric dialdehyde, amino acids, lysozyme, tetramethyl orthosilicate (TMOS), polyamines (1-4 diaminobutane, octadecyl amine, spermine, spermidine) and phosphate buffer prepared using monobasic sodium phosphate monohydrate and dibasic sodium phosphate were all obtained from Sigma Aldrich. 96 microwell glass bottom plates with a polystyrene sheet at the bottom of the plates were obtained from Nunc (164588). Polystyrene surfaces have some background fluorescence. Peptide (Pep 1 (KSLSRHDHIHHH)) a silica binding peptide identified by phage display (Patwardhan, et al. 2012) was obtained as a gift from Dr Marion Limo (NTU).

5.2.1 Silica fabrication procedure

The silica surface was prepared using an adaptation to a previously described protocol (Hickman, et al. 2012b, Nicklin, et al. 2014). Briefly, untreated tissue culture glass microwell plates was coated with a polyaniline film. This was performed by reacting 0.25 M aniline hydrochloride in 1 M HCl with 0.08 M ammonium persulfate in double distilled (dd) H_2O. Plates were then incubated at room temperature (RT) for 15 min followed by three washes with an excess of (dd)H_2O. Maintaining the same coating volumes, plates were treated with 2% (v/v) glutaric dialdehyde for 2 h at 57 °C followed by washing. Plates were then treated with 1 mg/ mL of lysozyme in phosphate buffer pH 7.2 for 2 h at RT and then washed. To prepare the silica surface, 0.5 M tetramethyl orthosilicate in (dd)H_2O was pre-hydrolysed in 1 mM HCl for 15 min. The pH of this solution was raised to 4 by adding 0.1 M NaOH in a drop-wise fashion prior to surface application (Nicklin, et al. 2014). Plates were incubated for 2 h at RT to allow for silica film formation and were then washed once more with distilled water.

5.2.2 Instrumentation

The confocal scanning laser microscope (CSLM) used was from Leica microsystems (Leica TCS SP5). The 405 nm laser line was used for excitation of PDMPO. Confocal parameters used are numerical aperture (0.5 NA) with objectives (20×) were used with a pinhole size of 84 µm with 400 steps of 0.5 µm. PMT gain (1000 V) offset (2.7 %) and laser intensity (29 %) were kept constant in all experiments. The axial response beginning from 80 µm above the polystyrene sheet was selected for binding studies as in (**Figure 5.1**.)

5.2.3 Theoretical section

The key part of confocal detection of OSPFA is a fluorescent thin layer (C1) formed between PDMPO and the silica surface which does not exceed the Stern layer on the silica surface (**Figure 5.1**). The thickness of the Stern layer is estimated to be less than 10 nm (Herbowski,

Gurgul and Staron 2009, Zhang, et al. 2011). The thickness of the silica PDMPO thin layer (C1) cannot be measured using CSLM due to the diffraction limit. However, the axial position of the thin layer (C1) and fluorescence light emissions from the thin layer (C1) can be measured using CSLM. The response of silica PDMPO interactions can be considered as the sum of the response of a thin layer (C1) (<10 nm) with a fluorescent concentration of (C_1) and a fluorescent over layer beginning 10 nm above the silica surface with concentration (C_2). In this study a semi empirical approach using the Cauchy-Lorentz function and the cumulative Cauchy-Lorentz function (Ghafari, et al. 2009, Ghafari, Parambath and Hanley 2012) was applied for fitting the data (eqn 5.1).

$$M(z) = C_1 \frac{1}{\pi\gamma\left[1+\left(\frac{(z-z_0)^2}{\gamma}\right)\right]} + C_2\left(\frac{1}{\pi} arctan\frac{(z-z_0)}{\gamma} + \frac{1}{2}\right) + B \qquad (eqn\ 5.1)$$

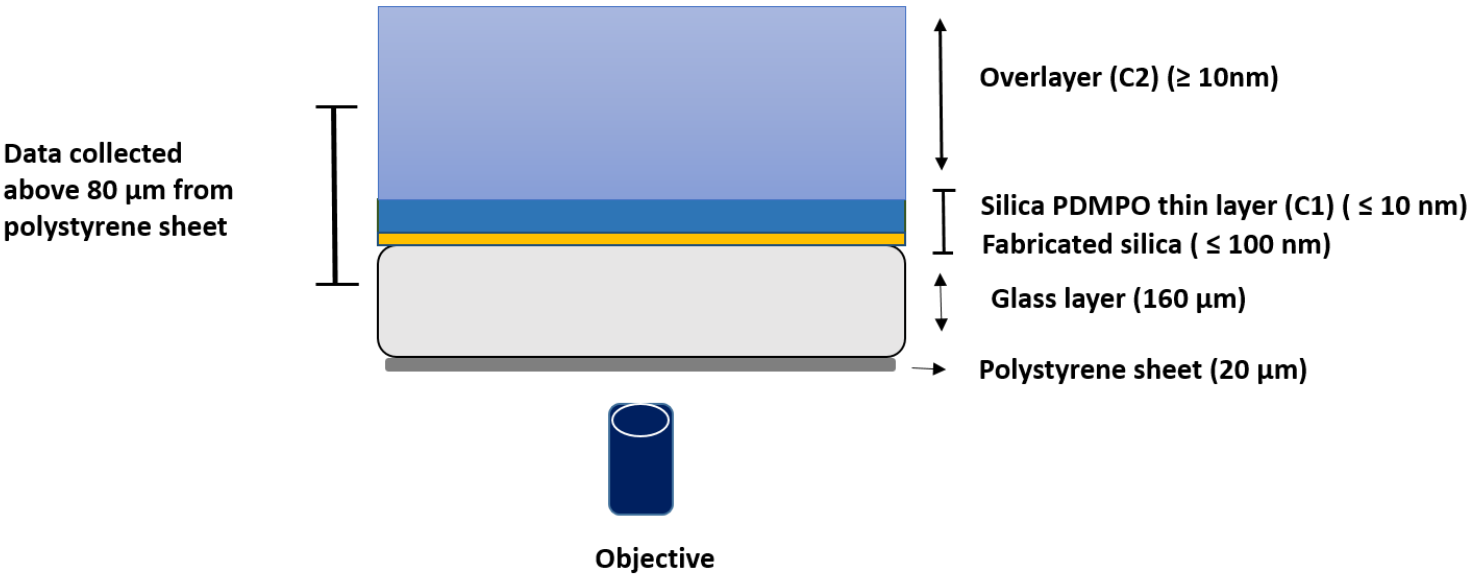

Figure 5.1: Schematic representation of the optical sectioned planar format assay for silica binding interaction using PDMPO in a 96 well glass bottom plate from Nunc (164588). (The figure is a schematic representation not drawn according to the scale.)

Where M (z) is the measured axial response from CSLM, Z_0 is the centre of silica PDMPO thin film, γ is the width of the response and B is the constant which corrects for electronic offset and the photomultiplier tube background in the confocal microscope. The first part of the equation is dependant and related to PDMPO on the silica thin layer (C1) while the second part is related to over layer concentration (C2) which is above the silica PDMPO thin layer (C1).

5.2.4 Fluorescence anisotropy

Fluorescence anisotropy was measured using a Tecan F200 with excitation filter 360/35 nm and emission filter 540/35 nm. The PMT gain setting was 40 and the G factor 1.256.

5.2.5 Estimation of silica on the fabricated surface: The fabricated silica surface was treated with 1 M NaOH. The dissolved silica concentration (200 µL) was determined by the molybdosilicate method. This consists of two solutions, Solution A is made of 20 g ammonium molybdate tetrahydrate and 60 ml of concentrated hydrochloric acid in deionized water. Solution B is prepared by adding oxalic acid (20 g), 4-methylaminophenol sulphate (6.67 g), anhydrous sodium sulfite (4 g), deionised water (500 mL) and concentrated sulphuric acid (100 mL) in a 1 L volumetric flask and filled to the mark with deionised water. In a typical experiment, 200 µL of the unknown silicic acid solution was sampled and diluted to 3.2 mL with deionised water. To this was added 300 µL of solution A. After 10 min, 1.5 mL of solution B was added to the assay solution. The blue colour was left to develop over 2 h at room temperature before measuring the optical density at λ = 810 nm using a Tecan M200. A standard solution of different silicic acid concentration ranges (0.05 PPM to 0.3 PPM) was used to estimate silica on the fabricated surface. The molar extinction coefficient of the molybdenum blue complex at 810 nm is 44700 ± 150 l mol^{-1} cm^{-1} making it suitable for the dynamic range (Coradin, Eglin and Livage 2004).

5.2.6 Silica PDMPO interaction.

Silica PDMPO interaction studies were performed with 1 µM PDMPO, in a 200 µL volume unless mentioned otherwise. Scanning using a confocal microscope was performed after 15 min incubation. A PDMPO dose response (1 nM to 10 µM) was analysed after dosing PDMPO onto the silica surface. Experiments were carried out in 200 µL volumes of phosphate buffer (0.1 M) at pH 7.1. Dose dependent curves were fitted to a Langmuir equation (Irving Langmuir 1918).

$$F = \frac{F_{max}[c]}{K_d + (c)} \qquad (eqn\ 5.2)$$

In this equation, F is the observed maximum thin layer intensity (C1), F_{max} is the maximal thin layer intensity for the highest concentration, [c] the concentration of PDMPO in the solution, and K_d is the thermodynamic dissociation constant at equilibrium. Three parameters are fitted for five data points.

5.2.7 Indicator displacement assays

5.2.7.1 Simultaneous indicator assay (SIDA)

SIDA requires three steps. The first step is fabrication of hydroxylated silica on a 96 well plate. The second step is presentation of PDMPO and a silicaphilic substrate (lysine) to the fabricated silica surface. The third is detection of fluorescence along the z axis using the confocal microscope. A constant amount of PDMPO (2 µM in 100 µL) was incubated with varying concentrations of silicaphilic substrates (2 nM to 2 mM in 100 µL). Binary solutions of PDMPO with lysine are presented to the silica surface with final concentrations of 1 µM of PDMPO and varying concentrations of lysine (1 nM to 1 mM) in a total volume of 200 µL followed by a 2 h incubation and confocal scanning. All experiments in this work were performed in phosphate buffer (0.1 M) at pH 7.1.

5.2.7.2 Subsequent indicator assay (SQIDA)

SQIDA requires four steps. The first step is fabrication of hydroxylated silica on a 96 well plate. The second step is presentation of PDMPO to the fabricated silica surface, followed by incubation for 2 h and washing of the plates using distilled water. The third is presentation of silicaphilic substrates followed by incubation for 2 h and the fourth step is detection of

fluorescence along the axis using confocal microscope. In a typical SQIDA PDMPO (1 µM) of 200 µL prepared in phosphate buffer (0.1 M) at pH 7 was added to a silica surface and incubated for 2 h. Microwell plates were washed in distilled water for three times and air dried followed by addition of the competitive analyte (lysine), (1 µM) in 200 µL was added subsequently to the silica surface. Microplates were incubated for 2 h before subjected to confocal scanning. A dose dependent analysis was performed using different concentrations of analyte from 1 mM to 1 nM.

5.2.8 IC_{50} calculation

IC_{50} is the concentration of silicaphilic substrate where silica PDMPO thin layer (C1) is reduced by half. IC_{50} was calculated using eqn. 5.3 (Cheng and Prusoff 1973).

Equation 2

$$Y(X) = \frac{A - B}{(1 + 10^{(X - LogIC_{50})})} \qquad \text{(eqn 5.3)}$$

Where Y(X) was the observed or normalised intensity (C1) at a particular concentration of unlabelled displacing ligand (X), A is the maximal signal, B is the non-specific interaction.

5.2.9 Z' Factor analysis

The efficiency of an indicator displacement assay was monitored using Z' factor analysis (Zhang, Chung and Oldenburg 1999). Z' factor analysis was performed for both SIDA and SQIDA. To evaluate Z' factor maximum thin layer intensity (C1) was used. Z' factor was calculated using equation 5.4.

Equation 3

$$Z' = 1 - \frac{(3SD_p + 3SD_n)}{|\mu_p - \mu_n|} \qquad \text{(eqn 5.4)}$$

SD_p is the standard deviation of the maximum thin layer (C1) intensity of three positive controls and μ_p is the mean of maximum thin layer (C1) intensity of the positive control. SD_n is the standard deviation of three negative controls and μ_n is the negative control. In the experiment the reagent blank is taken as the negative control. Assays with Z' factor values between 0.5 to 1 are considered good to excellent assays (Zhang, Chung and Oldenburg 1999).

5.2.10 Screening of silicaphilic substrates using subsequent indicator assay

The screening assay was applied to many silicaphilic reagents particularly with polyamines (1-4 diaminobutane, octadecyl amine, spermine, and spermidine) and amino acids (histidine, alanine, cystine, lysine, aspartic acid). SQIDA was used for screening assay.

5.2.11 Screening of silicaphilic substrates using fluorescence anisotropy.

The fluorescence anisotropy of the PDMPO in combination with different concentrations of silicaphillic substrates (amino acids and polyamines). Fluorescence anisotropy was performed on fabricated silica surfaces and non-fabricated silica surfaces. Fluorescence anisotropy on hydroxylated silica surfaces (fabricated surfaces) was used to compare SQIDA. Fluorescence anisotropy on non-fabricated surface was monitored to study substrate (amino acids and polyamines)-PDMPO interactions.

5.2.12 Charge determination on silicaphilic substrates was performed using SPARC.

The SPARC computational approach is based on the combination of well-established structure activity relationships, linear free energy relationships and perturbed molecular orbital theory to estimate pK_a and charge on molecules like polyamines (1- 4 diaminobutane,

octadecyl amine, spermine, spermidine) and amino acids (histidine, alanine, cysteine, lysine, aspartic acid).

5.2.13 Dose dependent assay on silicaphilic substrates using silicaphilic fluorescence of PDMPO

Dose dependent experiments (1 nM to 1 mM), were done using the peptide pep1 (KSLSRHDHIHHH from N to C terminal), a silica binding peptide identified by phage display (Patwardhan, et al. 2012), a positively charged amino acid (lysine) and with a negatively charged amino acid (aspartic acid).

5.2.14 Calculation of Inhibitor binding (K_i) constant from IC_{50}

IC_{50} is converted to inhibitor binding (K_i) using the Cheng prussoff competitive equation. K_i refers to the concentration of the silicaphilic substrate which would occupy 50% of the silica binding sites in the absence of PDMPO. IC_{50} is calculated using eqn. 5.3, L is the concentration of PDMPO, K_d is the dissociation constant of PDMPO calculated using eqn. 5.2 (Coleska et al 2004).

$$K_i = \frac{IC50}{\frac{L}{(K_d + 1)}} \qquad (eqn\ 5.5)$$

5.3 Results and discussion

5.3.1 Silica PDMPO interaction in a planar format confocal assay

Silica PDMPO interactions in a planar format assay (OSPFA) result in an axial response when scanned with CSLM as in the (**Figure 5.2)**. This axial response from a typical silica PDMPO interaction consisted of three distinctive features, one a region with decreasing fluorescence signal which is the glass surface below the silica surface (below 200 µm), second a prominent fluorescent layer formed due to silica PDMPO interaction between 200 µm to 300 µm, third a region above 300 µm of decreasing fluorescence and reaching to a constant value which results from fluorescence of the over layer generated by unbound PDMPO. Upon separation using the Cauchy Lorentz and cumulative Cauchy Lorentz function fluorescence from the silica PDMPO thin layer (C1) and unbound PDMPO over layer was separated as in (**Figure 5.2.b**). The sum of the thin layer (C1) and over layer was found to fit very well with the measured function from CSLM as in (**Figure 5.1.b.)** Maximum thin layer intensity obtained from (Figure 5.2.b) using eqn. 5.1 was used to study silica surface interactions. Dose dependent effects of PDMPO on silica surface were investigated. Binding affinity of PDMPO on the silica surface was determined using different PDMPO concentrations (1 nM to 1 µM) which was followed by decomposition into the silica PDMPO thin layer (C1) and unbound PDMPO over layer (C2). Dose dependent effects on PDMPO were monitored using increases in the concentration of silica PDMPO thin layer C1 calculated using eqn. 5.1 **(Figure 5.2.b.**) The amount of silica on each microwell plate was determined using the silicomolybdic assay using a standard solution of monosilicic acid (Appendix 1) and it was found to be 0.235 µg/mL.

a

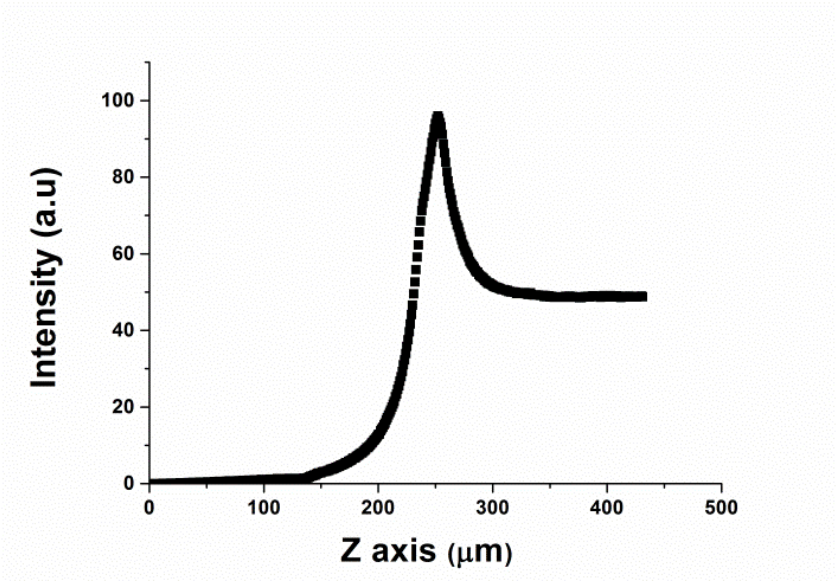

b

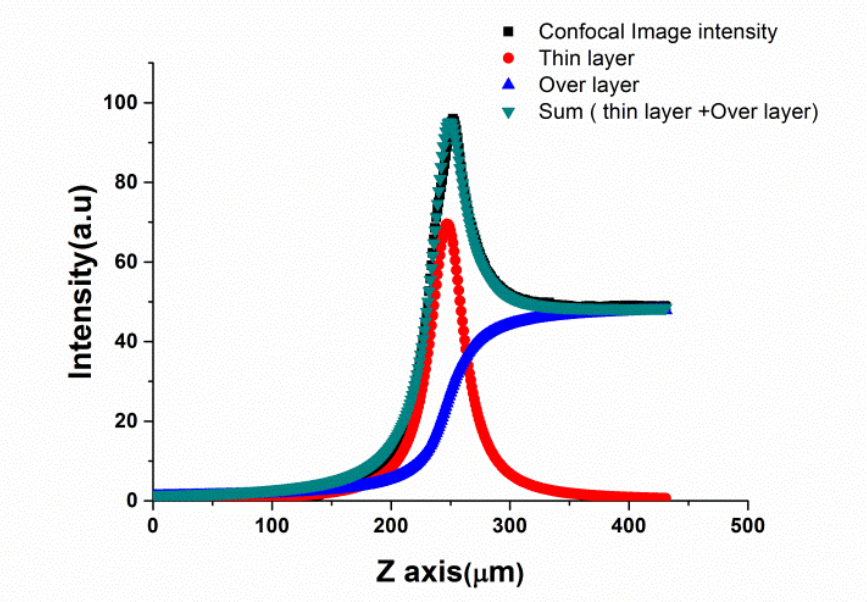

Figure 5.2: The Axial response of PDMPO on a silica surface has three distinct layers, (1) region below 200 µm which is the glass layer of the well plate, which is followed by a (2) silica PDMPO thin layer (C1) between 200-300 µm and (3) fluorescent overlayer above 200µm. (a) The measured response from CSLM (b) results following equ 5.1 (sum of thin layer and over layer fitted with measured response function).

a

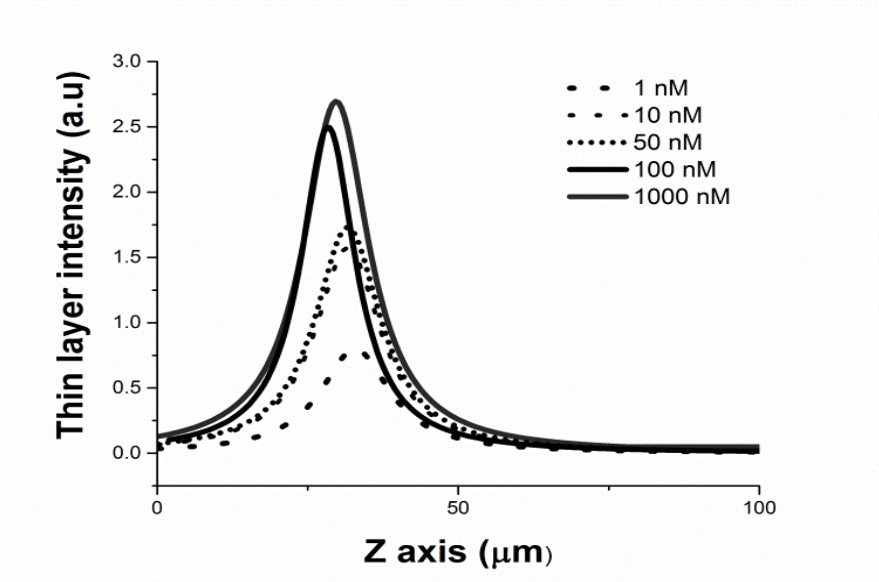

b

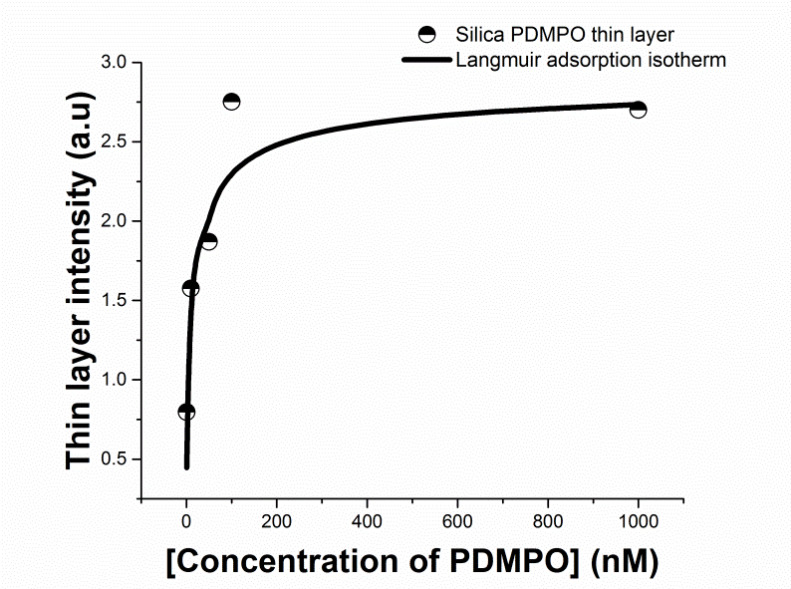

Figure 5.3: Decomposition of the measured response function for PDMPO thin layer (C1) and over layer. (a) Experimentally measured confocal response is decomposed to silica PDMPO thin layer (C1) upon dose dependent increases in PDMPO concentration. (b) Adsorption of PDMPO on silica surfaces fits with a Langmuir adsorption isotherm with a binding constant of 4.6 nM.

Adsorption of PDMPO onto silica surfaces fits with a Langmuir adsorption isotherm with a binding constant of 4.6 nM (**Figure 5.3.b**). With increases in PDMPO concentration there is corresponding increase in silica PDMPO thin layer (C1) formation (**Figure 5.3.a**) and the FWHM remains constant at 6 μm (+/- 0.5 μm) between different concentrations. FWHM of the intensity profile in the z direction is used as a measure of optical sectioning performance.

5.3.2 Indicator displacement assays

In an indicator displacement assay a fluorescent indicator PDMPO binds to silica, in the presence of other silica binding reagents the fluorescent indicator gets displaced and this can be detected OSFPA. We have designed two types of indicator displacement assay; simultaneous indicator assay (SIDA) and subsequent indicator assay (SQIDA).

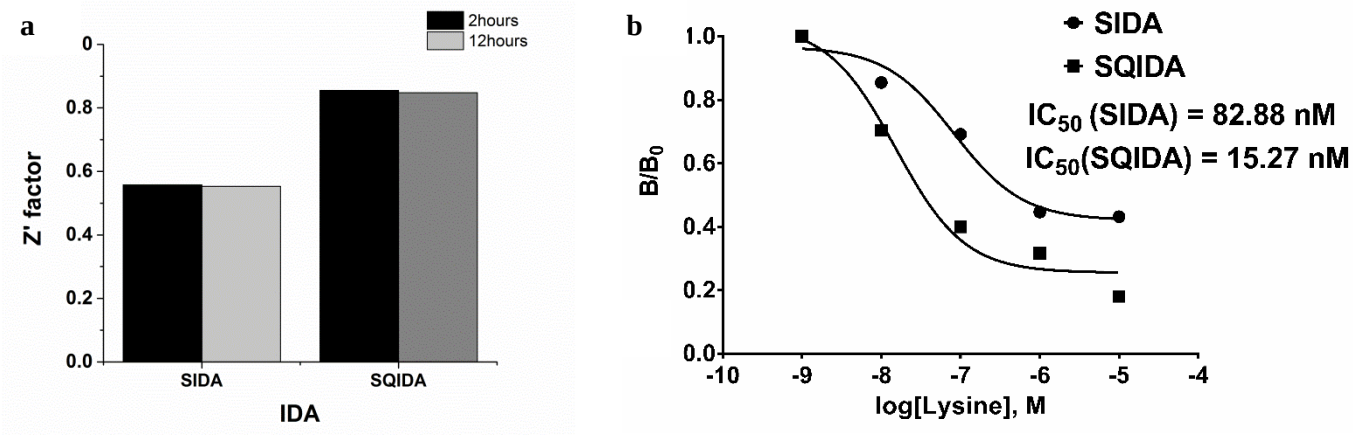

.

Figure 5.4: Indicator displacement assay: (a) Z' factor values estimated on SIDA and SQIDA. (b) IC_{50} values calculated based on maximum thin layer (C1) intensity on SIDA and SQIDA using a dose dependent study with lysine, B_0 is the maximum thin layer intensity in the absence of any silica binding reagents, B is thin layer intensity at different concentrations of silica binding reagents. IC_{50} values were calculated using a linear regression as in eqn. 5.3.

A comparative study between the simultaneous indicator assay (SIDA) and subsequent indicator assay (SQIDA) was performed with silica surfaces using different concentrations of lysine. Lysine has previously been demonstrated as a strong silica binder (Cherkouk, Rebohle and Skorupa 2011, Rimola, Sodupe and Ugliengo 2009). A dose dependent displacement of lysine was observed for both the simultaneous indicator assay and subsequent indicator assay. Adapting this assay for screening and to study silica biomolecule interactions requires a good statistical separation between positive and negative responses and this achieved by evaluating the Z' factor.

To evaluate the potential of SIDA and SQIDA three replicates of positive control (1 mM lysine) and negative control (no lysine) were used and experiments were carried after 2 h incubation. SIDA and SQIDA indicate a Z' factor of 0.55 and 0.85 receptively **(Figure 5.4.a)**. A longer incubation time up to 12 h did not result in a significant change in Z' factor value indicating that the reaction has reached equilibrium by two h. From Z' factor analysis we can infer that SQIDA is highly efficient for screening and silica biomolecule interaction. When SIDA and SQIDA was exposed to a series of lysine concentrations ranging from 1 nM to 10 µM plots of the concentration against maximum thin layer (C1) in equation 1 show a dose response. IC_{50} values were calculated as in equation (3) IC_{50} was calculated as 82.88 nM and 15.27 nM for SIDA and SQIDA respectively (**Figure 5.4.b)** A fivefold increases in IC_{50} values SIDA over SQIDA can be attributed to poor statistical separation between positive and negative responses. Non-specific fluorescence of 40% and 20% was observed for both SIDA and SQIDA respectively.

3.3 Screening of silicaphilic substrates using the silicaphilic fluorescence of PDMPO

The screening capability of SQIDA using OSPFA was demonstrated using the amino acids (**Figure 5.5.a)** histidine, lysine and pep 1 which exhibit a higher level of silica binding, resulting in a higher level of PDMPO displacement and subsequently a lower level of maximum thin layer intensity. For alanine and aspartic acid which exhibit a lower binding affinity, a lower level of PDMPO displacement occurs and subsequently a higher level of thin layer intensity. Fluorescence anisotropy studies (**Figure 5.5 b)** on fabricated silica surfaces were compared to OSPFA.

When PDMPO binds to silica it results in hindered rotation and higher anisotropy measurements, when amino acids and peptides with higher binding affinity bind with silica (histidine, lysine and pep 1) they displace PDMPO into solution, resulting in a higher rotational diffusion hence lower anisotropy while lower affinity amino acids (alanine, aspartic acid) exhibits higher anisotropy.

a

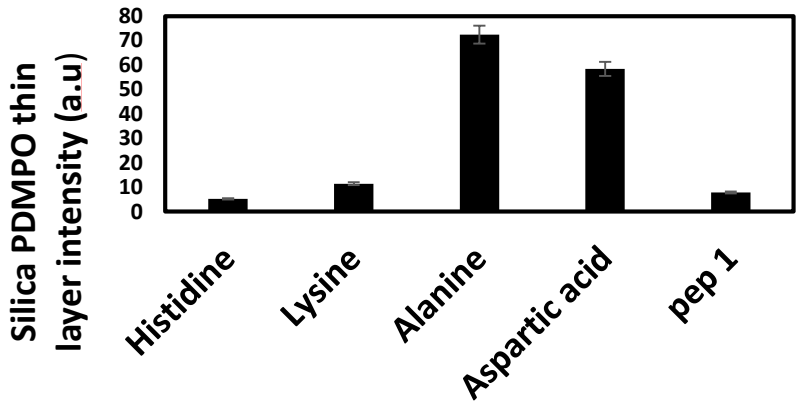

Figure legend on page 131

b

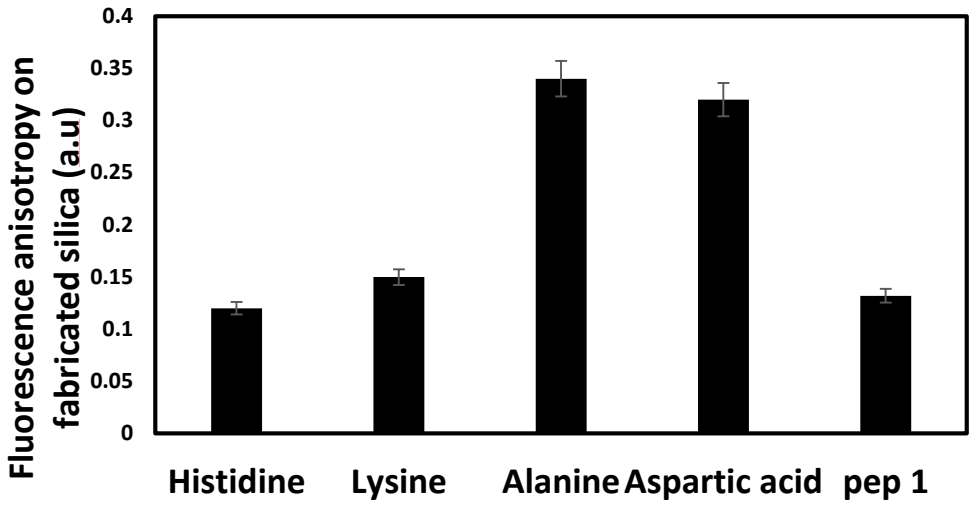

c

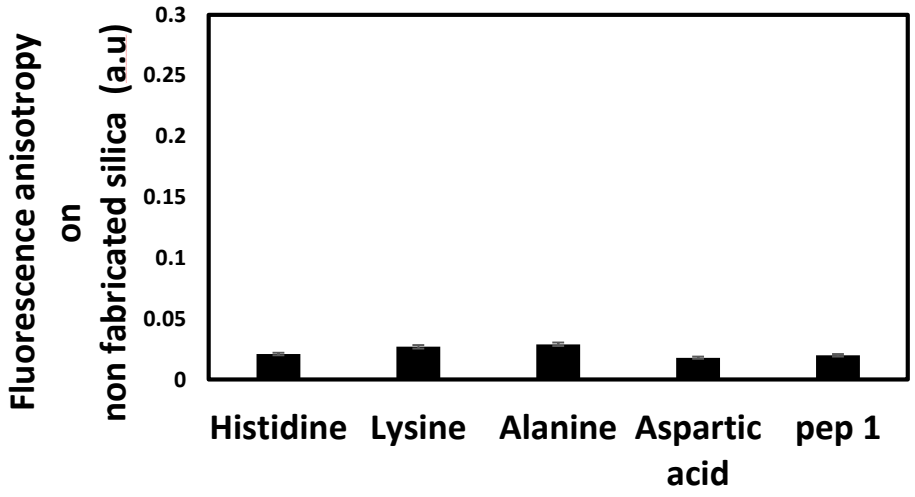

Figure 5.5: Screening of amino acids interacting with silica using SQIDA (a) Screening by SQIDA using an optical sectioned planar format assay (b) Screening by SQIDA using fluorescence anisotropy on a silica fabricated surface (c) Screening by SQIDA using fluorescence anisotropy on a non-fabricated surface

a

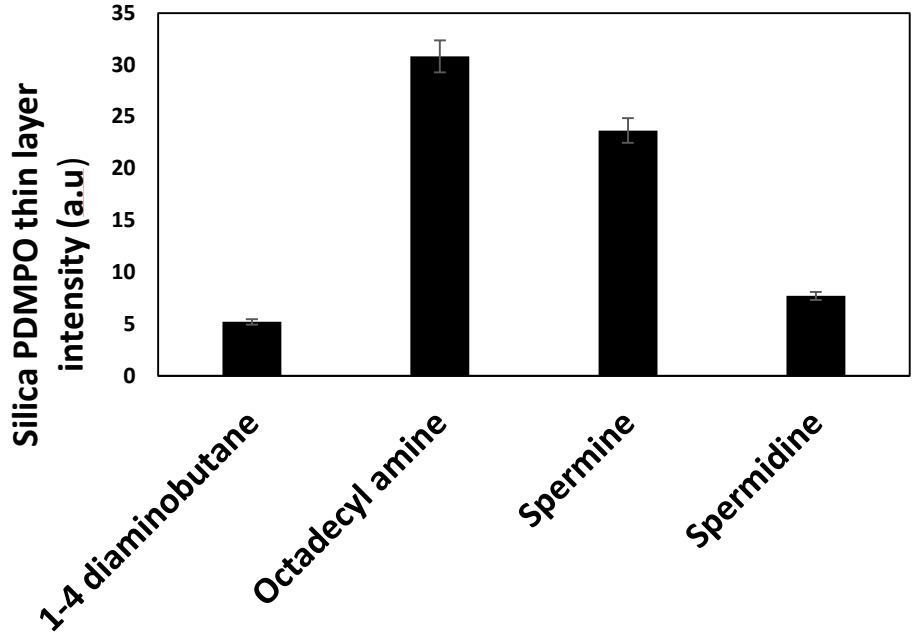

b

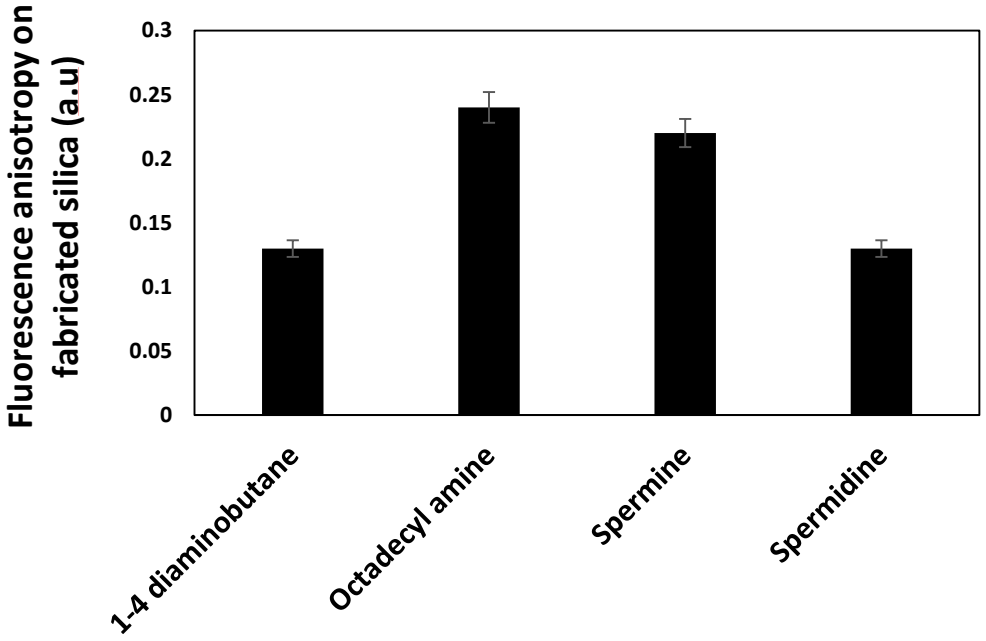

Figure legend on page 133

c

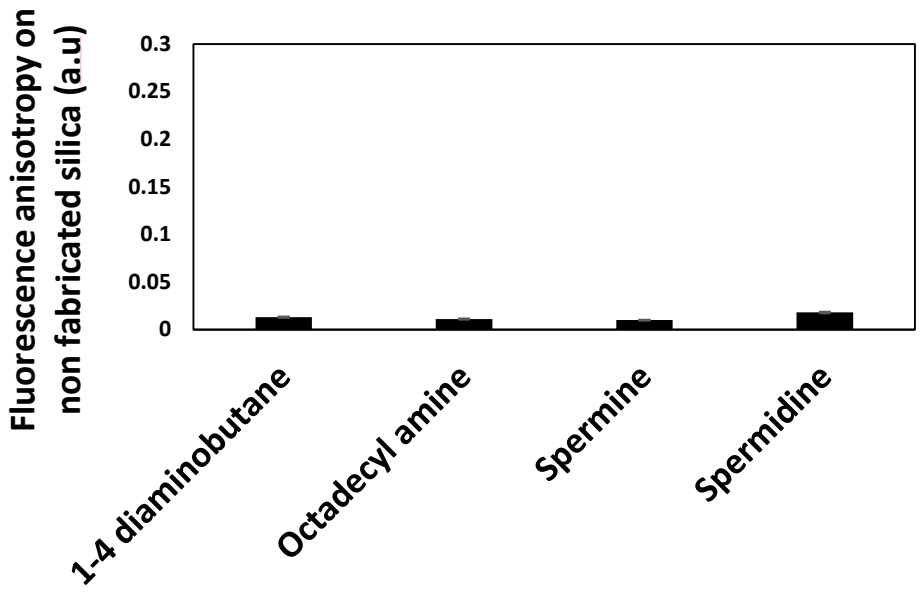

Figure 5.6: Screening of polyamines interacting with silica using SQIDA (a) Screening by SQIDA using an optical sectioned planar format assay (b) Screening by SQIDA using fluorescence anisotropy on a silica fabricated surface (c) Screening by SQIDA using fluorescence anisotropy on a non-fabricated surface

Correlation between OSPFA results (**Figure 5.5 b**) with fluorescence anisotropy results indicate that these techniques are complimentary techniques. Fluorescence anisotropy on non-fabricated silica surfaces (**Figure 5.5 c**) monitor nonspecific interactions between the screened amino acids and PDMPO, a higher rotational diffusion (lower anisotropy) indicates no complexation between the screened molecules and PDMPO either in the ground or excited state. The screening capability of the OSPFA was further studied using polyamines and SQIDA. Polyamines are organic molecules which are involved in species specific mineral patterns in bio silicifying organisms (Sumper and Brunner 2006, Belton, et al. 2008).

Table 1

Screening compounds	**pK_a**	**Net Charge at pH 7**
14 dibutamine	pK_1=8.82	+1.991
Octa decylamine	pK_1 =10.41	+1
Spemidine trihydrochloride	pK_1 =6.97, pK_2 =8.25	+2.7
Spermine tetrahydrochloride	pK_1 = 6.97 pK_2 = 8.25	+3.
Aspartic Acid	pK_1=1.86,pK_2 =4.18	-0.999
Alanine	pK_1=2.36,pK_2 =9.65	-0.001
Histidine	pK_1 =1.94, pK_2 =5.86	+0.1
Lysine	pK_1=2.19, pK_2=9.06	+0.995

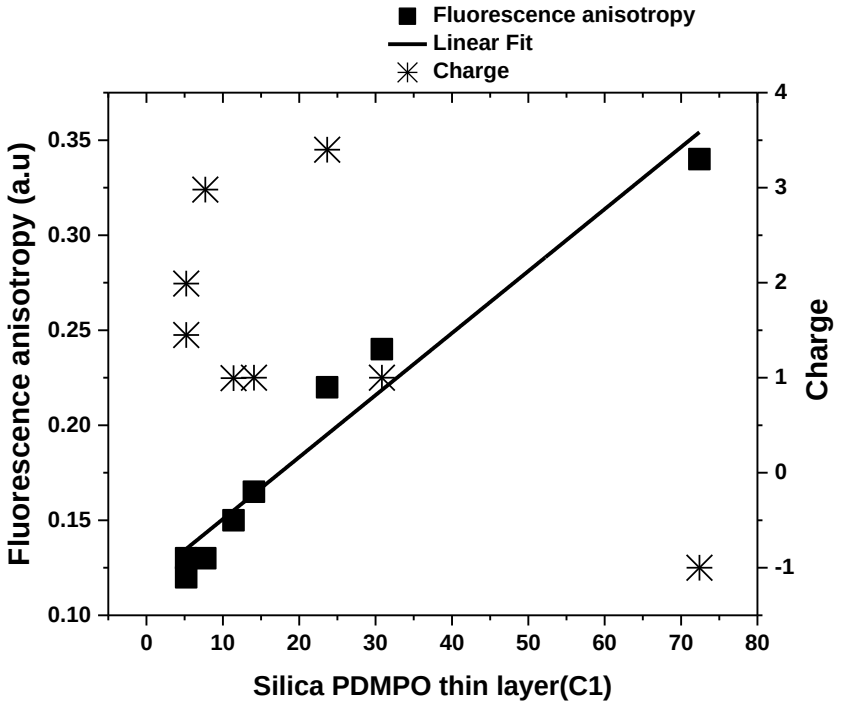

Figure 5.7: (a) Linear response between fluorescence anisotropy and confocal thin layer (C1) intensity demonstrate that SQIDA can be used as a complimentary technique to fluorescence anisotropy and responses between charges on the substrate with thin layer (C1) intensity.

OSPFA was performed on the polyamines (**Figure 5.6.a**) spermine and spermidine which have a higher rate of displacement (lower thin layer intensity) compared to Putrescine (1,4 diaminobutane) and octadecylamine. These results correlate with fluorescence anisotropy measurements on silica surfaces (**Figure 5.6.b**) with a higher rotational diffusion of PDMPO (lower anisotropy) for polyamines with higher binding affinity for silica (spermine and spermidine) compared to polyamines with lower binding affinity with silica (octadecyl amine and 1,4 diaminobutane). There is no evidence of interactions between polyamines and PDMPO **(Figure 5.6.c**). Studies on silica polyamine interactions using two techniques infer that OSPFA along with SQIDA can be used as an auxiliary techniques to study silica binding interactions.

To further understand the relation between charge and displacement of PDMPO from the silica surface the charge of silicaphilic substrates was determined using the SPARC online calculator. Relationships between charge and the displacement of the indicator represents a linear relationship in the case of amino acids however in the case of polyamines the number of charges along with the length of the side chain influence the mechanism of PDMPO release from the silica surface. A linear relationship was observed between confocal thin layer (C1) intensity and fluorescence anisotropy on silica surfaces (**Figure 5.7)** which suggests that both the techniques can used to complement each other.

3.4 Binding studies on silicaphilic substrates using the silicaphilic fluorescence of PDMPO.

To demonstrate the ability of OSPFA as a tool for binding studies, a negatively charged amino acid (aspartic acid), positively charged amino acid (lysine) and a silica binding peptide (pep1) were selected for the study. These binding interactions were then further compared with fluorescence anisotropy measurements. The negatively charged amino acid aspartic acid upon encountering the silica surface was not able to displace PDMPO compared to the positively charged amino acid lysine and the positively charged peptide in the concentration range between 10 mM to 1 nM.

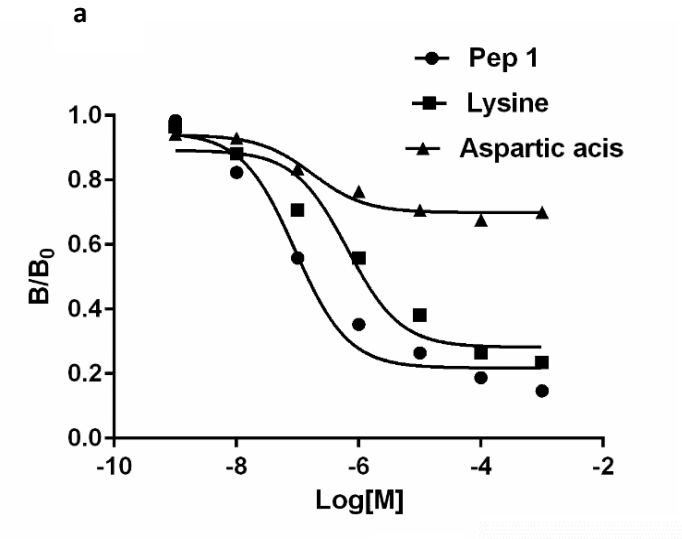

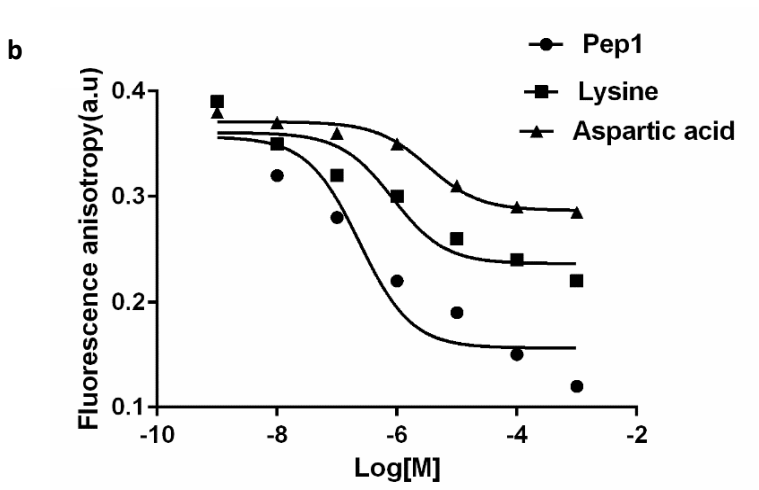

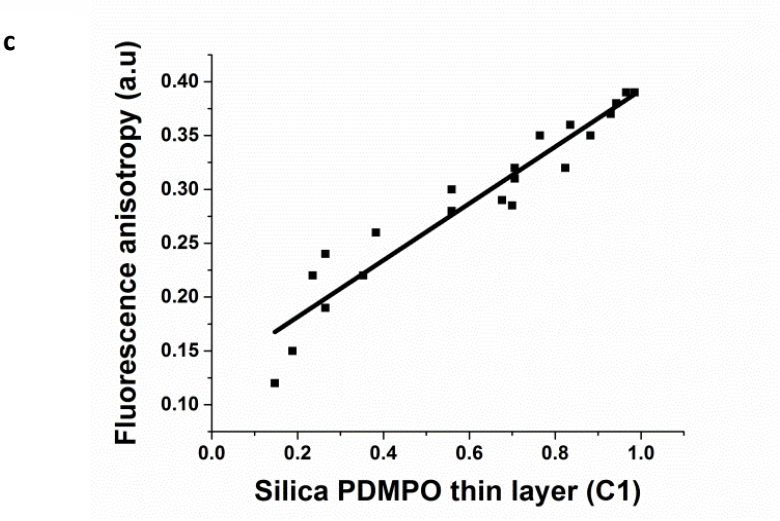

Figure 5.8: Binding curve of displacement assay. (a) Binding curve obtained using confocal indicator displacement assay. (b) Binding curve obtained using fluorescence anisotropy. (c) Linear correlation between the fluorescence anisotropy and confocal thin layer intensity.

A direct comparison of IC50 using OSPFA, $IC5_0$ is 50% displacement of PDMPO upon addition of silicaphilic substrates between negatively charged amino acids and positively charged amino acids was not possible as there is less than a 30% fold reduction in silica PDMPO thin layer intensity for a negatively charged amino acid compared to a 70% fold reduction in the silica PDMPO thin layer intensity in the presence of a positively charged amino acid (**Figure 5.8 a**). Both OSPFA and fluorescence anisotropy studies (**Figure 5.8 b**) indicate that negatively charged amino acids are unable to displace PDMPO compared to positively charged amino acids like lysine. Binding constant K_i refers to the concentration of the silicaphilic substrate which would occupy 50% of silica binding sites in the absence of PDMPO. K_i for lysine was calculated as 0.124 µM using OSPFA and 0.124 µM fluorescence anisotropy respectively whereas K_i for pep 1 was calculated as 2.53 nM for OSPFA and and 2.92 nM for fluorescence anisotropy respectively. Binding constants calculated using the two techniques are comparable with experimental uncertainty. There was a linear correlation between fluorescence anisotropy and maximum thin layer intensity measurements (**Figure 5.8 c**).

5.7 Discussion

5.7.1 Why do polyamines, amino acids and PDMPO bind to silica?

The silica water interface is very important to understanding the adsorption properties of amino acids, polyamines and fluorescent dyes such as PDMPO. The hydroxyl groups (silanol

groups) on the surface of silica dictate the properties of the silica water interface. Silanol groups are formed on the silica surface by two main process, one during condensation and polymerisation where a super saturated solution of monosilicic acid is converted into a polymeric form, even upon drying they retain silanol groups on the surface (Ong, Zhao and Eisenthal 1992). Secondly silanol groups can be formed by rehydroxylation of a dehydroxylated surface by treating with an aqueous solution. These silanol groups on silica surfaces make its surface hydrophilic, they act as centres of molecular adsorption during silica's interaction with adsorbates capable of forming a hydrogen bond which results in donor acceptor interactions. We have used a bioinspired silica condensation process to fabricate silica surfaces which catalyse silica formation using proteins such as lysozyme (Nicklin, et al. 2014). These interactions result in a fabricated silica surface with plenty of silanol groups which can be involved in adsorption processes. PDMPO is an excellent fluorescent dye which has a unique interaction with silica and widely used as silicaphilic probe. It is widely used to study silica precipitation in diatoms and silica deposition in *Equisetum* (Durkin, et al. 2012, Hazelaar, et al. 2005) PDMPO upon interacting with silica remains in the Stern layer. PDMPO has a pyridinium moiety and our previous work indicates that the pyridinium form is stabilised by interaction with negatively charged silica resulting in a proton being taken from the bulk solution. This proton is shared between a siloxide group and the pyridinium moiety on PDMPO leading to two points binding PDMPO at neutral pH. SQIDA a competitive assay was used to screen silica binding molecules and to determine silica binding constants, the data from fluorescence anisotropy studies on nanofabricated surfaces, which do not have hydroxylated silica indicate no evidence of any allosteric modification of PDMPO upon interacting with screening molecules.

5.7.2 What are the factors which affect binding of amino acids, polyamines and peptides on silica?

There are 20 different amino acids which constitute all proteins and peptides. All amino acids are characterised by both carboxyl and amino groups. However the side chain of amino acids determines the molecular properties of the amino acid and peptides they forms. In my experiments I have used four different amino acids; histidine, lysine, alanine and aspartic acid which possess different side chains. Histidine shows higher binding affinity on silica compared to all other amino acids (**Figure 5.a and b**). Histidine is an amino acid which is much more reactive than hydroxide ions in terms of its basicity, apart from that it is a tertiary amine which is intrinsically more nucleophilic than primary or secondary amines (Rimola, Sodupe and Ugliengo 2009). The pK_a of histidine calculated as 1.94 and 5.86 (Table 1) make this molecule the strongest base that can exist at neutral pH. When histidine is protonated the positive charge is shared by two nitrogen atoms (N1 and N3) by resonance. Because these amino acids have a basic group in their lateral chains, it is reasonable to assume positively charged nitrogen have protons which can interact with silanol groups on the silica surface. The main interaction of histidine is between silanol groups and the protons on N atoms of imidazole groups. After histidine the second highest affinity for silica was exhibited by lysine, interaction of lysine with silanol groups is similar to histidine however in the case of lysine interactions are between protons of the amine group of the lysine side chain with silanol groups. Aspartic acid has a carboxylic group in the side chain, its interactions with the silica surface takes place mainly through the backbone carboxyl group. Alanine is a non-polar amino acid which shows the least binding affinity with silica surfaces. The interaction of alanine is mostly governed by $-NH_2$ and -COOH groups of the amino acids. OPSFA results and fluorescence anisotropy results confirmed that the affinity of amino acids are in order histidine > lysine > aspartic acid > alanine which correlates with silica-amino acid binding studies using the computational cluster approach based on the *ab initio* ONIOM2(B3LYP/6-

311++G(d,p):MNDO) method (Rimola, Sodupe and Ugliengo 2009). The the case of Polyamine, silica interaction was tested using a monoamine (octa decylamine), diamine (1-4 diaminobutane) and oligoamines (spemidine trihydrochloride, spermine tetrahydrochloride). Affinity of polyamines to silica are in the order of oligoamines > diamines > monoamines. A direct correlation between charges on the amine groups to the rate displacement of PDMPO from the silica surface is observed. Our observations align with the experimental findings of Verzola et al. who demonstrated the inhibition of protein adsorption in the presence of silica binding amines (Verzola, Gelfi and Righetti 2000). The silica binding peptide pep 1 (KSLSRHDHIHHH) has exhibited very high binding affinity to silica, which can be attributed to the higher binding affinity of histidine motifs that we have observed with amino acids (**Figure 5.4a, b**) using OSPFA.

5.7.3 What are the advantages and disadvantages of OPSFA

To the best of my knowledge this is the first report of using confocal microscopy to study silica binding interaction using PDMPO. Lysine PDMPO binding was used to demonstrate SQIDA in measurements of binding interaction and screening assays on silica fabricated surfaces. The results suggest that confocal assays can be used for screening and study binding interactions. Our method of decomposition of the signals from the silica PDMPO thin layer and unbounded PDMPO over layer integrated with an indicator displacement assay can used to study dose dependent binding and screening of small and big molecules on silica surfaces. We have demonstrated this assay using monoamines, diamines, polyamines, amino acids and peptides but this can be adapted to any silica binding interactions where the binding reaction occurs at the boundary of liquid-solid surface. This technique, based on confocal scanning is non-invasive and it also provide the advantage of restricting the imaging to small portions of the xy, xz and yz planes so unfabricated silica surface in the microplates can be eliminated.

This assay can save time as there is no need of a final washing step and this does not require sensors or specialized reagents beyond those commonly available in many laboratories. Due to the ability to eliminate final washing steps this assay is potentially quite attractive for the study of weak interactions like electrostatic, π-effects, van der waals forces, and hydrophobic effects.

One of the main limitations of confocal scanning is the slow speed of image formation due to raster scanning of the sample by point-by–point illumination and detection. The frame rate of the confocal microscope is roughly 1 sec per frame, this limits confocal microscopy in the study of kinetic interactions happening at millisecond timescale. Confocal assays also possess photo bleaching of the fluorophore in focal planes above and below the plane being observed, which can be problematic as focusing on one plane can influence those that have not yet been observed.

5.7.4 Future work

Comparative studies with fluorescence anisotropy demonstrate that SQIDA can be a complimentary technique for high throughput screening assays for silica binders. This method can be used to screen number of silica binders and can be used to screen different types of chemical libraries including those from combinatorial chemistry, proteomics and peptide libraries. The main goal of using this technique in high throughput screening is to accelerate silica binding research by screening large compound libraries at a rate that may exceed a few a few thousand compounds per day or per week. Silica biomolecule interaction has a fundamental role in biomineralisation and have direct implications in material science, medicine and bionanotechnology. OSPFA provides an excellent analytical tool for work in this arena.

6 References

Böhlen, P., Stein, S., Imai, K. and Udenfriend, S., 1974. A simplified protein assay with fluorescamine in samples containing interfering material. *Analytical Biochemistry,* 58 (2), 559-562.

Cheng Y, P.W.H., Relationship between the inhibition constant (KI) and the concentration of inhibitor which causes 50 per cent inhibition (I50) of an enzymatic reaction. . *Biochem Pharmacol,* 22, 3099.

Cheng, Y., and Prusoff, W.H., 1973. Relationship between Inhibition Constant (K1) and Concentration of Inhibitor which Causes 50 Per Cent Inhibition (I50) of an Enzymatic-Reaction. *Biochemical Pharmacology,* 22 (23), 3099-3108.

Cherkouk, C., Rebohle, L. and Skorupa, W., 2011. Lysine adsorption on the silanized SiO2-surface for immobilization of the estrogen receptor hER(alpha). *Applied Surface Science,* 257 (11), 4831-4835.

Coleska, N., Wang, R., Fang, X., Pan, H., Tomita, Y., Li, P., Roller, P.P., Krajewski, K., Saito, N.G., Stuckey, J.A., Wang, S., 2004. Development and optimization of a binding assay for the XIAP BIR3 domain using fluorescence polarization. *Anal Biochem,* 15;332(2):261-73

Conchello, J., and Lichtman, J., 2005. Optical sectioning microscopy. *Nature Methods,* 2 (12), 920-931.

Coradin, T., Eglin, D. and Livage, J., 2004. The silicomolybdic acid spectrophotometric method and its application to silicate/biopolymer interaction studies. *Spectroscopy-an International Journal,* 18 (4), 567-576.

Dennis, M.K., Bowles, H.J.C., MacKenzie, D.A., Burchiel, S.W., Edwards, B.S., Sldar, L.A., Prossnitz, E.R. and Thompson, T.A., 2008a. A multifunctional androgen receptor screening assay using the high-throughput HyperCyt (R) flow cytometry system. *Cytometry Part A,* 73A (5), 390-399.

Esposito, A., Federici, F., Usai, C., Cannone, F., Chirico, G., Collini, M. and Diaspro, A., 2004. Notes on theory and experimental conditions behind two-photon excitation microscopy. *Microscopy Research and Technique,* 63 (1), 12-17.

Ghafari, H., Parambath, M. and Hanley, Q.S., 2012. Macromolecular binding and kinetic analysis with optically sectioned planar format assays. *The Analyst,* .

Ghafari, H., Zhou, Y.Z., Ali, S. and Hanley, Q.S., 2009. Confocal detection of planar homogeneous and heterogeneous immunosorbent assays. *Journal of Biomedical Optics,* 14 (6).

Gustafsson, M.G.L., 2005. Nonlinear structured-illumination microscopy: Wide-field fluorescence imaging with theoretically unlimited resolution. *Proceedings of the National Academy of Sciences of the United States of America,* 102 (37), 13081-13086.

Hell, S.W., Stelzer, E.H.K., Lindek, S. and Cremer, C., 1994. Confocal Microscopy with an Increased Detection Aperture - Type-B 4pi Confocal Microscopy. *Optics Letters,* 19 (3), 222-224.

Herbowski, L., Gurgul, H. and Staron, W., 2009. Experimental determination of the Stern layer thickness at the interface of the human arachnoid membrane and the cerebrospinal fluid. *Zeitschrift Fur Medizinische Physik,* 19 (3), 189-192.

Hickman, G.J., Rai, A., Boocock, D.J., Rees, R.C. and Perry, C.C., 2012a. Fabrication, characterisation and performance of hydrophilic and super-hydrophilic silica as cell culture surfaces. *Journal of Materials Chemistry,* 22 (24), 12141-12148.

Hyun, J.W., Kim, S.Y., Lee, S., Park, H., Pyee, J. and Kim, S., 2002. Protein adsorption on the nickel-coated glass slide for protein chips. *Bulletin of the Korean Chemical Society,* 23 (12), 1724-1728.

Irving Langmuir, 1918. The Adsorption of gases on plane surfaces of glass, mica and platinum. *J. Am. Chem. Soc.*, 40 (9), 1361–1403.

Ishikawa-Ankerhold, H.C., Ankerhold, R. and Drummen, G.P.C., 2012. Advanced Fluorescence Microscopy Techniques-FRAP, FLIP, FLAP, FRET and FLIM. *Molecules,* 17 (4), 4047-4132.

Jachimska, B., Tokarczyk, K., Lapczynska, M., Puciul-Malinowska, A. and Zapotoczny, S., 2016. Structure of bovine serum albumin adsorbed on silica investigated by quartz crystal microbalance. *Colloids and Surfaces A-Physicochemical and Engineering Aspects,* 489, 163-172.

Kristensen, T.B., and Pedersen, K., 2004. Second-harmonic generation pulse splitting in quartz observed by frequency-domain interferometry. *Optics Communications,* 233 (1-3), 219-223.

Liu, A., Peng, J. and Li, G., 2014. Characterizing penetration depths of multi-wavelength surface plasmon resonance sensor using silica beads. *Applied Physics Letters,* 104 (21), 211103.

Marvin Minsky, 1957. *Microscopy apparatus.* Microscopy apparatus US3013467 A. Microscopy apparatus.

Matveeva, E., Gryczynski, Z., Malicka, J., Gryczynski, I. and Lakowicz, J.R., 2004. Metal-enhanced fluorescence immunoassays using total internal reflection and silver island-coated surfaces. *Analytical Biochemistry,* 334 (2), 303-311.

Monton, M.R.N., Forsberg, E.M. and Brennan, J.D., 2012. Tailoring Sol-Gel-Derived Silica Materials for Optical Biosensing. *Chemistry of Materials,* 24 (5), 796-811.

Nicklin, M., Rees, R.C., Pockley, A.G. and Perry, C.C., 2014. Development of an hydrophobic fluoro-silica surface for studying homotypic cancer cell aggregation-disaggregation as a single dynamic process in vitro. *Biomaterials Science,* 2 (10), 1486-1496.

Ong, S.W., Zhao, X.L. and Eisenthal, K.B., 1992. Polarization of Water-Molecules at a Charged Interface - 2nd Harmonic Studies of the Silica Water Interface. *Chemical Physics Letters,* 191 (3-4), 327-335.

Parambath, M., Hanley, Q.S., Martin-Martinez, F.J., Giesa, T., Buehler, M.J. and Perry, C.C., 2015. The nature of the silicaphilic fluorescence of PDMPO. *Physical Chemistry Chemical Physics : PCCP,* .

Patwardhan, S.V., Emami, F.S., Berry, R.J., Jones, S.E., Naik, R.R., Deschaume, O., Heinz, H. and Perry, C.C., 2012. Chemistry of Aqueous Silica Nanoparticle Surfaces and the Mechanism of Selective Peptide Adsorption. *Journal of the American Chemical Society,* 134 (14), 6244-6256.

Reindl, W., Strebhardt, K. and Berg, T., 2008. A high-throughput assay based on fluorescence polarization for inhibitors of the polo-box domain of polo-like kinase 1. *Analytical Biochemistry,* 383 (2), 205-209.

Rimola, A., Sodupe, M. and Ugliengo, P., 2009. Affinity Scale for the Interaction of Amino Acids with Silica Surfaces. *Journal of Physical Chemistry C,* 113 (14), 5741-5750.

Schaeferling, M., 2012. The Art of Fluorescence Imaging with Chemical Sensors. *Angewandte Chemie-International Edition,* 51 (15), 3532-3554.

Sergeyev, A., Geiss, R., Solntsev, A.S., Sukhorukov, A.A., Schrempel, F., Pertsch, T. and Grange, R., 2015. Enhancing Guided Second-Harmonic Light in Lithium Niobate Nanowires. *Acs Photonics,* 2 (6), 687-691.

Spallino, L., Vaccaro, L., Sciortino, L., Agnello, S., Buscarino, G., Cannas, M. and Gelardi, F.M., 2014. Visible-ultraviolet vibronic emission of silica nanoparticles. *Physical Chemistry Chemical Physics,* 16 (40), 22028-22034.

Tam, J., and Merino, D., 2015. Stochastic optical reconstruction microscopy (STORM) in comparison with stimulated emission depletion (STED) and other imaging methods. *Journal of Neurochemistry,* 135 (4), 643-658.

Vashist, S.K., and Vashist, P., 2011. Recent Advances in Quartz Crystal Microbalance-Based Sensors. *Journal of Sensors, ,* 571405.

Veeranarayanan, S., Poulose, A.C., Mohamed, S., Aravind, A., Nagaoka, Y., Yoshida, Y., Maekawa, T. and Kumar, D.S., 2012. FITC Labeled Silica Nanoparticles as Efficient Cell Tags: Uptake and Photostability Study in Endothelial Cells. *Journal of Fluorescence,* 22 (2), 537-548.

Verzola, B., Gelfi, C. and Righetti, P.G., 2000. Protein adsorption to the bare silica wall in capillary electrophoresis: Quantitative study on the chemical composition of the background electrolyte for minimising the phenomenon. *Journal of Chromatography A,* 868 (1), 85-99.

Wang, D., Yang, M., Dong, Z., Bo, S. and Ji, X., 2013. Interaction between poly (ethylene oxide) and silica nanoparticles in dilute solutions. *Chinese Journal of Polymer Science*, 31 (9), 1290-1298.

Yirdaw, R.B., and Mchaourab, H.S., 2012. Direct Observation of T4 Lysozyme Hinge-Bending Motion by Fluorescence Correlation Spectroscopy. *Biophysical Journal*, 103 (7), 1525-1536.

Zhang, H., Hassanali, A.A., Shin, Y.K., Knight, C. and Singer, S.J., 2011. The water-amorphous silica interface: Analysis of the Stern layer and surface conduction. *Journal of Chemical Physics*, 134 (2), 024705.

Zhang, J.H., Chung, T.D.Y. and Oldenburg, K.R., 1999. A simple statistical parameter for use in evaluation and validation of high throughput screening assays. *Journal of Biomolecular Screening*, 4 (2), 67-73.

Chapter 6 Discussion

6.1 PDMPO its unique photophysics and its silicaphilic fluorescence

In my study I has found out that PDMPO is a unique dye which exhibit intramolecular charge transfer and inter molecular proton transfer. In experiments with binary mixtures of water and acetonitrile (**Figure 3.5 b**) with increases in water content we observe a solvent depend emission change this property of dye establish intramolecular charge transfer (ICT) property, However, ICT is not sufficient to explain all data particularly the pH dependent behaviour of the dye. pH behaviour of PDMPO (**Figure 3.2.5**) is very unique this can be only explained by inter molecular proton transfer. pH behaviour of the dye can be divided into three regime (1) pH≤4.3, (2) 4.3<pH<13.7 and (3) pH>13.7. Lower pH 4.3 fluorescent emission is from protonated state ($PDMPOH_2^{2+}$) and below pH 13.7 emission is from deprotonated state ($PDMPOH^{+}$), However between 4.3 and 13.7 there are two species present; the excited state deprotonated species ($PDMPOH^{+}*$) and excited state protonated species ($PDMPOH_2^{2+}*$) formed during the lifetime of excited state deprotonated species ($PDMPOH^{+}*$). Our discovery of inter molecular protonation of ($PDMPOH^{+*}$) at excited state to form $PDMPOH_2^{2+*}$ by grabbing a proton from water unravel the confusion surrounding the dye. My new understanding about the intermolecular proton transfer can be used to develop analytical techniques to determine water content in any organic solvents which can act a complimentary technique for Karl Fischer, the most common analytical technique in the market to measure the moisture (water) content in solids, liquids or gases.

In the case of Silicaphilic nature of PDMPO we do not see this an inter molecular proton transfer and in the presence of silica, pK_a of the dye is shifted to 6.4 pka units. Amine side chain of PDMPO which do not have any role in the spectroscopic property was involved in the binding interaction between silica and PDMPO. This shift in the pK_a of the dye upon in interacting with the silica is highly depended on the surface chemistry, particularly the charge on the silica surface making this dye a proxy probe to measure the pH and the surface charge density.

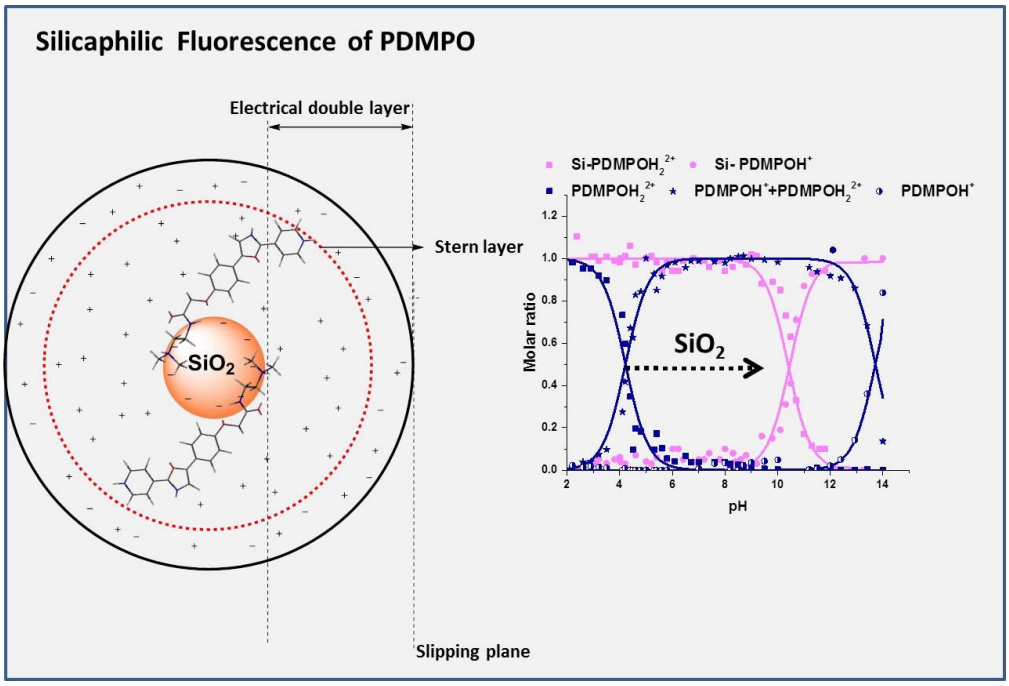

Figure 6.1: Silicaphilic fluorescence of PDMPO due to preferential location of dye in Stern layer and pK_a shift with silica nanoparticles (50 nm)

In my PhD thesis I have translated my understanding of the the photophyscics of the dye to elucidate the surface properties of silica. We were able to exploit the preferential location of fluorescent probe in side stern layer to monitor silica biomolecule interaction, silica

polymerization and study surface acidity. During the process of silica polymerization monosilicic acid get converted into from monomers, dimers to oligomers to polymeric form of silica and the surface charge on silica consecutively increased and this increase in surface charge can be detected using fluorescence emission ratios from PDMPO. Another area of silica chemistry that we have applications is surface charge determination of biosilica, we demonstrated this using *Equisetum arvense* and *Nitzchia stellate* but this can be further developed to any silicifying organisms and can be used to understand silica formation in nature. In my study I was able combine spectroscopic capabilities of PDMPO with microscopic capabilities of confocal microscopy to generate new technique which provides a new approach in silica chemistry.

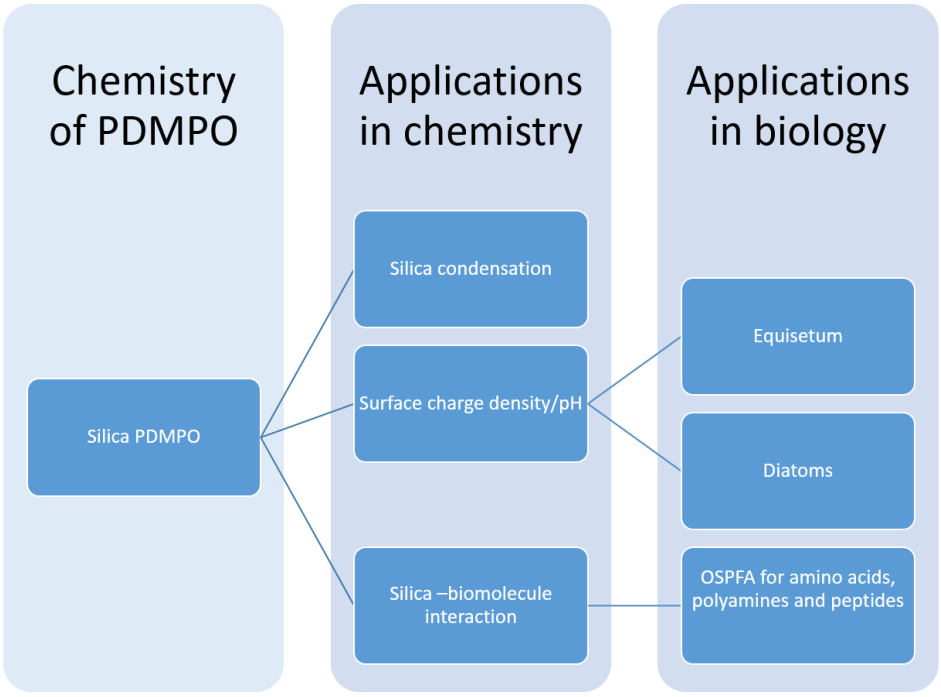

Figure 6.2: Silicaphilic fluorescence of PDMPO and its applications in chemistry and biology.

Our experiments have comprehensively shown that PDMPO when used along with the optical sectioned planar format assay with the confocal microscopy can be used for silica binding and to study screen silica binders. Our experimental results with our newly adapted

optical sectioned planar format assay and fluorescence anisotropy provide compelling evidence that these techniques offer a greater understanding in silica biomolecule interaction.

6.2 Future applications of PDMPO in Biomineralization

Silica formation in nature require the uptake, transport, condensation, growth, precipitation and moulding of species involving silicic acid. Significant progress has been made in role played by biomacromolecules in the controlled formation of silica structure. However much is not understood and there are many unresolved controversies particularly (1) concerning uptake transport silicic acid (2) predicting the pH and micro environment inside silica deposition vesicle(SDV) in diatoms, as it has always been a black box in the process of understanding biosilicification. As SDV itself has not been isolated. From our understanding of acid base interaction of PDMPO, PDMPO interaction after adsorption of silica nanoparticle and PDMPO emission upon entrapment in silica matrix we can propose a simple analytical model based on fluorescence emission ratio and wavelength shift which can be used to understand transport of silicic acid, predict pH change and silica condensation. Acid base balance in cytosol and SDV of silicon starved cultures can be monitored by fluorescence emissions at $PDMPOH_2^{2+}$ and $PDMPOH^+$ when excited at 360 nm which is the isobestic point of the dye.

Silicon uptake from the environment is the key step in the process of biomineralization, and it has been shown that most diatoms use un ionized form of silicic acid (Del Amo and Brzezinski 1999). Fluorescence emission of PDMPO in the presence of uncharged silicic acid will be typical of unhydrolysed silicic acid. In our study we have characterized fluorescence emission of unhydrolysed silicic acid there is no emission from protonated state of the PDMPO in the presence of unhydrolysed silicic acid. Fluorescence emission of unhdyolysed

TEOS was at $PDMPOH^{+}$. Monitoring fluorescence emission at this range can be used to study efflux of silicic acid into diatoms. Silicified cell compartments of diatoms are precisely sculpted in both time and space by two interactive mechanisms micromorphogenesis and macromorphogenesis (Hildebrand and Wetherbee 2003, Wetherbee 2002).

Micromorphogesis define the process like silica polymerization, formation of distinct nanostructures that develop in the lumen of the SDV and macromorphogenesis involve molding of developing SDV by organelles and cytoskeletal components that interact with cytoplasmic surface to generate large scale complex shape (Hildebrand and Wetherbee 2003). In our study we have demonstrated in the presence of silica PDMPO fluorescence is typical of that of that of $PDMPOH_2^{2+}$. We have also demonstrated $PDMPOH_2^{2+}$ adsorbed on silica nanoparticles have a size dependent effect on fluorescence emission. Dye binding on silica nanoparticles is dependent on surface charge and pH. There is a correlation between the surface charge of silica and fluorescence emission ratio of PDMPO based on its surface acidity of silica. This fluorescence emission ratio can be used to distinguish process of micromorphogenesis and macromorphogenesis. In our studies we identified that there is increases in fluorescence emission intensity with increases in size of silica nano particles. These findings can be used as a new research tool in investigating and understanding the process of silicified cell wall formation in diatoms.

6.3 Future applications of PDMPO in silica biomolecule interaction

Fluorescence spectroscopy can be applied to wide range of problems in the chemical and biological sciences (Cambi and Lidke 2012). Fluorescence measurements can provide information on a wide array of molecular processes, including interaction of solvent molecules with flurophores, rotational diffusion of molecules, distance between molecules, molecular conformation and binding(An 2009, Jaeger, Brand and Eggeling 2003). PDMPO

based interactions can be used to investigate some of the unsolved questions in the area of silicification. Biomolecules are suggested to be involved in silicification kinetics through a phase separation mechanisim.(Sumper and Brunner 2006) Silica precipitation guided by polyamine microemulsions produces a strikingly different morphology when a stabilized sol is replaced by monosilicic acid as the silicon source. Negatively charged SiO_2 particles are arranged around the emulsion droplet. Polyamine microemulsions play a dual role, they stabilize the silica sol and secondarily undergo a phase separation process to give mesoporous silica. The key property of the polyamine is its ability to form a microemulsion carrying positive charge there by providing a water free microenvironment and the removal of water from the condensation reaction provides the driving force for the proton donor/acceptor condensation mechanism this occur when polyamine is in close vicinity with silica particles (Belton, et al. 2008). The present understanding of (bio)silicification in relation to silica formation in the presence of polyamines is able to explain the catalytic effect of polyamines, the influence of pattern of polyamine methylation, the formation of polyamine microemulsions and the proton donor/ acceptor mechanism (Belton, et al. 2008). However there are still many factors that are unknowns from the studies and we believe that only through a combined thermochemical and structural approach the exact nature and mechanisms of (bio)inspired silicification can be fully explained. These question can be studied using fluoresce based approaches like anisotropy, FRET and using super resolution microscopy. Fluorescence anisotropy will be used to obtain rotational correlation time and microviscosity of fluorescent polyamines (Geddes 2002) such as the molecules developed by the C.C. Perry group collaborators VV. Annenkov *et al* and coworkers (Annenkov, et al. 2010). Fluorescence anisotropy measurements to study the size of polyamine complexes during (bio)silicification have not been performed. The proximity of polyamine molecules and silica species during polyamine mediated (bio)silicification has not been studied. This

can be studied using fluorescent resonance energy transfer (FRET). (Ishikawa-Ankerhold, Ankerhold and Drummen 2012) The efficiency of FRET is dependent on the inverse sixth power of the intermolecular separation, making it useful over distances comparable to the dimensions of silica and polyamines during the process of silicification.(Matsumoto, et al. 2000, May, et al. 2012) Thus, FRET is an important technique for investigating a variety of biological phenomena that produce changes in molecular proximity.(Gopich and Szabo 2012) Adaptation of FRET to study silicification by attaching fluorescent labels to polyamines and using silica PDMPO complex will be a good model to study the interaction between fluorescently labelled silica species and fluorescently labelled polyamines during silicification.

Conclusion

PDMPO (2-(4-pyridyl)-5-((4-(2dimethylaminoethylaminocarbamoyl)methoxy)phenyl) oxazole), has unique silica specific fluorescence and is used to study biosilicification. Using UV-vis and fluorescence spectroscopy, computational data, dynamic light scattering and zeta potential measurements we understood the PDMPO-silica interaction. A unique combinatory approach of chromaticity and excited state dynamics allowed the dye to monitor pH from 3 to 13. We have also demonstrated a simple fluorescent spectroscopic method for measurement of surface charge density on silica particles using fluorescent emissions ratios of $PDMPOH_2^{2+}$ and $PDMPOH^+$. There is size dependent and ion dependent change in surface charge potential on silica surface was identified . PDMPO distributed in the electrical double layer was revealed Depending upon the strength of the double layer there is change in fluorescence emissions from protonated and deprotonated state of the dye. When there is change in surface charge either by the change in morphology of silica nanostructure or by the presence of other cations there is corresponding change fluorescence emission ratio. Fluorescent emission ratio can be used as proxy method to calculate zeta potential in the

dynamic range between -15 mv to -40 mV. The Silicaphilic fluorescence of PDMPO was then combined with a optical sectioned planar format assay (OSPFA) using confocal microscopy. The combination of these two techniques provided a new approach to study molecular binding on silica and can be used to screen silicaphilic substrates.

References

An, W.F., 2009. Fluorescence-Based Assays. *Cell-Based Assays for High-Throughput Screening*, , 97-107.

Annenkov, V.V., Danilovtseva, E.N., Zelinskiy, S.N., Basharina, T.N., Safonova, T.A., Korneva, E.S., Likhoshway, Y.V. and Grachev, M.A., 2010. Novel fluorescent dyes based on oligopropylamines for the in vivo staining of eukaryotic unicellular algae. *Analytical Biochemistry*, 407 (1), 44-51.

Belton, D.J., Patwardhan, S.V., Annenkov, V.V., Danilovtseva, E.N. and Perry, C.C., 2008. From biosilicification to tailored materials: Optimizing hydrophobic domains and resistance to protonation of polyamines. *Proceedings of the National Academy of Sciences of the United States of America*, 105 (16), 5963-5968.

Cambi, A., and Lidke, D.S., 2012. Nanoscale Membrane Organization: Where Biochemistry Meets Advanced Microscopy. *Acs Chemical Biology*, 7 (1), 139-149.

Del Amo, Y., and Brzezinski, M., 1999. The chemical form of dissolved SI taken up by marine diatoms. *Journal of Phycology*, 35 (6), 1162-1170.

Geddes, C.D., 2002. 1 and 2-photon fluorescence anisotropy decay to probe the kinetic and structural evolution of sol-gel glasses: A summary. *Journal of Fluorescence*, 12 (3-4), 343-367.

Gopich, I.V., and Szabo, A., 2012. Theory of the energy transfer efficiency and fluorescence lifetime distribution in single-molecule FRET. *Proceedings of the National Academy of Sciences of the United States of America*, 109 (20), 7747-7752.

Hildebrand, M., and Wetherbee, R., 2003. Components and control of silicification in diatoms. *Silicon Biomineralization: Biology, Biochemistry, Molecular Biology, Biotechnology*, Volume 33, 11-57.

Ishikawa-Ankerhold, H.C., Ankerhold, R. and Drummen, G.P.C., 2012. Advanced Fluorescence Microscopy Techniques-FRAP, FLIP, FLAP, FRET and FLIM. *Molecules*, 17 (4), 4047-4132.

Jaeger, S., Brand, L. and Eggeling, C., 2003. New fluorescence techniques for high-throughput drug discovery. *Current Pharmaceutical Biotechnology,* 4 (6), 463-476.

Lokesh, G.L., Rachamallu, A., Kumar, G.D.K. and Natarajan, A., 2006. High-throughput fluorescence polarization assay to identify small molecule inhibitors of BRCT domains of breast cancer gene 1. *Analytical Biochemistry,* 352 (1), 135-141.

Matsumoto, C., Hamasaki, K., Mihara, H. and Ueno, A., 2000. a high-throughput screening utilizing intramolecular fluorescence resonance energy transfer for the discovery of the molecules that bind hiv-1 tar rna specifically. *Bioorganic & Medicinal Chemistry Letters,* 10 (16), 1857-1861.

May, F., Peter, M., Huetten, A., Prodi, L. and Mattay, J., 2012. Synthesis and Characterization of Photoswitchable Fluorescent SiO2 Nanoparticles. *Chemistry-a European Journal,* 18 (3), 814-821.

Sumper, M., and Brunner, E., 2006. Learning from diatoms: Nature's tools for the production of nanostructured silica. *Advanced Functional Materials,* 16 (1), 17-26.

Wetherbee, R., 2002. The diatom glasshouse. *Science,* 298 (5593), 547-547.

Appendix

Appendix 1.1 pH determination

pH determination using the sigma function of $PDMPOH^+$

The sigma values (σ) obtained from Gaussian fitting relate to the full width at half maximum (FWHM) of the peak according to equation ($2\sqrt{\ln \sigma}$). This can also be used as a pH indicator. The peak width values of $PDMPOH^+$ in the presence of silica diverge from the free dye at intermediate pH range but converge at high and low pH.

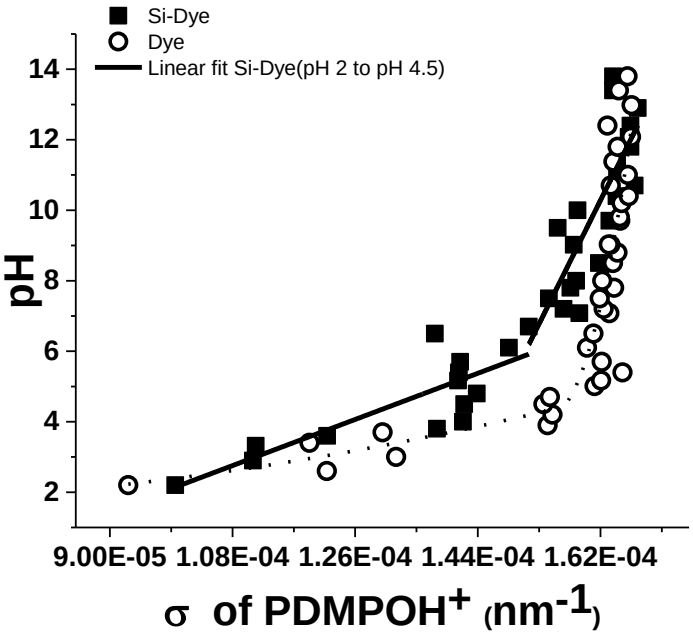

Figure A.3.1 : pH estimation using peak width of PDMPO

Appendix 1.2: pH determination on silica in the pH range 5.4 to 9.7 using the wavelength shift of PDMPOH22^{+}

The pH dependent chromaticity of $PDMPOH_2^{2+}$ is linear between pH 5.4 and 9.7 allowing the chromaticity of the dye in the presence of silica nanoparticles to be used as a probe of pH. In the presence of silica, the dye exhibits a blue shift from pH 2.2 (540 nm) to pH 4.5 (519nm) followed by a red shift up to pH 9.7 (531 nm). At a very high basic pH wavelengths of $PDMPOH_2^{2+}$ for the dye by itself and on silica roughly overlap.

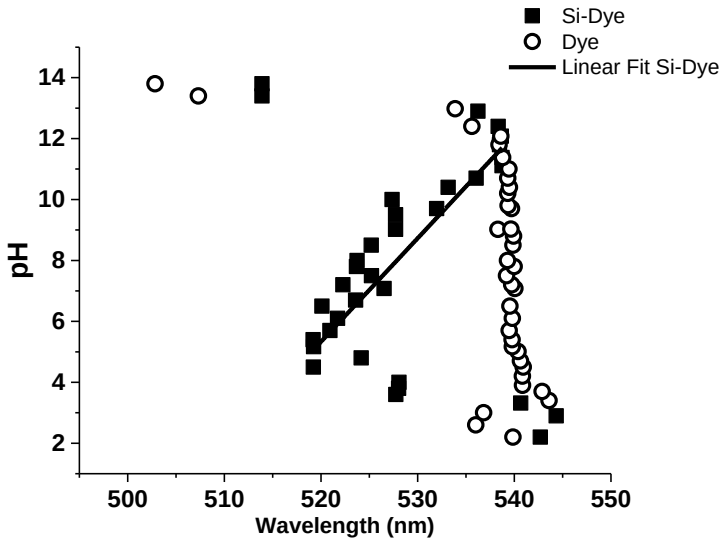

Figure A.2: pH determination on silica in the pH range 5.4 to 9.7 using the chromaticity of $PDMPOH_2^{2+}$.

Appendix 2.1 : Size of silica particles determine charge on the silica particles. We characterized the size of the nano particles using dynamic light scattering

22 nm

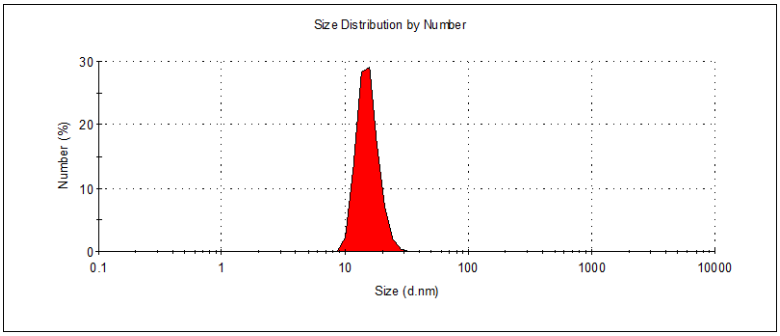

33 nm

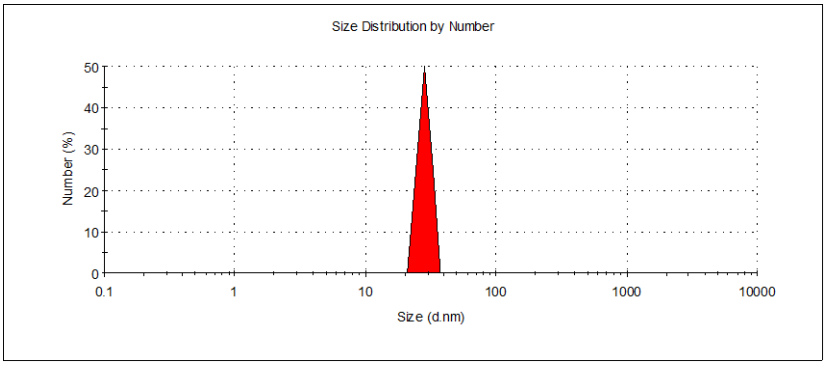

50 nm

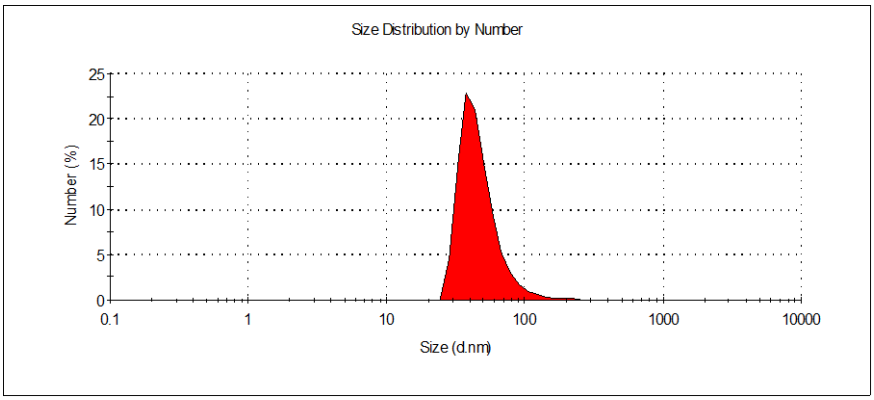

77 nm

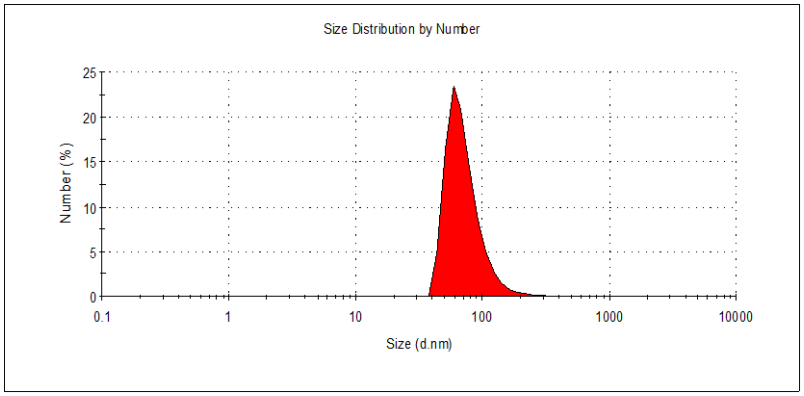

133 nm

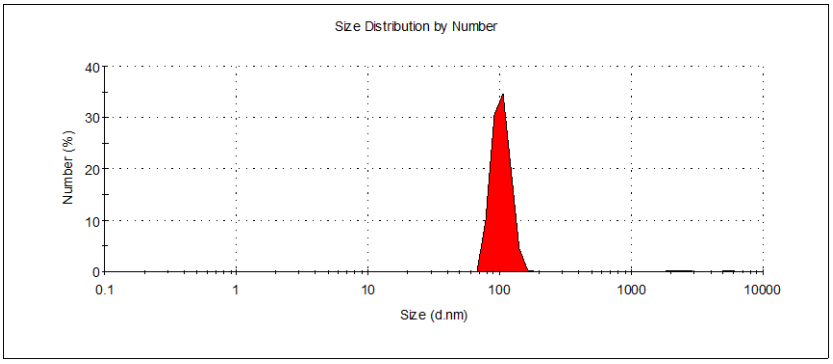

Figure A .2.1: Silica particles were synthesized and size of particles were measured using Dynamic light scattering,

Appendix 2.2. : Charge estimation on the upper and lower ridges of of *Equisetum arvense* using PDMPO

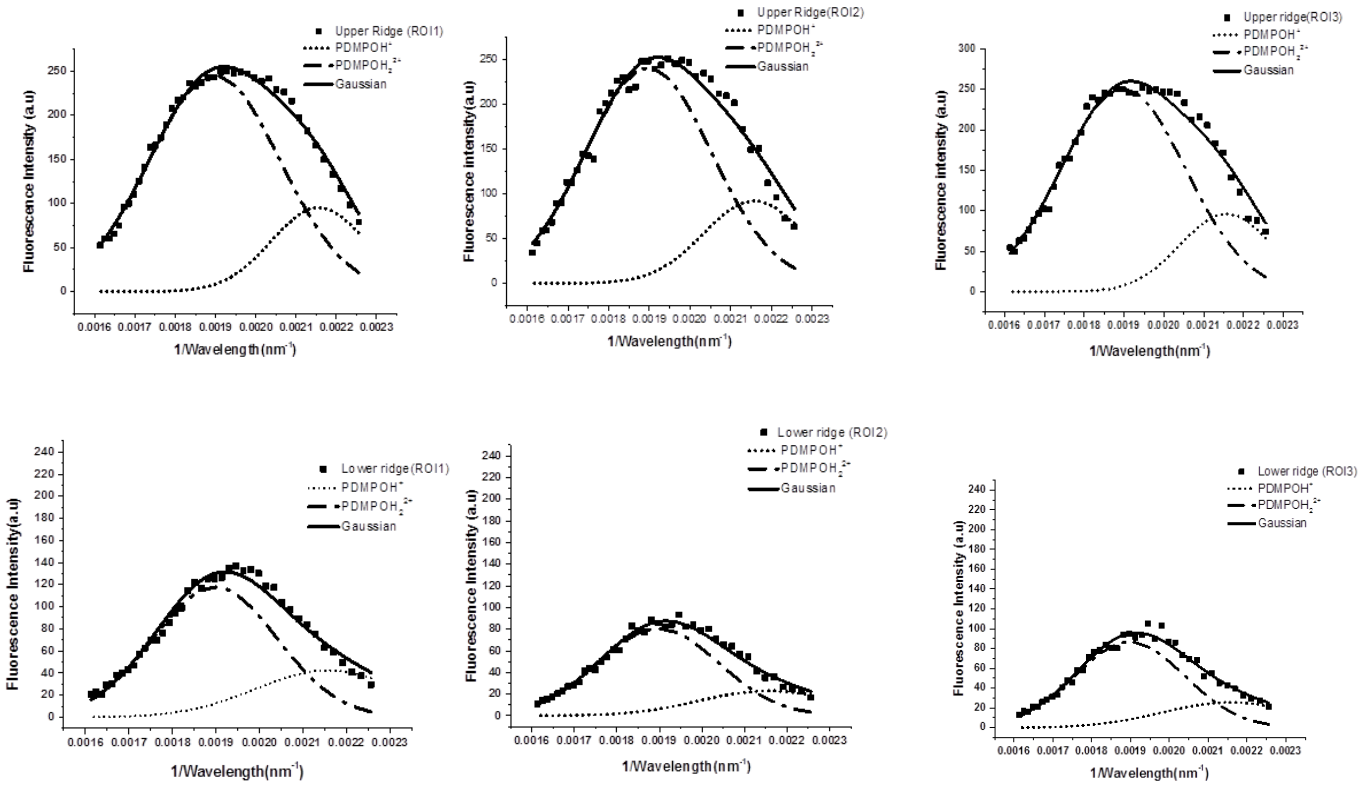

Figure A.2.2 : Fluorescence emission collected from the upper and lower ridges. Three regions of interest (ROI) was selected for each nanostructure. The fluorescence emission spectrum obtained from confocal spectrum imaging was further subjected to Gaussian decomposition.

Appendix 2.3: Charge estimation on the star-shaped rosettes and nodal plane of *Equisetum arvense* using PDMPO

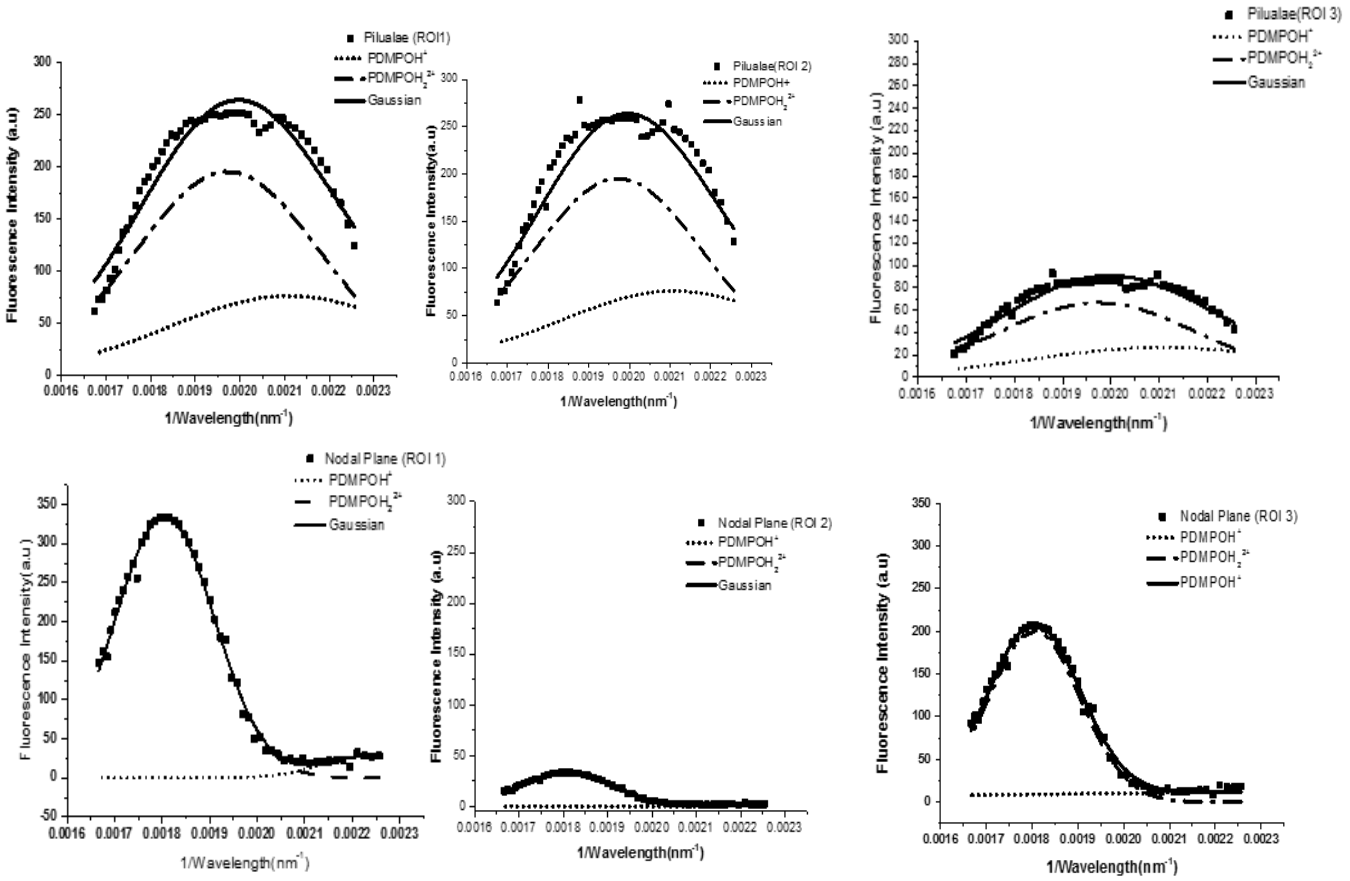

Figure A.2.3 : Fluorescence emission collected from the star shaped rosettes (piluale) and nodal planes Three regions of interest (ROI) was selected for each nanostructure. The fluorescence emission spectrum obtained from confocal spectrum imaging was further subjected to Gaussian decomposition.

Appendix 2.4: Charge estimation on the stomata and basal plane of *Equisetum arvense* using PDMPO

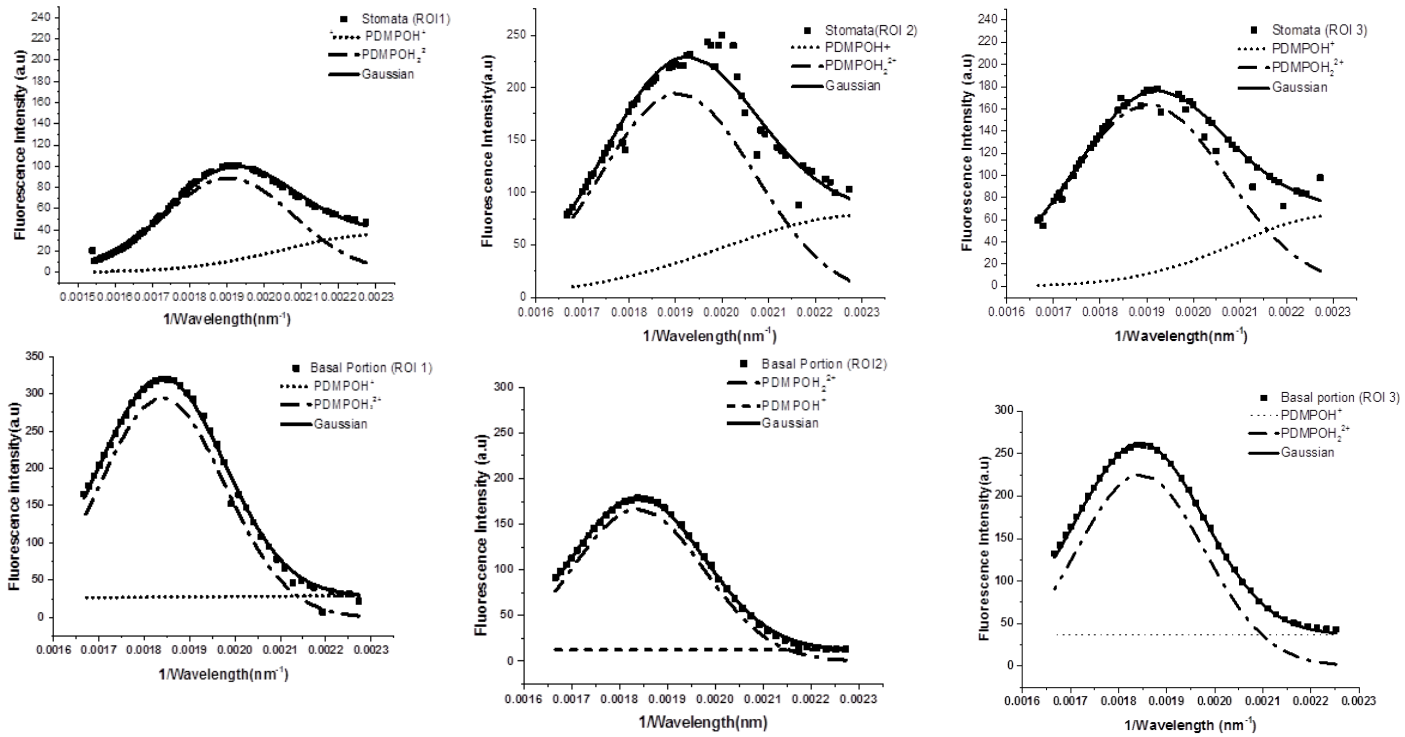

Figure A.2.4 : Fluorescence emission collected from the stomata and basal planes of *Equisetum arvense.* For the spectral analysis three regions of interest (ROI) was selected for each nanostructure. The fluorescence emission spectrum obtained from confocal spectrum imaging was further subjected to Gaussian decomposition.

Appendix 2.5: Charge estimation on apical and trans apical axis of *Nitzschia stellate* using PDMPO

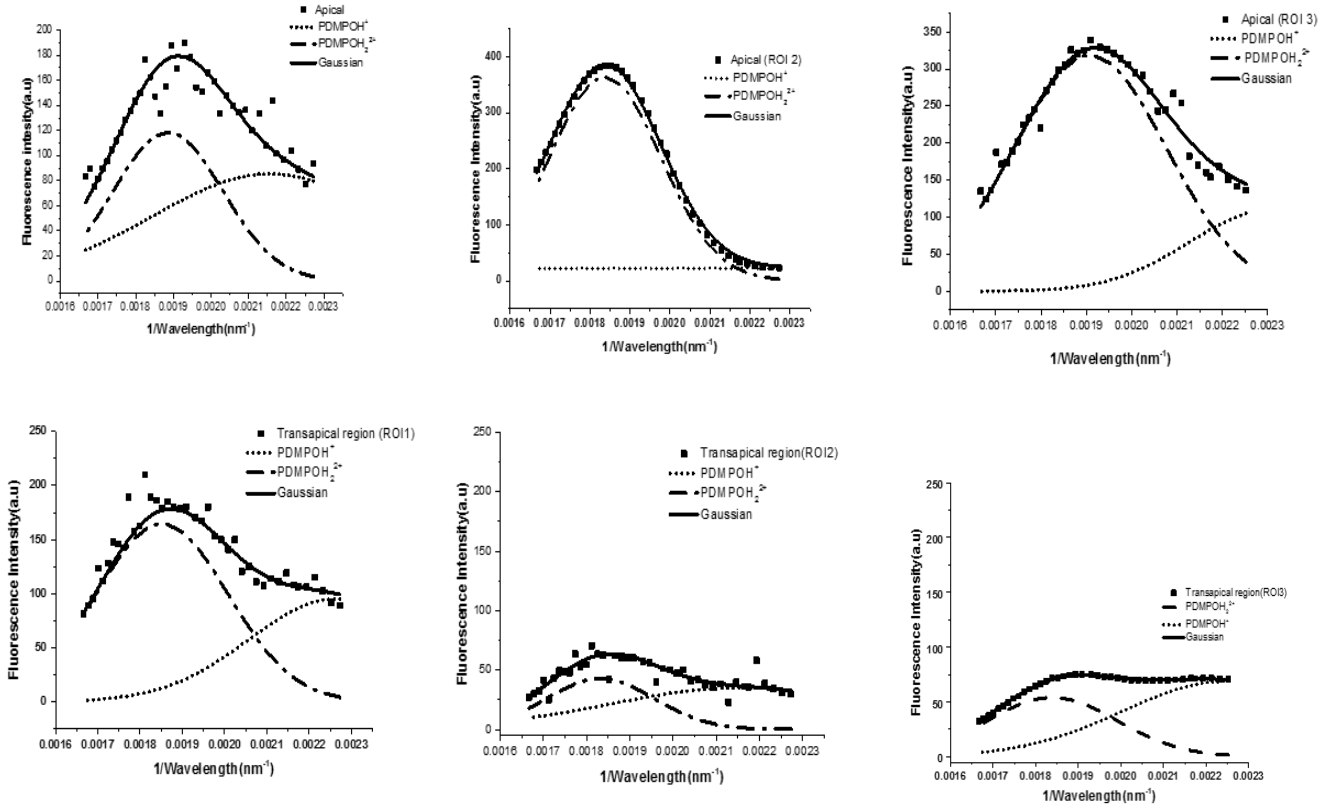

Figure A.2.5 : Fluorescence emission collected from the apical and trans apical axis of Nitzschia stellate using PDMPO. For the spectral analysis three regions of interest (ROI) was selected for each nanostructure. The fluorescence emission spectrum obtained from confocal spectrum imaging was further subjected to Gaussian decomposition.

Appendix 2.6 : Calculation of Pseudo first order rate constants

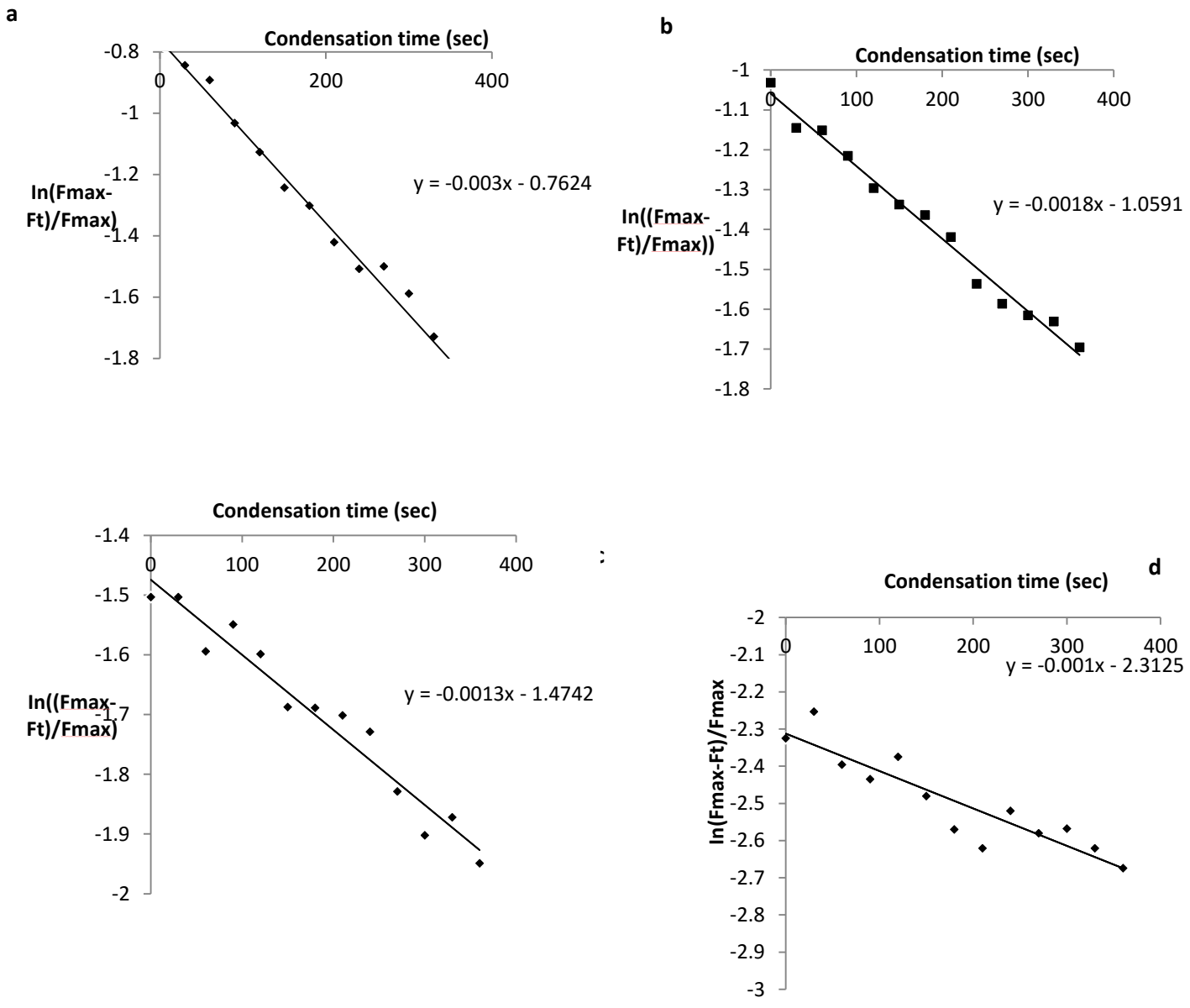

Figure A.2. 6: Pseudo first order rate constants were calculated from the slopes (A) pH 7.08, (B) pH 6.5, (C) pH 6.2 and (D) pH 5.5 as 0.003 sec-1, 0.0018 sec-1, 0.0013 sec-1 and 0.001 sec-1 respectively for the initial 350 seconds

Appendix 3:

Appendix 3.1: Standard curve for Molybdenum blue experiment

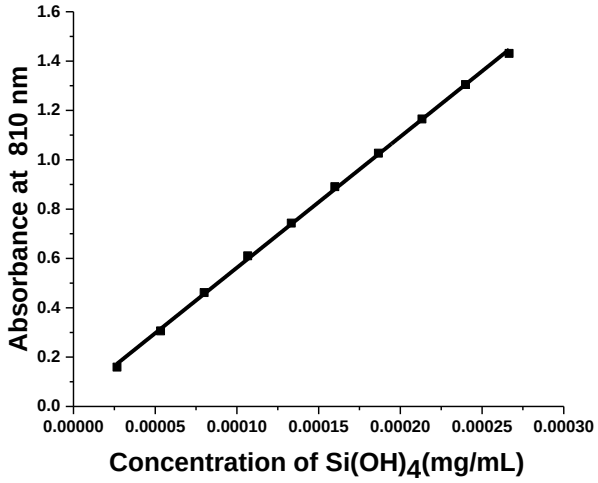

Figure A 3.1. Standard curve for molybdic acid assay used to determine silica concentration in microwell plate

Appendix 3.2 : Decomposition of confocal response of dose dependent increase of PDMPO on silica surface. Measured thin layered intensity was used to fit Lagmuir adsorption isotherm

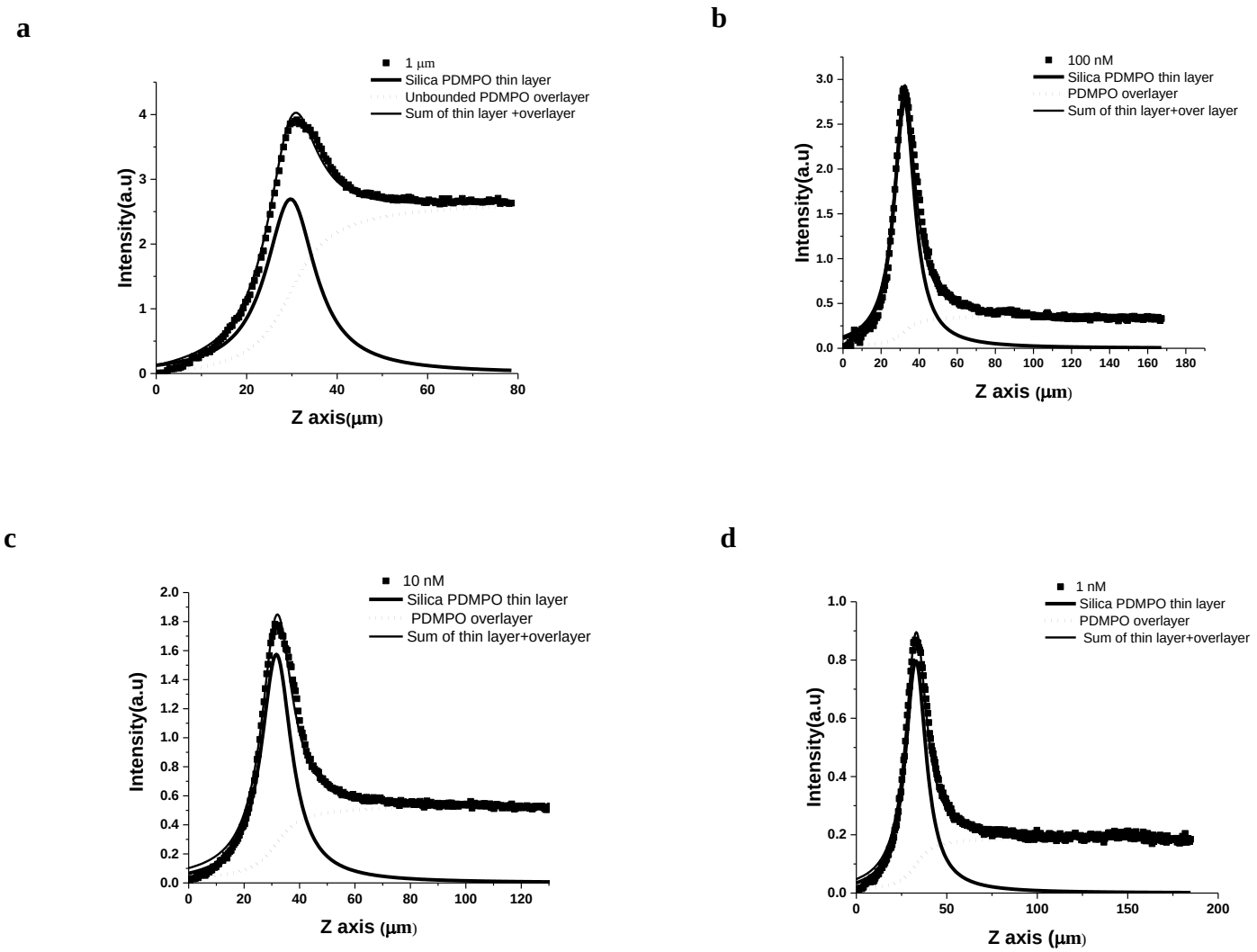

Figure A2: Dose dependent effect of PDMPO concentration on silica surface (a) 1 μm (b) 100 μm (c) 10 μm (d) 1nM

Appendix 3.3 :Measured response function and decomposition of signal Cauchy Lorentz function and cumulative Lorentzian function for thin layer and over layer respectively for dose dependent displacement of lysine.

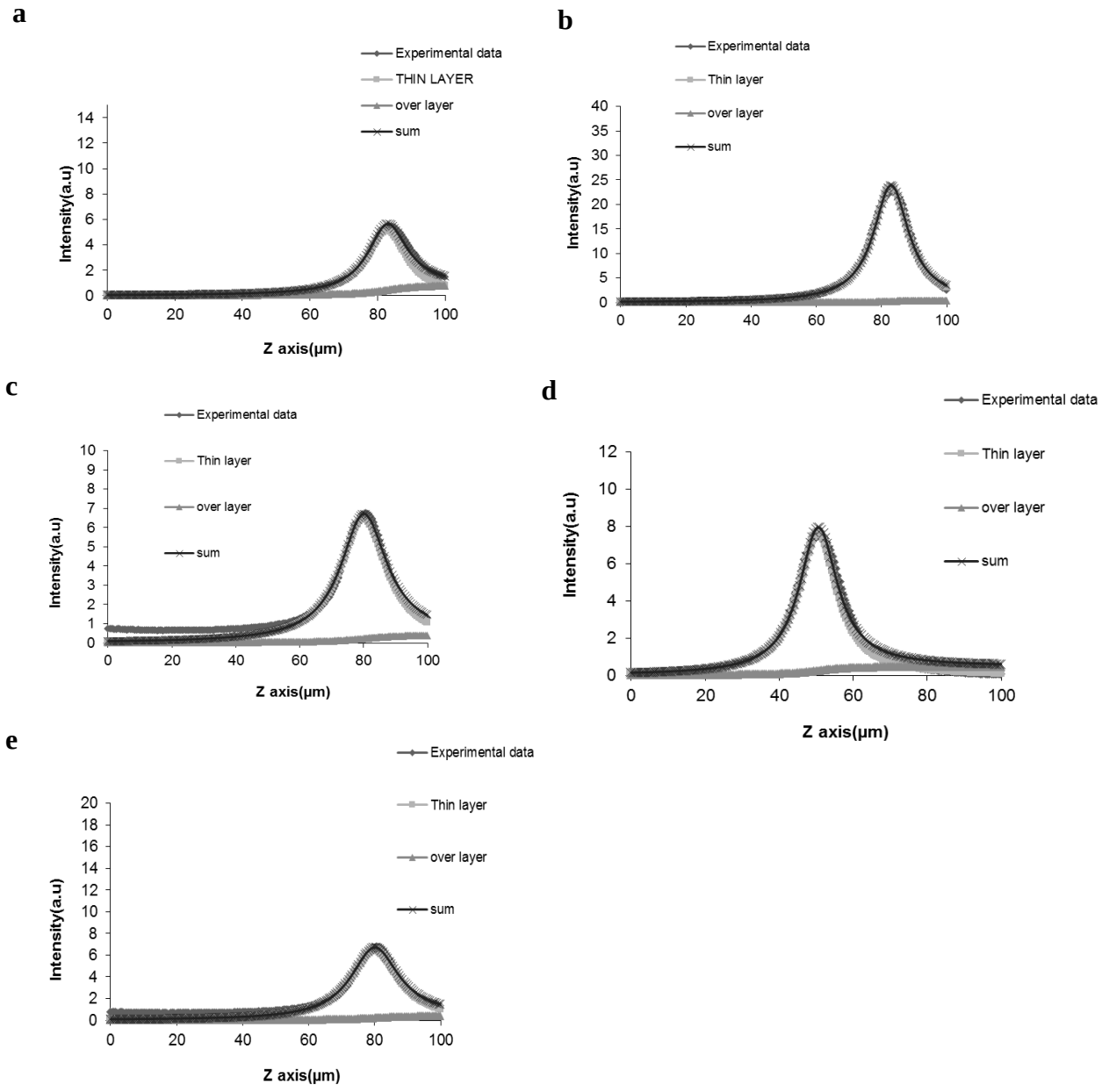

Figure A 3 : Screening of silica binders Experimental data is decomposed into thin layer and overlayer and sum of thin layer and overlayer is fitted with Cauchy-Lorentz function and the cumulative Cauchy-Lorentz functions as in (eqn 5.1) (a) 14 butadiene (b) Spermine (c) Spermidine (d) Alanine (e) Histidine (C1 values for Lysine, Aspartic acid and pep 1 was selected from dose curve. 1 µM concentration of screening molecules was used in screening assa

Appendix 3.4: Calculation of Binding Constant (Ki) for silica binding peptide pep 1

a

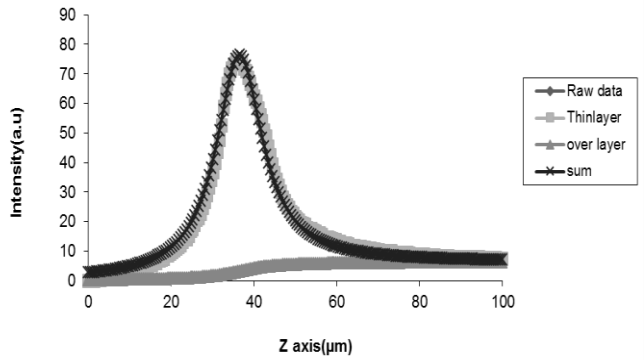

b

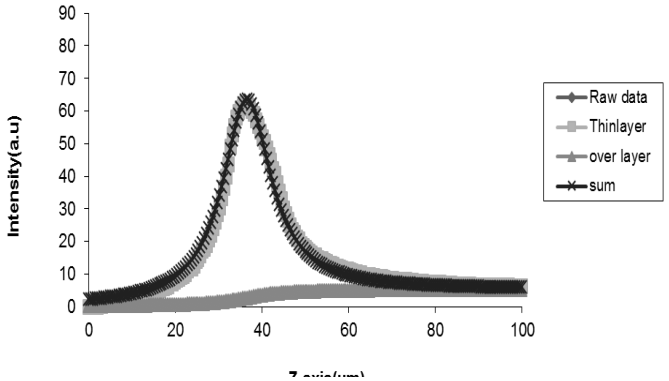

c

d

e

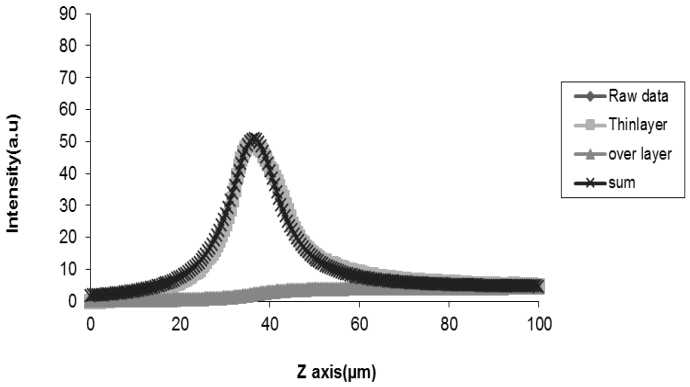

f

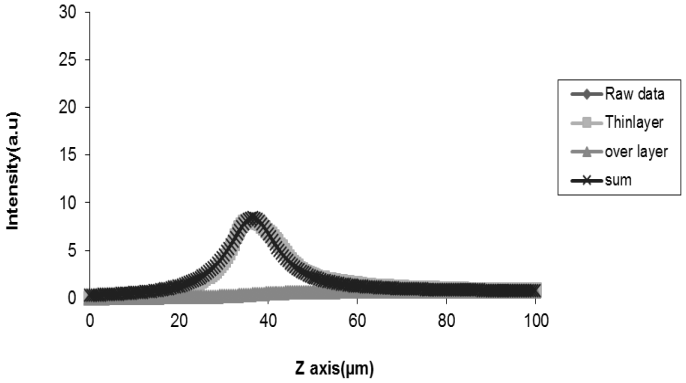

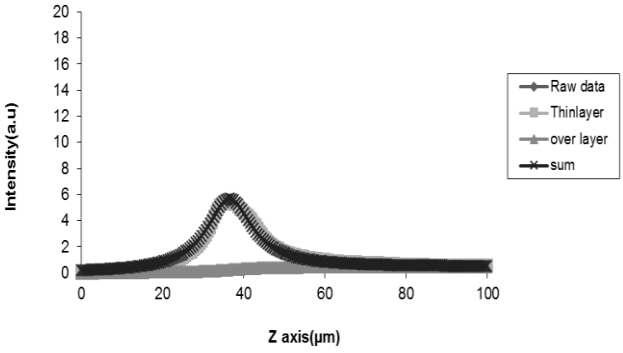

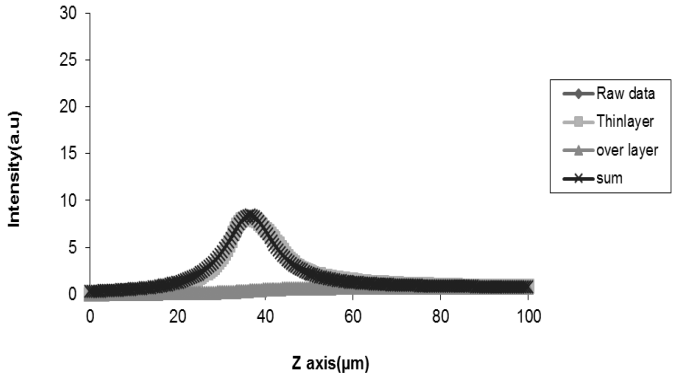

g

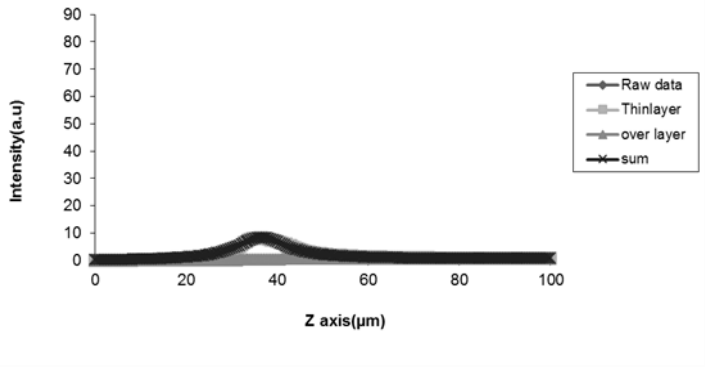

Figure A.3.5: Measured response function for different dose of pep 1 (1 mM to 1 mM) (a) 1 nM (b) 10 nM (c) 100 nM (d) 1000 nM (e) 10 µM (f) 100 µM (g) 1 mM. There is dose dependent displacement of PDMPO is observed

Appendix 3.5 : Calculation of Binding Constant (Ki) for Aspartic acid

a

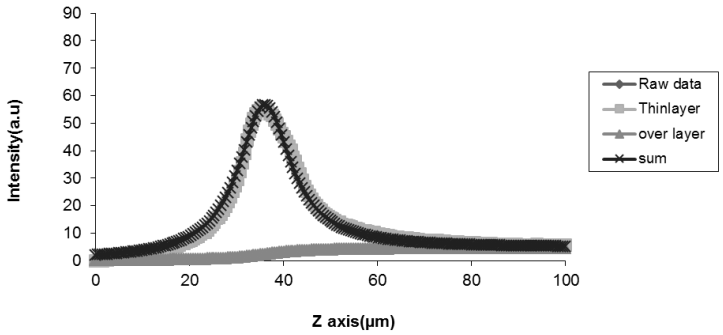

b

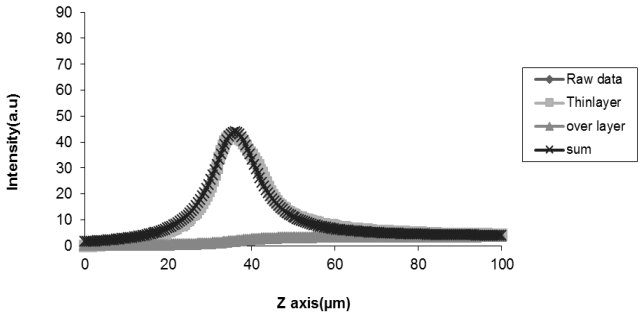

c

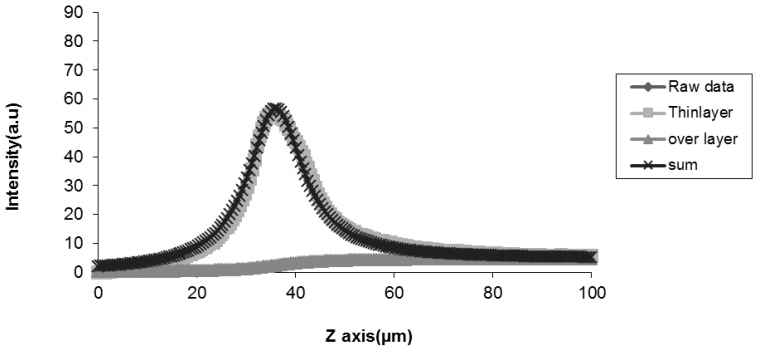

d

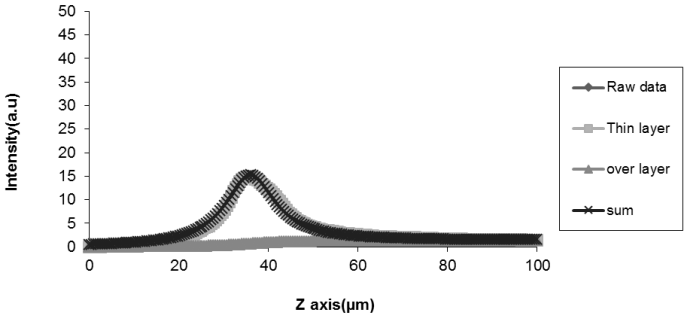

e

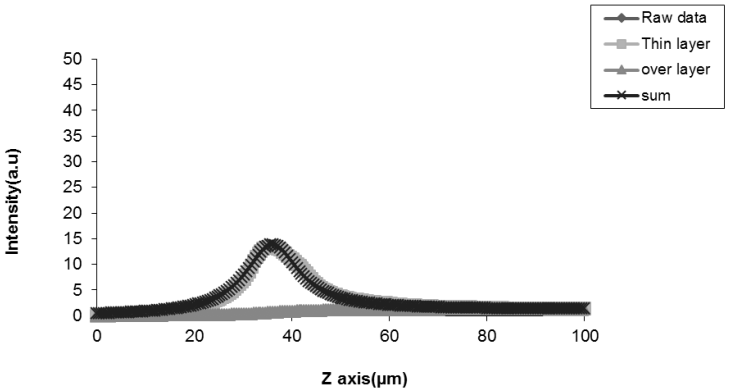

f

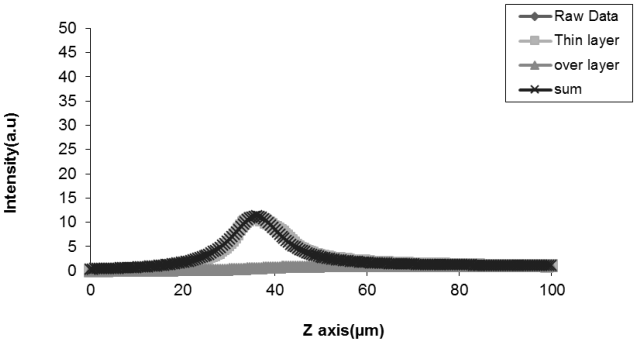

g

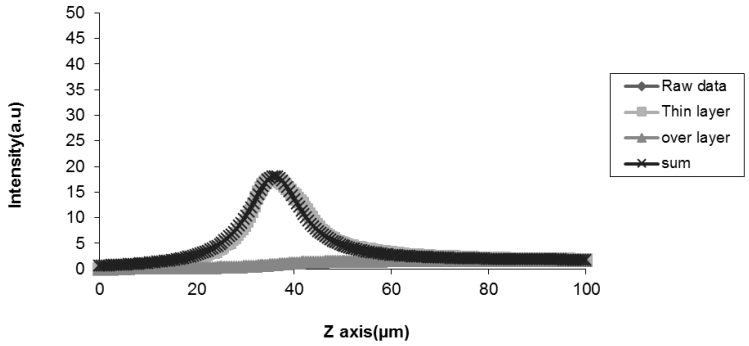

Figure A.3.5: Measured response function for different dose of Aspartic acid (1 mM to 1 mM) (a) 1 nM (b) 10 nM (c) 100 nM (d) 1000 nM (e) 10 µM (f) 100 µM (g) 1 mM. There is dose dependent displacement of PDMPO is observed